

May 2017

Performance Optimization of Onboard Lithium Ion Batteries for Electric Vehicles

Rohit Anil Ugle

University of Wisconsin-Milwaukee

Follow this and additional works at: <https://dc.uwm.edu/etd>



Part of the [Mathematics Commons](#), and the [Mechanical Engineering Commons](#)

Recommended Citation

Ugle, Rohit Anil, "Performance Optimization of Onboard Lithium Ion Batteries for Electric Vehicles" (2017). *Theses and Dissertations*. 1547.

<https://dc.uwm.edu/etd/1547>

This Dissertation is brought to you for free and open access by UWM Digital Commons. It has been accepted for inclusion in Theses and Dissertations by an authorized administrator of UWM Digital Commons. For more information, please contact open-access@uwm.edu.

PERFORMANCE OPTIMIZATION OF ONBOARD
LITHIUM ION BATTERIES FOR ELECTRIC VEHICLES

by

ROHIT UGLE

A Dissertation Submitted in
Partial Fulfillment of the
Requirements for the Degree of
Doctor of Philosophy
in Engineering

at

The University of Wisconsin – Milwaukee

May 2017

ABSTRACT

PERFORMANCE OPTIMIZATION OF ONBOARD LITHIUM ION BATTERIES FOR ELECTRIC VEHICLES

by

Rohit Ugle

The University of Wisconsin-Milwaukee, 2017
Under the Supervision of Professor Anoop Dhingra

Next generation of transportation in the form of electric vehicles relies on better operation and control of large battery packs. The individual modules in large battery packs generally do not have identical characteristics and may degrade differently due to manufacturing variability and other factors. Degraded battery modules waste more power, affecting the performance and economy for the whole battery pack. Also, such impact varies with different trip patterns. It will be cost effective if we evaluate the performance of the battery modules prior to replacing the complete battery pack. The knowledge of the driving cycle and battery internal resistance will help to make decision to replace the worst battery modules and directly cut down on user expenditure to replace the battery.

Also, optimizing the performance of battery during the driving trip is the challenging task to achieve. The knowledge of energy prices of the grid, internal resistance of the lithium

ion battery pack on the electric vehicle, the age of the battery and distance travelled by the electric vehicle are very important factors on which the cost of daily driving cycle is dependent.

In near future, the energy consumed by the electric vehicles will create a major consumer market for the smart grids. The smart grid system is complemented by the renewable energy sources that contribute and support the grid. The electric vehicles are not only predicted as energy consumers but also as dynamic sources of energy. These vehicles can now travel more than 100 miles with a single charging cycle whereas average day to day commute is well below the maximum capacity of these vehicles. This leaves the driver with the extra energy on the battery pack which can be used later for supporting energy requirement from the grid. As we know that cells/modules in large battery packs do not have identical properties and these degrade at different rates during the course of their lifespan. It is beneficial for the user to quantify the amount of energy that can be used to support the grid.

The improvement of the electric grid to the next generation infrastructure ie 'Smart Grid' will enable diverse opportunities to contribute the energy and balance the load on the grid. The information about the grid like price quality, load etc will be available to the people very easily. This information can be useful to make the energy grid more economical and environment friendly. We have used the information for price of energy on the grid to optimize the cost of daily driving cycle.

The goal of this research is to accurately predict the battery behavior for the daily driving cycle. The prediction of battery behavior will help the driver to decide the optimum charging patterns, energy consumed during driving and the surplus energy available in the

batteries. The prior knowledge of the battery behavior, price of the energy on the grid and the trip travel will help the driver to minimize the cost of travel on daily basis as well as throughout the life of the battery.

TABLE OF CONTENTS

1	Introduction.....	1
1.1	Hybrid and Plug-in Hybrid Electric Vehicles	4
1.1.1	Parallel Hybrid Vehicle	5
1.1.2	Series Hybrid Vehicle	6
1.1.3	Power-Split Hybrid Vehicle	7
1.2	Organization of Material	10
2	Literature Review	12
2.1	Battery Modeling	12
2.2	Battery Equalization.....	13
2.3	Electric Vehicles in Smart Grid Market.....	14
2.4	Thermal Modeling of Lithium-Ion Batteries.....	17
2.5	Summary	17
3	Electric Vehicle Battery Performance	18
3.1	Electric Vehicle Model	18
3.1.1	Aerodynamic Force	18
3.1.2	Rolling Resistance.....	19
3.1.3	Acceleration Force	19
3.1.4	Wheel Torque.....	19
3.1.5	Motor Torque.....	20
3.2	Electric Motor Model.....	20

3.3	Electric Vehicle Battery	23
3.3.1	Lithium Ion Batteries.....	25
3.3.2	Battery Modeling Technique	27
3.3.3	Battery Equivalent Circuit Representation	28
3.3.4	Battery Internal Resistance	33
3.3.5	Battery Charging Strategies	37
3.3.6	Battery Equalization.....	39
3.4	Smart Grid	45
3.4.1	Smart Grid Optimization	54
3.5	Summary	58
4	Battery Health and Internal Resistance	60
4.1	Battery Health.....	60
4.1.1	Battery SOC Calibration.....	61
4.2	Driving Cycle	64
4.3	Battery Equalization.....	66
4.4	Worthiness of Replacement.....	67
4.4.1	Two Module Equalization	68
4.4.2	Three Module Equalization	71
4.5	Estimation of Battery Parameters	75
4.5.1	Subspace Estimation of Internal Resistance Map of EV Battery Pack	77
4.5.2	Results with Subspace State Space Parameter Estimation	81

4.6	Summary	88
5	Optimizing the Trip Cost	90
5.1	Battery Discharging	91
5.2	Charging the Battery	94
5.3	Cost Function for the Trip	97
5.4	Opportunity Cost	99
5.5	Optimization Problem	100
5.6	Simulation Results	103
5.6.1	Case 1	103
5.6.2	Case 2	105
5.6.3	Summer Battery Cycle	106
5.6.4	Winter Battery Cycle	110
5.6.5	Summer Battery Cycle - Reducing Charging Time	114
5.6.6	Winter Battery Cycle - Reducing Charging Time	118
5.7	Summary	122
6	Effect of Temperature on Battery Performance	123
6.1	Battery Modeling	123
6.2	Simulations of Battery Behavior	131
6.3	Summary	139
7	Summary	140
8	Bibliography	143
9	Curriculum Vitae	149

LIST OF FIGURES

Figure 1.1 USA Energy sources and consumption from May 2014 (Energy Information Administration, 2014).....	2
Figure 1.2. Smart grid architecture.....	3
Figure 1.3. Parallel hybrid vehicle architecture	5
Figure 1.4. Series hybrid vehicle architecture	6
Figure 1.5. Power-split hybrid vehicle architecture	7
Figure 3.1. Typical initial Lithium ion battery pack	26
Figure 3.2. Battery model examples (a) Thevenin electrical model (b) Impedance based electrical model (Min Chen, 2006).....	28
Figure 3.3. Runtime Based Electrical Battery Models (Min Chen, 2006)	30
Figure 3.4. Non-Linear RC battery proposed for estimation of SOC (Vasebi A, 2008)...	31
Figure 3.5. Remapped battery model (C.R. Gould, 2009).....	32
Figure 3.6. Total resistance R_{tot} , Ohmic resistance R_{hf} , Semicircle resistance R_c and.....	34
Figure 3.7. The electric circuit model of lithium ion battery (M. Ecker, 2012)	35
Figure 3.8. (a) & (b) Internal resistance with variation in temperature (M. Ecker, 2012)	36
Figure 3.9. Multiwinding transformer (a) Conventional Approach (b) Modularized Approach (Park H.S, 2009).....	41
Figure 3.10. Battery Equalization Circuit (Cheng, 2005)	42
Figure 3.11. Typical switching waveform of the battery equalizer when $V_{B1} > V_{B2}$ (Cheng, 2005).....	43
Figure 3.12. a] Diurnal electric pattern on July workday for large school in San Francisco b] Diurnal electric pattern for S2 on January workday for large school in San	

Francisco c] Diurnal electric pattern for point S3 on a January workday for large school in San Francisco d] Diurnal electric pattern on a July workday for minimal costs for healthcare facility. (M. Stadler, 2012)	48
Figure 3.13. California daily load with PHEV and without PHEV load (Christophe Guille, 2009)	49
Figure 3.14. Load and price for a day in winter (Christophe Guille, 2009)	50
Figure 3.15. Battery vehicle as controlled load and storage (Christophe Guille, 2009) ...	51
Figure 3.16. The vehicle to grid implementation framework (Christophe Guille, 2009) .	52
Figure 3.17. (a) Power generation cost curve (b) CO ₂ emission curve	55
Figure 3.18. Average Non-EV power demand in DTE service area (Changsun Ahn, 2011)	55
Figure 3.19. Generation cost and CO ₂ emission, the carbon tax of \$12/t CO ₂ is used. (Changsun Ahn, 2011).....	56
Figure 3.20. PHEV load sensitivity to vehicle age (Changsun Ahn, 2011)	57
Figure 3.21. Electric car load profile (P. Finn, 2012)	58
Figure 4.1. The battery equivalent circuit model	60
Figure 4.2. Route map of the sample trip	64
Figure 4.3. (a) Motor speed during driving, (b) Motor torque profile during driving	65
Figure 4.4. Battery with equalization circuit	66
Figure 4.5 Battery module SOC trajectories with Case 1 example driving cycle	69
Figure 4.6 Two module battery SOC for example driving cycle for Case-2.....	70
Figure 4.7. SOC trajectory for case1 of three-module battery pack	72
Figure 4.8. SOC trajectory for case 2 of three-module battery pack	73

Figure 4.9. Battery SOC trajectories for three modules for Case3 for intermediate equalization	74
Figure 4.10. Switch Q_1 as conductor	76
Figure 4.11. Diode D_2 as conductor	76
Figure 4.12. Online estimation of Battery-1 internal resistance for the 2-module case....	83
Figure 4.13. Online estimation of Battery-2 internal resistance for the 2-module case....	83
Figure 4.14. Relative error in estimating Battery-1 internal resistance for the two-module case.	84
Figure 4.15. Relative error in estimating Battery-2 internal resistance for the two-module case.	84
Figure 4.16. Estimation of Battery-1 internal resistance for the 3-module case.....	85
Figure 4.17. Estimation of Battery-2 internal resistance for the 3-module case	85
Figure 4.18. Estimation of Battery-3 internal resistance for the 3-module case.....	86
Figure 4.19. Relative error in estimating the Battery-1, Battery-2 and Battery-3 internal resistance for 3-module case.	87
Figure 4.20. Maximum eigenvalue and condition number for the input signal throughout the trip.	88
Figure 5.1. Battery performance for 100 vehicles on a given driving torque and speed ..	93
Figure 5.2. Charging time for batteries in all the groups.....	95
Figure 5.3. Batteries performance during charge from and discharge to grid	105
Figure 5.4. Limited batteries performance during charge from and discharge to grid ...	106
Figure 5.5. Performance of batteries during a week in summer	107
Figure 5.6. The average performance of batteries in summer	109

Figure 5.7. Performance of batteries during a week in winter	111
Figure 5.8. Costs incurred and gained during charging and exchanging energy with grid in winter	112
Figure 5.9. Performance of batteries during a week in summer with varied state of charge	116
Figure 5.10. Costs incurred and gained during charging and exchanging energy with grid in summer.....	117
Figure 5.11. Performance of batteries during a week in winter with varied state of charge	120
Figure 5.12. Costs incurred and gained during charging and exchanging energy with grid in winter	121
Figure 6.1. Physical model of a lithium ion battery model	123
Figure 6.2. C-rate for battery driving cycle	133
Figure 6.3. Operational temperature of the batteries during the driving cycle	134
Figure 6.4. Estimated internal resistance for battery 1 from response surface method ..	135
Figure 6.5. Estimated internal resistance for battery 2 from response surface method ..	136
Figure 6.6. Estimated simulated internal resistance for battery 2 vs actual internal resistance applied during the simulation of the trip.....	137
Figure 6.7. Battery SOC with two module equalization with constant internal resistance and varying internal resistance.	138

LIST OF TABLES

Table 3-1 Typical permanent magnetic electric motor configurations	22
Table 3-2. Commercially available batteries	24
Table 3-3. Comparison for lithium ion and lead acid batteries	25
Table 3-4. U.S. standard electric vehicle charging levels	37
Table 3-5. Typical electric vehicle charging time.....	38
Table 4-1. Initial conditions of the two module simulation study	68
Table 4-2. Initial conditions of individual battery modules for simulation study	71
Table 5-1. Battery internal resistance as per the age of battery	90
Table 5-2. Battery internal resistance as per the age of battery during charging.....	94
Table 5-3. Battery energy capacity available for exchange.....	104
Table 5-4. Cost of battery cycle per day in summer	108
Table 5-5. Opportunity cost for a week in summer	110
Table 5-6. Cost of battery cycle per day in winter	112
Table 5-7. Opportunity Cost for a week in winter	113
Table 5-8. Charging Batteries with variation in SOC during summer	114
Table 5-9. Cost of battery cycle per day for a week in summer with varied SOC	115
Table 5-10. Opportunity Cost for a week in summer.....	118
Table 5-11. Charging Batteries with variation in SOC during winter	119
Table 5-12. Cost of battery cycle per day for a week in winter with varied SOC	119
Table 5-13. Opportunity Cost for a week in winter	121
Table 6-1. Battery Parameter used for modeling	132

Dedicated to my dear parents and wife Mithila who have encouraged me and always been supporting pillars during my education.

My daughter Romila is the cherry on the cake towards the end of my doctoral journey.

ACKNOWLEDGEMENTS

My deepest gratitude goes to Professor Anoop Dhingra. He expertly guided me through my graduate education and shared the same excitement during the research study. His resolute enthusiasm for engineering design optimization kept me constantly engaged with my research. His personal magnanimity has helped me make my time at University of Wisconsin Milwaukee enjoyable.

I would like to thank my committee members Dr. Ronald Perez, Dr. Ilya Avdeev, Dr. Istvan Lauko and Dr. Wilkistar Otieno for their valuable suggestions, support and insights. The Design Optimization Group has always been a source of inspiration. I would like to express my regards to all. I will continue to appreciate their inputs. I would also extend my sincere thanks to Bill Paterson and UW Milwaukee staff who helped me in critical situations.

I owe my degree to all those who have supported and strongly stood beside me during the testing times. Above ground, I am indebted to my family, whose value to me only grows with age. Last but not the least, I acknowledge my wife Mithila, who is my champion. She has blessed me with a life of joy in the hours when the lab lights were off.

1 Introduction

An ever increasing need for better and efficient transportation has motivated the automobile industry to look for alternative sources of energy in lieu of conventional energy sources. This has led to a resurgence of hybrid or electric vehicles in recent years. The electric vehicles are clean, i.e. they have lower CO₂, CO and hydrocarbon emissions than conventional energy resources. Vehicles which use non-conventional energy sources are multi-sourced vehicles which use petroleum-battery, diesel-battery or fuel cell-battery etc. The battery forms a critical element for driving non-conventional vehicles. Electric vehicles (EV) require large battery packs with high energy and power densities to become a competitive choice of transport. These batteries have many cells/modules in series and parallel. Acceptance of these vehicles results from better operation and control of large battery packs.

Recently, addressing the problems of green-house effect, clean energy requirements and the need for renewable energy resources, electric vehicles have gained ground (Fiji Times Online, 2010). Today, research in electric vehicle design and improved battery technology is an active area of research. The automobile industry is adjusting to the requirements to minimize pollution, to limited availability of conventional energy resources and to minimize the cost of travelling (Chang, 1993).

There is a continuous increase in the need for energy around the globe. The sources of energy have been changing dramatically over the last couple of decades. As more and more people appreciate that conventional energy sources such as gasoline, coal etc are finite, the

need to find alternative energy sources to cater our ever increasing energy requirements is growing. Renewable energy resources have been fulfilling a portion of the overall energy requirement. An effort to reduce the cost of renewable energy sources like wind energy and solar energy is the need of the hour.

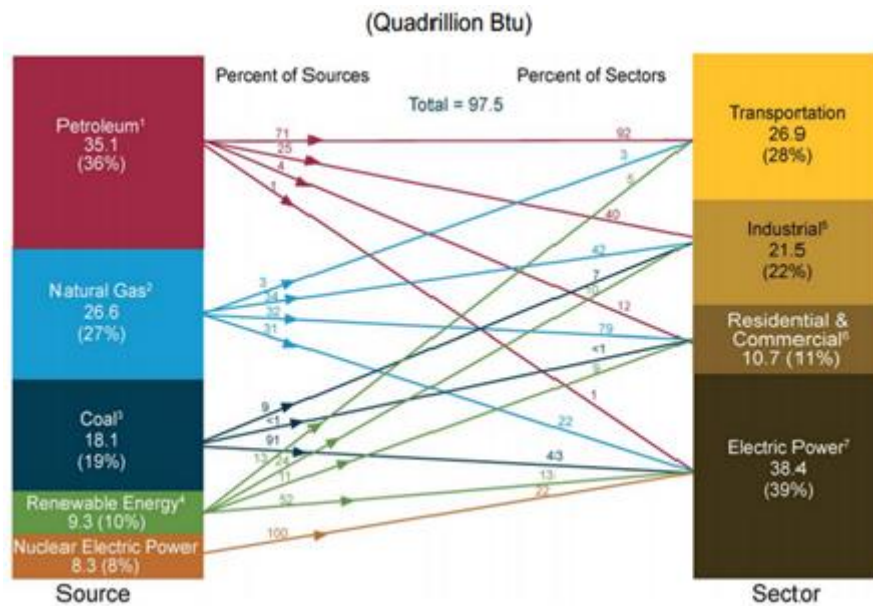


Figure 1.1 USA Energy sources and consumption from May 2014 (Energy Information Administration, 2014)

In Figure 1.1, it can be observed that the major source of energy for transportation is petroleum, i.e. 92 % and only 5% comes of the energy from renewable energy sources (Energy Information Administration, 2014). The major reason for this is the availability of renewable energy sources to drive the vehicles on their own is not a practical option; whatever comes in the 5% is the energy from the grid which is stored in the electric vehicle battery or electric locomotives which are connected to the grid. Hence, to satisfy our growing energy needs, we have to depend more on the energy from the grid and limit the use of internal combustion engine. But, the current supply system electricity has limitations on the infrastructural support.

In order to move from non-renewable energy resources to renewable energy resources, it is important that we have a very robust grid which can support the energy needs. The grid should be able to support the additional loads from the electric vehicles. Also, it should be able to meet variable energy loads which vary depending on the time of the day and the season. The cost of energy should not increase with an increase in the energy requirements and the grid should also not fail under additional loads.

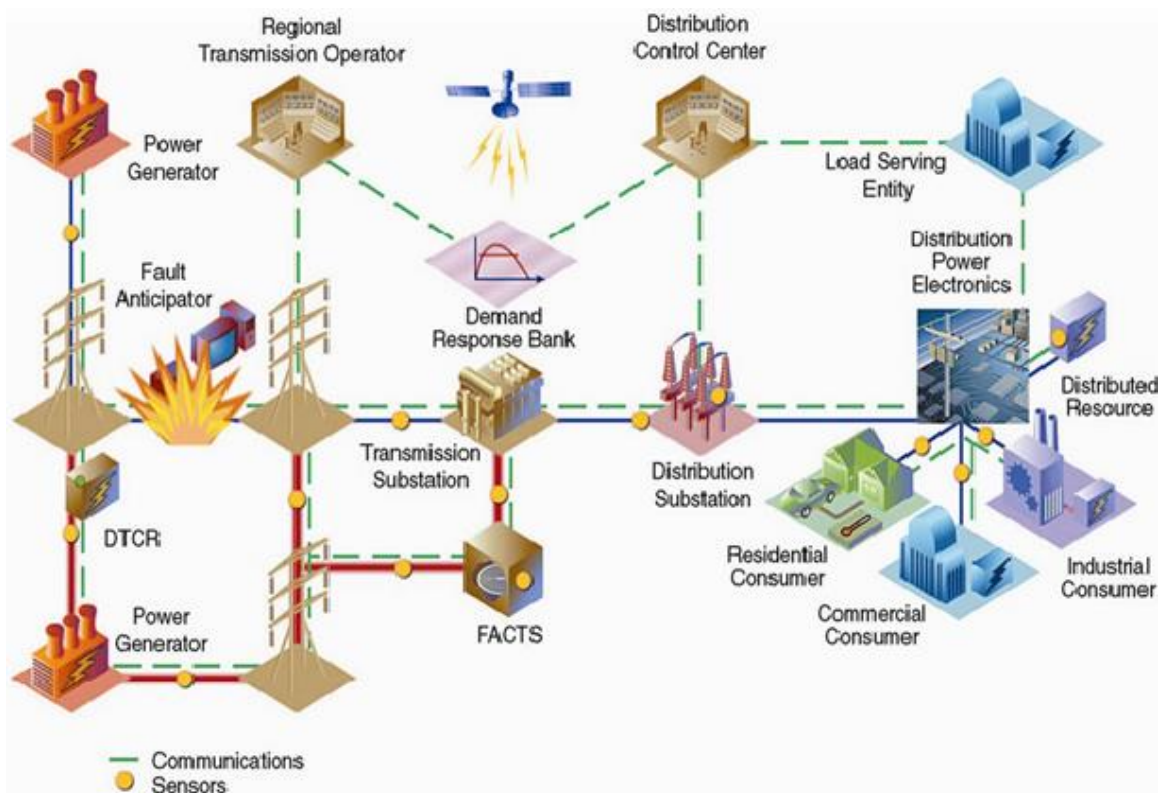


Figure 1.2. Smart grid architecture

The modern grid, which incorporates provisions for advanced load and provides energy efficient solutions is shown in Figure 1.2. The modern grid is also known as “smart grid” as it can keep a track on the energy price per hour as well as the source of energy during an hour. Such a grid would be a self-healing grid which solves problems like voltage

fluctuations, black outs etc. It can adjust its own operating fixed voltage and can correctly monitor the high voltage on the grid.

The best feature in a smart grid is that a user can be a buyer of energy from the grid or can sell excess energy, back to the grid, which means that there would be a two way interaction between the user and grid. This will help in monitoring energy levels at peak hours. In this thesis we will limit our application of the smart grid to electric vehicles and their operation.

1.1 Hybrid and Plug-in Hybrid Electric Vehicles

Vehicles which utilize two sources of energy in combination for propulsion are termed hybrid or plug-in hybrid electric vehicles. The source of energy used for driving the vehicle can be a combination of any of the following: diesel, gasoline, battery, bio-fuels, fuel cells etc. Hybrid-vehicles are recognized in today's market and are appreciated for their low operation cost and low exhaust emissions. Hybrid-vehicles with a diesel and battery combination are less efficient than a gasoline and battery combination.

Hybrid-vehicles with fuel cell and battery are more efficient than gasoline and battery hybrid-vehicle, but they are commercially less successful because of the flammable properties of hydrogen. Also, hydrogen has storage limitations. Hence, more work is required to make hydrogen and battery combination successful. Hybrid and Plug-in hybrid electric vehicles are classified based on their power train configuration. Three commonly used hybrid electric vehicles include:

- Parallel hybrid vehicle
- Series hybrid vehicle

- Power split hybrid vehicle

1.1.1 Parallel Hybrid Vehicle

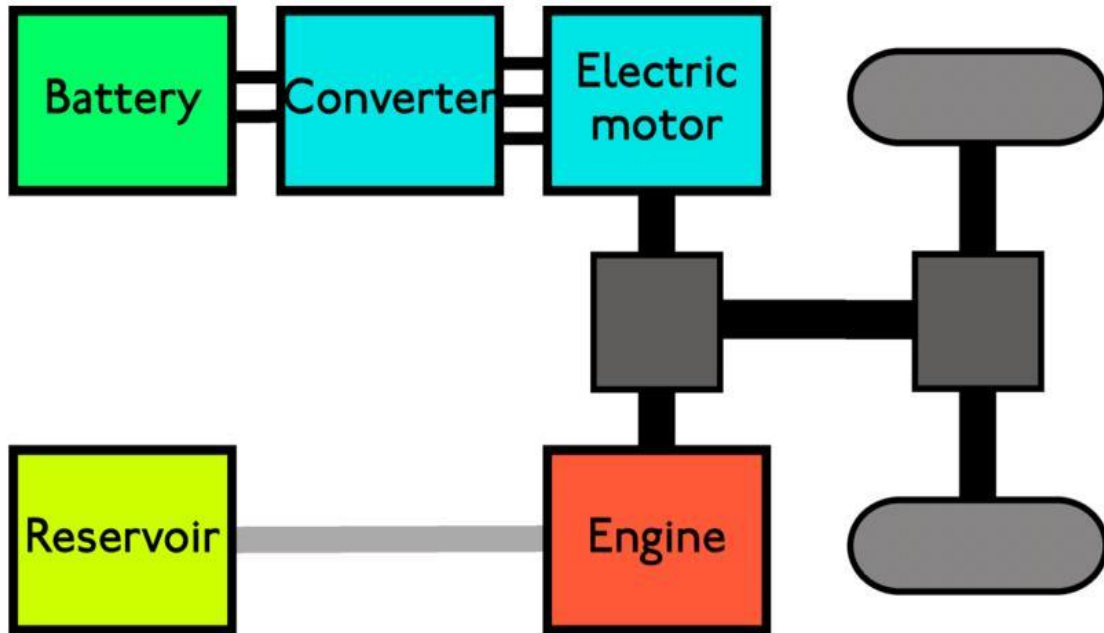


Figure 1.3. Parallel hybrid vehicle architecture

In parallel hybrid vehicles, the electric motor and IC engine are coupled together. In this type of hybrids, the energy from the two sources is applied on the same shaft and the speed of the two shafts is equal. The output torque is the sum of torques from the engine and the battery. The electric motor torque is positive when the vehicle is driven and negative when regenerative charging is done during braking. This type of architecture is found in cars with start-stop application such as Accord-Hybrid, Camry-Hybrid, Cadillac CTS to name a few.

1.1.2 Series Hybrid Vehicle

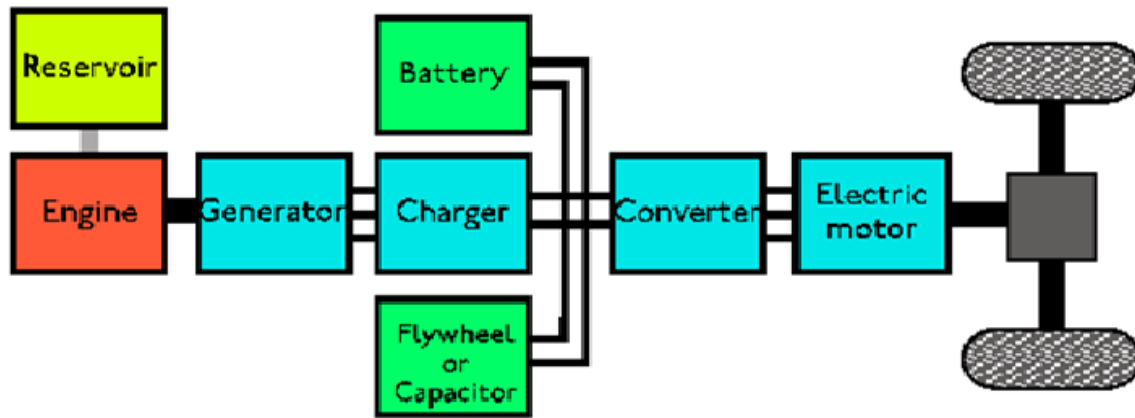


Figure 1.4. Series hybrid vehicle architecture

This type of architecture is mainly observed in electric vehicles which are manufactured for extended driving range. They are also known as range extended electric vehicles (REEV). They are typically battery driven electric vehicles. The internal combustion engine charges the battery and drives the vehicle when the battery state of charge drops to lower limits of the operational range. This arrangement is common in diesel electric locomotives and ship.

1.1.3 Power-Split Hybrid Vehicle

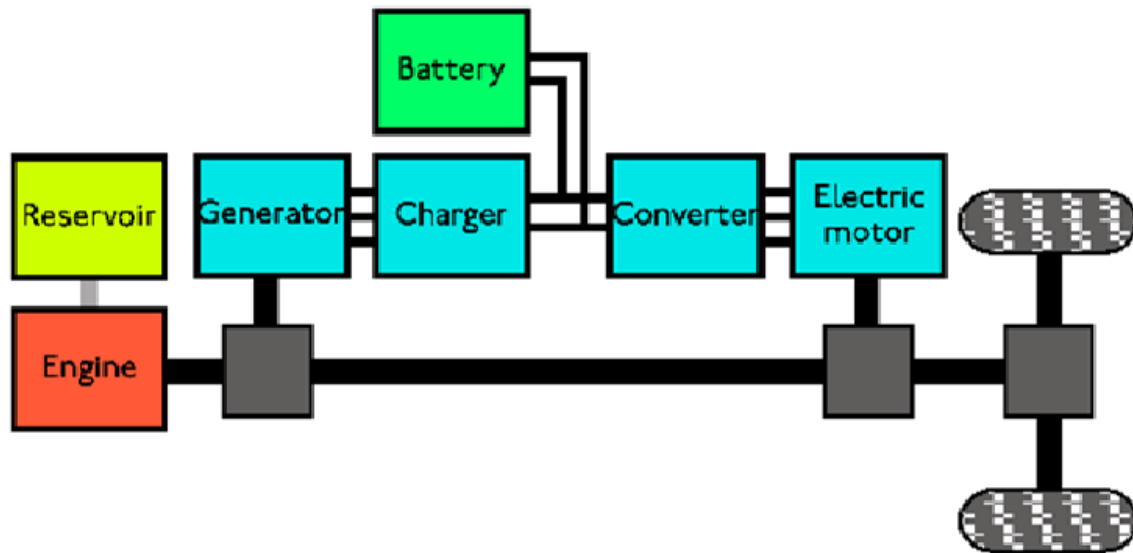


Figure 1.5. Power-split hybrid vehicle architecture

The power split hybrid vehicle works on the principle of decoupling of the power supplied by the engine from the power demanded by the driver. The power split hybrid incorporate devices allowing for power paths from the engine to the wheels that can be either mechanical or electrical. This type of hybrid powertrains are used in vehicles such as Toyota Prius.

Power split hybrid vehicle architecture and parallel hybrid vehicle are applied to short range electric vehicle hybrids. The series hybrids powertrain are applicable for long range electric vehicles which have onboard internal combustibile engine.

The most crucial component for plug-in hybrid electric vehicle or electric vehicle which are completely driven by the electric motor is the battery. Battery capacity and size determine the range of electric vehicles. The battery capacity and size is controlled by

available space and is subjected to design restrictions. So, we intend to utilize the available onboard energy to its maximum capacity. The battery performance and available onboard energy is critically dependent on status of the state of health of the battery in the vehicle.

The electric vehicle battery is divided into various modules and these modules are further sub-divided in series and parallel arrangement of cells. The health of these modules is not uniform and can be determined from the internal resistance of the module. The internal resistance varies with each module in the battery pack. Modules with high internal resistance perform poorly during the battery discharge cycle and reach the lowest point of the battery capacity earliest. This in turn, restricts the battery from driving the electric vehicle with the electric motor. To increase the electric range of a battery, it is necessary to transfer energy from a high energy level module to a low energy level module.

It is also known that with a rise in the internal resistance, the battery performance deviates and degrades. This results in an increase in the charging time and degraded performance of the battery pack during the driving cycle. Also, with the charging scenario in the smart grid, we have the opportunity to decide when to charge the battery (when the electricity cost is the lowest), and supply excess stored energy in the battery to the grid to reduce the overall trip cost. A prior knowledge of the trip/driving cycle, cost of energy on the grid, the battery internal resistance and the energy requirement of the trip enables us to decide the charging and discharging times.

In this dissertation, the research objectives are three fold. Firstly, we propose an on-line battery module degradation diagnostic scheme using the intrinsic signals of battery module equalization. Without need for additional sensors or offline tests, this scheme is cost-effective for constructing and updating the battery pack “health map” in real time during

the vehicle operation. Based on the derived battery health map, the Worthiness of Replacement (WOR) for certain modules/cells is proposed to evaluate the performance of the battery pack for customer specified trip. Such evaluation index provides a quantitative measure for module replacement and battery pack swapping.

Secondly, our research objectives are to quantify the energy available from various battery packs to support the grid. We will optimize the driving cost for all the vehicles and their individual trips. Based on battery age, cost of charging from the grid, daily driving trip and energy available to exchange with grid, we specify the operating patterns for electric vehicles.

Finally, the temperature effect on the performance of lithium ion battery during the driving cycle is very critical to performance of the battery. The internal resistance change during the driving cycle is estimated using the response surface method. Next a model of the lithium ion battery is constructed. This model accounts for the effect of changes in the temperature on the internal resistance of the lithium ion battery during the active driving. Simulation study is performed throughout our study to validate the proposed ideas using an actual driving cycle recorded for a commuting trip.

1.2 Organization of Material

This dissertation is organized in chapters as mentioned below.

Chapter 2 presents a broad overview of the existing literature available on the electric vehicle batteries. The methods adopted for modeling lithium ion batteries to predict accurate parameters of the battery are discussed. The techniques used for identification of system parameters are discussed in this section.

The literature on smart grid, battery behavior on the smart grid is briefly mentioned. Also, the literature on optimizing battery performance is discussed.

The batteries are analyzed in this thesis for their thermal behavior during actual operating conditions. The literature on thermal modeling and effect of operating temperatures on the performance of the batteries is reviewed.

Chapter 3 includes the details of the electric vehicle model with the forces acting on the electric vehicle. The torque on the electric vehicle and motor torque are calculated. Then we list various types of batteries and specify the advantages of lithium ion batteries.

Different battery models are studied with various parameter estimation methods. The open circuit voltage, internal resistance, state of charge and state of health are estimated with these techniques.

Battery charging strategies which do not create adverse effects on the batteries are discussed in brief from the literature review. Also, battery equalization techniques are mentioned, with a prospective strategy to be implemented in this research is discussed in detail.

The smart grid system is explained in brief with the diurnal cost of the energy price per hour on the grid. The role of renewable energy resources to support the grid is discussed. The energy from the battery in the vehicles can be used as energy resource to support the grid decreasing the load from the conventional energy resources. This will reduce the cost of energy.

Chapter 4 deals with battery health modeling and battery equalization technique for a specific driving cycle. The battery internal resistance is estimated for the driven cycle. The concept of worthiness of replacement of lithium ion battery modules is discussed in this section. The sub-space-state-space estimation technique is discussed in this chapter, along with results of the algorithm.

Chapter 5 explains the charging and discharging strategies implemented for the lithium ion batteries of electric vehicles. The algorithm designed for charging and discharging of the electric vehicle battery optimizes the operational cost of lithium ion batteries. We will explain the impact of internal resistance on the performance of electric vehicles. We optimize the daily driving cycle using linear programming techniques.

In **Chapter 6**, we highlight the loss caused by the higher operating temperature of the lithium ion batteries. We create a multi-physics based model for the batteries with an intention to study the effect of internal resistance on the battery performance. We estimated the internal resistance including the temperature effects using the response surface method.

Chapter 7 includes the summary and future scope of our research. Main findings and applications of this research are discussed in this chapter. Based on the research results suggestions are also made for areas that need further exploration.

2 Literature Review

Ever increasing need for energy has motivated the society to find alternative sources of energy. Batteries are assumed to be reliable source of energy required by the automobiles. Several aspects of battery design are explored by research community. The batteries are studied to improve their power to weight ratio, optimize the onboard energy of the battery pack and look at the safety aspects of the lithium ion batteries. The field of battery managements systems is challenging and prospective. In the next parts of literature review aspects of battery modeling, optimizing the electric vehicle performance in the smart grid and thermal behavior of the battery is discussed.

2.1 Battery Modeling

As the batteries are used as source of energy, it is required to identify the state of charge during the driving trip. This has led to the creation of chemistry based battery models and circuit based battery models (M. Kassem, 2012) (M. Dubbarry, 2009). Circuit based models are robust, and practical to implement in electric vehicles. The circuit based models are rigorously tested to accurately predict the performance of the actual battery. Some of the techniques applied to estimate the performance of the lithium ion battery are least square method, Kalman filters, extended Kalman filters, ARMA models etc (K.M. Tsang, 2010).

The age of lithium ion battery pack can be identified from the internal resistance of the battery (X. Wei, 2011). An estimate of battery state of charge can be used to quantify the energy available in the battery pack (J. Xu, 2009).

2.2 Battery Equalization

The electric vehicle battery pack consists of large number of cells which are packed in modules. These modules have variable voltages. The power quality of the battery is good if the battery is operated at one specific voltage. Hence to maintain the whole battery pack at one energy level and voltage energy is transferred from higher energy battery module to the lower energy battery module. Battery equalization is the process to balance the energy levels of the modules of lithium ion battery pack.

The battery pack has limitation on the its maximum current to charge or discharge, maximum and minimum operating voltage, quantization error and noise (C. Moo, 2008). This is addressed with equalizing the battery pack. The energy from higher energy module is transferred to lower energy module (Cassani & Williamson , 2010). The high energy modules have lower internal resistance whereas the lower energy modules have higher internal resistance. The energy level of the battery is equalized to minimize the loss of energy. The battery pack is operated at equalized module as a benchmark and not the lowest energy module as the benchmark.

Cassani et al in 2010 designed a control scheme to equalize battery modules based on open circuit voltage estimation. A novel cell equalization approach was proposed to achieve a low cost operation, large current exposure and high efficiency. A practical approach to solve the cell equalization problem is with a voltage equalization scheme. Voltage based power electronics scheme for cell equalization is a practical solution for electric vehicles and plug-in hybrid electric vehicles (Park H.S, 2009).

The equalization schemes are applied to single battery cells for specific currents and voltages. The equalization schemes are not applied to battery packs of electric vehicles. The batteries are not exposed to actual driving cycles which involve variable currents and voltages. Based on the equalization schemes it is possible to estimate the internal resistance or the age of the battery. Techniques like sliding mode observer, Luenberger observer etc are used to estimate the internal resistance of electric vehicle batteries (X. Hu, 2010).

2.3 Electric Vehicles in Smart Grid Market

The major hurdle in penetration of electric vehicles in the market is energy carrying capacity of batteries. Though performance of the lithium ion batteries has improved, it does have limitation on miles per charge. Charging the batteries on the residential grid is a widely accepted solution in near future applications. The batteries should penetrate in the residential grid in coordination, arbitrarily charging the batteries can adversely affect the performance of the grid

Coordinated charging of electric vehicles and plug-in hybrid electric vehicles decreases power losses and voltage deviations by flattening the peak power requirement. However, if the penetration of the grid is arbitrary, the impact on the grid is heavy (K.C.Nyns, 2010).

One of the solutions to charge batteries faster is by charging them with a higher current. This, however, has adverse effect on battery health. As the charging current increases, the internal resistance of the battery rises over a period of time. There is a trade-off between the charging the batteries with higher current levels and the health of the batteries. The charging current for lithium ion battery and the battery degradation is optimized by Bashash et al (S. Bashash, 2011).

Ideally, the batteries should not degrade during the charging process. Degradation of the batteries during charging leads to increase in the trip cost of electric vehicles. The battery replacement cost will add up in the use of electric vehicles. A practical approach to charging electric vehicles on the residential grids is to charge the batteries during the nights as the peak loads and energy cost/unit are highest during the day and fall sharply at the night time. The trade-off in the process of quick charging strategies and battery degradation cost is studied by Lunz et al (Benedikt Lunz, 2012). They have concluded that saving realized from controlled charging of the battery are more than twice than those obtained by exchanging energy from vehicle to grid.

The future for charging electric vehicles on the grid lies with the availability of charging stations (M. Armstrong, 2013). The charging stations could drastically lower the time period for charging batteries. The electric vehicles will no longer have limitation of trips per charge as the depleted battery could be easily replaced at the charging station. The charging stations are further researched by Saber et al to utilize other renewable energy resources in the smart grid (A.Y. Saber, 2012).

The hourly impacts of electric vehicle charging are studied in greater details by Weiller (Weiller, 2011). In the battery charging stations, the batteries have varied state of charge and require different times to charge. This problem of charge scheduling is addressed in Tal's research (Raviv, 2012).

The overall emission from manufacturing to daily driving of electric vehicle is compared to the manufacturing and emissions of the gasoline vehicle in research by Nansai et al in

2001. It is concluded that the CO₂ and other emissions are greater in gasoline vehicles than the electric vehicles charged on the grid (K. Nansai, 2001).

There has been a study carried out to maximize the profit in the smart grid with vehicle-to-grid exchange of energy (Scott B. Peterson, 2010). The authors have calculated the amount of profit earned by exchanging energy with the grid and replacement cost of the battery due to over use of batteries.

The advantage of using electric vehicles to supply energy to the grid can shift the peak load and frequency. The load and frequency shifting are studied with linear programming techniques by Ahn et al (Changsun Ahn, 2011).

A very important approach that reduces charging cost and increases the earnings is by making the electric vehicles smart. In this research the authors compared the energy cost of charging vehicles. Which means the electric vehicle starts charging when it is connected to the plug. This cost is compared to the charging cost of the vehicles when the electric vehicle is charged at minimum prices on the grid (J. Kiviluoma, 2011).

Optimization of the process of charging the batteries in the open market has been conducted by Rotering et al in 2011. They have concluded that the cost of saving the energy over a period of 10 years can cover the initial cost of the equipment (N. Rotering, 2011).

2.4 Thermal Modeling of Lithium-Ion Batteries

In this section, research work related to thermal modeling of lithium-ion batteries is reviewed.

A factor limiting widespread use of electric vehicles is performance of the batteries. The lithium-ion batteries explode at high temperatures. Their performance drastically degrades if their operating temperatures are high (Millner, 2010).

The thermal behavior of the lithium ion battery is modeled by Cai et al (L. Cai, 2011). The battery temperatures change with the application of the loads. The temperature of the battery rises with the operation of the battery. Proper cooling system should be implemented to keep the battery temperature within the operating range (Y. Ye, 2012).

2.5 Summary

Though a lot of research has been conducted in the field of battery modeling, battery equalization and performance of electric vehicle batteries, there are specific issues that need to be addressed. The battery performance can be improved by knowing its state of health and state of charge. Accurately identifying the internal resistance of the battery pack helps us to predict the behavior of the batteries. The reviewed literature directs to use voltage equalization scheme which is a robust technique to equalize batteries. For equalization technique to work, we must be able to estimate the internal resistance of the battery pack during the trip. Further mathematical programming technique can be used to determine energy exchange patterns between the electrical vehicle batteries and the grid.

3 Electric Vehicle Battery Performance

In this chapter the electric vehicle model is reviewed. We formulate all the equations which are useful to model an electric vehicle under driving conditions. Also, various types of batteries and battery models are studied with their application. Large battery packs have varied properties and performance under same or different operating conditions. These batteries are subjected to equalization to optimize and improve their performance. We review current controlled as well as voltage controlled equalization schemes.

3.1 Electric Vehicle Model

In order to derive expressions for motor driving torque and motor driving current, we need explore propulsion dynamics (Karen L. Butler, 1999). Vehicle propulsion dynamics is dependent on aerodynamic force, acceleration force on the vehicle as well as the rolling resistance force.

3.1.1 Aerodynamic Force

The aerodynamic force is the force due to friction on the moving body from the air. This force takes into consideration protruding shapes and surfaces, ducts passages, spoilers, frontal area of the vehicle and is given as

$$F_{ad} = \frac{1}{2} \rho A C_d v^2 \quad (3.1)$$

where, ρ is the air density, A is frontal area, C_d is the coefficient of drag and v is the velocity of the vehicle.

A good design can effectively reduce the drag force by reducing the frontal area from the shape as well as reducing the coefficient of drag.

3.1.2 Rolling Resistance

The rolling resistance force is due to the contact of tires with the road. This force is independent of the velocity of the vehicle. The type of tire and tire pressure are the major factors contributing to this force which is given as

$$F_{rr} = \mu_{rr}Mg \quad (3.2)$$

where, μ_{rr} is the coefficient of rolling resistance, M is the mass of the vehicle and g is the acceleration due to gravity. Proper tire pressure and tire quality can minimize the resistance force.

3.1.3 Acceleration Force

The acceleration force is responsible for linear acceleration of the vehicle. The acceleration force is given by Newton's second law of motion as

$$F_{acc} = Ma \quad (3.3)$$

This is the actual acceleration applied to the vehicle during its motion. This includes the rotating as well as translating parts in the vehicle.

3.1.4 Wheel Torque

All the forces acting on the vehicle contribute to the torque at wheels which propels the vehicle. The torque at the wheels from these forces is

$$T_{wh} = (F_{ad} + F_{rr} + F_{acc}) * r \quad (3.4)$$

where, F_{ad} is the aerodynamic force, F_{rr} is the rolling resistance force, F_{acc} is the accelerating force, and r is the radius of the wheel.

3.1.5 Motor Torque

In case of electric vehicles, the output torque requirement is satisfied by the electric motor. To complete specified motion of the wheel, electric motor produces torque at the motor shaft. The torque at the motor shaft is

$$T_m = \frac{T_{wh}}{G \cdot \eta_g} \quad (3.5)$$

where, T_{wh} is the torque at the wheels, T_m is the torque at the motor, G is the gear ratio of the transmission and η_g is the gear efficiency.

3.2 Electric Motor Model

Modeling electric motor to satisfy the required motion of the vehicle is the primary requirement of the electric vehicle. The propulsion of the electric vehicle is completely dependent on the electric motor. The factors which are considered for electric vehicles are acceleration requirement, speed requirements, life of the motor and regeneration requirements. Also, there are limiting factors for modeling the performance of the motors which are motor torque requirement, angular speed and acceleration. The performance of the motor helps to keep a check on the maximum speed at which the vehicle can be driven.

If these design requirements are not considered, the performance of the electric vehicle is adversely affected.

We have the design requirements and the expected performance from the electric motor. The parameters to design the electric motor are resistance (Ω), motor inductance (L), back emf constant (volt-sec/rad), torque constant (N-m/a), rotor inertia ($\text{kg}\cdot\text{m}^2$) and mechanical damping. The automotive parameters considered are vehicle damping (friction), transmission dynamics, gear ratio and tire friction on the pavement. The electric motor is scaled based on motor speed and torque range. We have limit on the torque and speed of the motor. Also, to safeguard motor from burning out, we set a limit for maximum current and voltage. Efficiency of the motor varies with motor torque, power and motor size. Thus interpolating efficiency with the motor torque and speed is used calculate input and output power of the motor at wheels.

The power delivered by the motor is

$$P_i = \frac{P_o}{\eta_o} \quad (3.6)$$

where, P_i is the input power from the battery and η_o is the motor efficiency. Further,

$$P_o = \frac{P_w}{\eta} \quad (3.7)$$

where, P_o is the output power, P_w is the power available at the wheels and η is the gear efficiency.

The type of electric motor selected for electric vehicle is dependent on the type of load applied to the motor. AC motors have robust performance, but they fail to react to sudden changes in speed; DC motors perform ideally under sudden acceleration and deceleration. Hence, DC motors are first choice for motors applied in electric vehicles. In the case of three-phase AC motors induction motors are a common choice. Recently, permanent magnet synchronous motors are widely accepted as it has advantages of DC and AC motors.

Therefore the choice of motor is a tradeoff between performance during acceleration and running under high speeds. Following are some of the typical configurations of permanent magnetic synchronous motors used for electric racing cars.

Table 3-1 Typical permanent magnetic electric motor configurations

Motor Name	YASA-400	YASA-750	YASA-750H
Peak torque 400A	400Nm	750Nm	750Nm
Continuous torque	220Nm	400Nm	400Nm
Peak power ~ 400V	100kW	100kW	150kW
Continuous power	85kW	50kW	70kW
Peak efficiency	95%	95%	95%

Yasa motors is a leading manufacturer of electric motor drives. They specialize in high power and high torque density electric motors to market. The Yasa motors in Table 3-1 are permanent magnetic synchronous motors that can be used in hybrid electric vehicles

and pure electric vehicles. These motors have varied applications from industrial machines to electric cars.

Commonly, DC motors are used for electric vehicle. The permanent magnetic synchronous motors are suitable to battery operated electric vehicles.

3.3 Electric Vehicle Battery

Electric vehicle battery consists of long series and parallel connected batteries. Batteries convert chemical energy into electrical energy. Direct current (DC) is generated in the batteries from the positive and negative electrodes in the electrolyte. The cells which convert chemical energy to electricity only once in their life time are called primary cell whereas the rechargeable cells are called secondary or rechargeable batteries. The rechargeable batteries can be charged by reversing the chemical reactions in the battery. There by bringing the batteries to their original state of charge. The batteries used for electric vehicles are rechargeable batteries which propel the electric motor. Electric vehicle batteries undergo deep discharge so as to satisfy the need of power. Hence the electric vehicle batteries should have high ampere-hour (Ah) capacity. The following are the characteristics the electric vehicle battery must have:

- High energy density batteries
- High calendar life of lithium ion batteries
- Low cost batteries
- Low replacement cost of batteries
- High reliability
- Robustness

- Low weight and smaller sizes
- Higher power to weight ratio

The major drawback for electric and plug-in hybrid electric vehicles is their range of travel. Vehicle with internal combustion engine (ICE) have no limiting range for travel whereas electric vehicles have maximum of 30-350 miles all electric range. Electric vehicles have lower specific energy which results in poor performance during initial acceleration compared to internal combustion engines. This means that the electric vehicles have lower initial acceleration as the batteries are restricted from performing sudden deep discharging cycles which degrade the battery life, and also the motor responds slowly to changes in acceleration. On the other hand, the internal combustion engines can provide power efficiently starting the vehicle from rest without degrading the life of engine. The types of batteries commercially available are given below

Table 3-2. Commercially available batteries

Battery	Sp. Energy (Wh/Kg)	Engy Density (Wh/L)	Sp. Power (W/Kg)
Lead Acid	30-40	60-70	180
NiCad	40-60	50-150	150
NiMH	60-120	140-300	250-1000
Li-Ion	100-265	250-730	250-340
Zinc-Air	470	270	100

The two main commercially available batteries are lead acid and Lithium ion batteries. Currently, there is extensive research conducted for using Nickel metal hydride batteries and Zinc Air batteries for driving commercially available electric vehicles. The batteries

are also used with fuel cells but there is no commercial application of fuel cell and battery hybrids. Two commonly used, lithium ion and lead acid batteries are compared in table below.

Table 3-3. Comparison for lithium ion and lead acid batteries

Property	Lithium Ion	Lead Acid
Nominal cell voltage	3.5 V	2 V
Amp-hour efficiency	~90-95%	~80%
Internal resistance	Very low	Extremely low
Operating temperature	Ambient	Ambient
Self-discharge	~10% per month	~2% every day
Number of life cycles	geater than 1000	Up to 800
Recharge time	2-3h	8h

3.3.1 Lithium Ion Batteries

The lithium ion battery is a member of the rechargeable battery family. In lithium ion batteries, the lithium ion moves from positive electrode to negative electrode during charging and moves from negative to positive electrode while discharging. The three primary components of the lithium ion batteries are the positive electrode, negative electrode and electrolyte. The negative electrode anode is made from carbon, positive electrode cathode is a lithium metal oxide and the electrolytic solution is the lithium salt in an organic solvent. The direction of the lithium ions change between anode and cathode based on the direction of the current flow and whether the battery is charging or discharging.



Figure 3.1. Typical initial Lithium ion battery pack

A typical lithium ion battery pack during its early formations is as shown in Figure 3.1. Lithium batteries first came into existence in 1970 by M.S. Whittingham, while he worked for Exxon (M.S, 1976). The major drawback with the lithium ion batteries is that lithium is highly explosive and there are safety issues working with lithium ion batteries. The present form of lithium ion batteries came into existence in 1985, by Akira Yoshino (Akira, 1985). He assembled lithium ion electrodes, lithium cobalt oxide and carbonaceous electrolyte. The performance of lithium ion batteries are best suited for applications like electric vehicle as the batteries are light weight and have high energy density.

3.3.2 Battery Modeling Technique

To model a particular type and application of the battery with R-C circuits, we must know the behavior of the battery. The performance of a battery is dependent on 30-40 variables. The model of battery generated is strictly for that specific battery. The models of batteries are used to understand the performance of the battery and its behavior which requires the knowledge of fundamental physics and chemistry. Parameters like temperature, voltage, resistance and current can be measured with greater accuracy. Based on these parameters we can model the performance of electric vehicle batteries using lesser complicated R-C circuits. The battery models generate accurate state of charge (SOC) and open circuit voltage (VOC) of the battery. If the battery SOC or VOC fall below a certain limit, their characteristics change permanently, this degrades their performance. The charging and discharging resistance of the batteries is of considerable importance as it is a critical performance determining factor. It can be calculated based on the type of the battery (Nazri, 2004). Electric vehicle battery model must account for self-discharging resistance and the operating temperature of the vehicle.

The model we consider for our research does not include self-discharge resistance as we do not simulate behavior of the model over a long term in standby mode in which case this resistance would be meaningful. Also, we do not account for the effect of temperature on the battery performance as we assume that the operating range of the temperature is small therefore, influence of temperature changes on the overall performance of the electric vehicle battery is small.

3.3.3 Battery Equivalent Circuit Representation

The crucial parts for electric vehicles are low power dissipation and maximum battery run time. An accurate circuit model can solve the problem of predicting and optimizing battery run time and circuit performance.

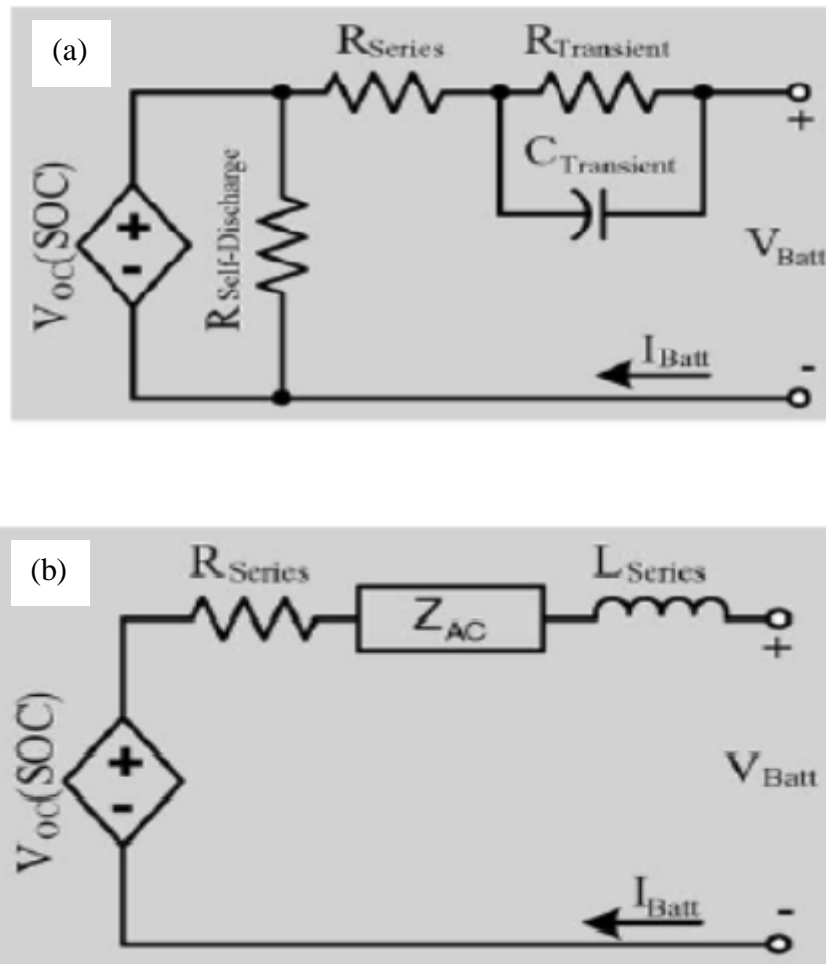


Figure 3.2. Battery model examples (a) Thevenin electrical model (b) Impedance based electrical model (Min Chen, 2006)

Battery circuit model must account for all dynamic characteristics of the non-linear open circuit voltage, current, temperature, cycle number and storage time dependent capacity to transient response.

The most basic form of battery equivalent R-C model is as shown in Figure 3.2(a). The battery consists of a series resistance and a parallel R-C connection to predict the open circuit voltage and SOC of the battery (Salameh Z.M., 1992) (Valvo M. Wicks F.E., 1996). The major drawback of the battery model is that it assumes open circuit voltage as constant and this assumption makes it impossible to predict steady state battery variation (M, 2000).

In Figure 3.2(b) an AC equivalent impedance model in the frequency domain is described. The authors then use an equivalent network (Z_{ac}) to fit the impedance spectra using electrochemical impedance spectroscopy. The drawback for this method is that it is difficult, complex and non-intuitive. Also, they only work for fixed SOC and temperature setting (Buller.S, 2003). Hence they have limitation to predict DC response or battery runtime.

Since, the battery models in Figure 3.2 have their limitation for calculating the state of charge and predicting the health of the batteries a new approach to model the battery is reviewed. The runtime based battery model shown in Figure 3.3 uses a complex circuit network and a DC voltage (S.C, 1993). A very high speed integrated circuit hardware description language (VHDL) is used to simulate a discrete-time implementation. They perform effectively to calculate the SOC of the battery in three stages i.e. the transient stage, the overall SOC estimation and the self-discharge resistance.

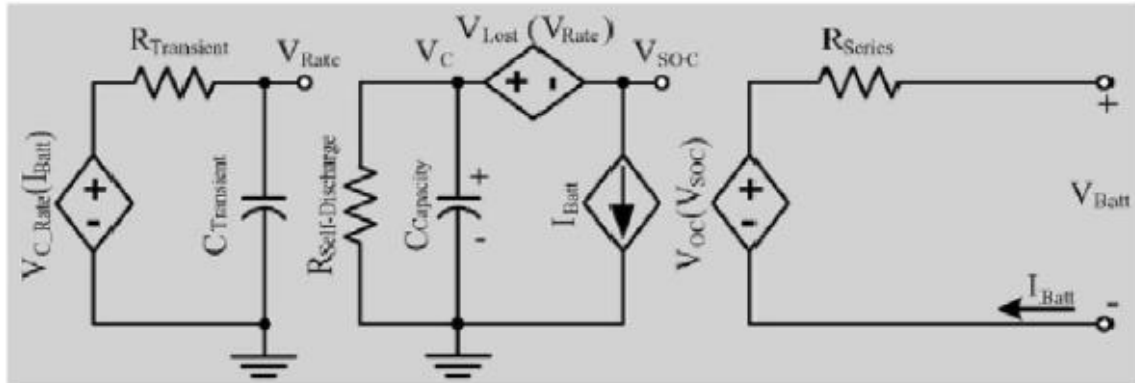


Figure 3.3. Runtime Based Electrical Battery Models (Min Chen, 2006)

The limitation of the estimation technique is that it cannot predict voltage response with varying loads and runtime voltage (Gold, 1997).

Since, the battery models in Figure 3.2 have their limitation for calculating the state of charge and predicting the health of the batteries a new approach to model the battery is reviewed. The runtime based battery model shown in Figure 3.3 uses a complex circuit network and a DC voltage (S.C, 1993). A very high speed integrated circuit hardware description language (VHDL) is used to simulate a discrete-time implementation. They perform effectively to calculate the SOC of the battery in three stages i.e. the transient stage, the overall SOC estimation and the self-discharge resistance. The limitation of the estimation technique is that it cannot predict voltage response with varying loads and runtime voltage (Gold, 1997).

In 2008, Vasebi et al developed an extended Kalman filter for estimating the SOC which uses a nonlinear estimating technique for accurate prediction performance of the SOC (Vasebi A, 2008).

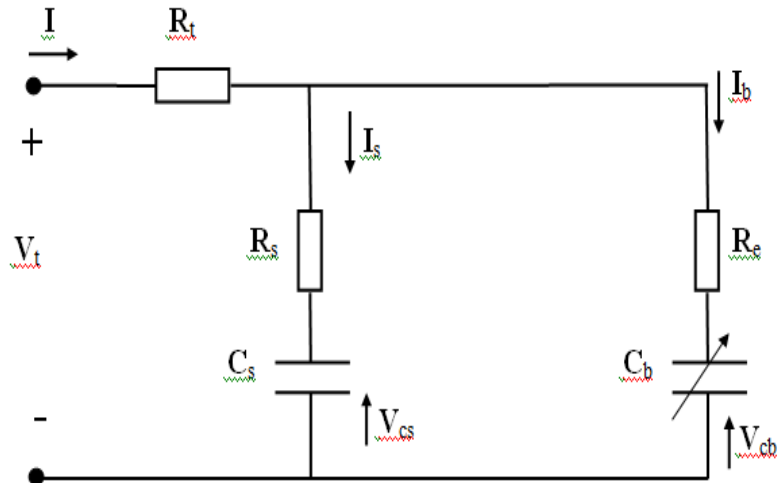


Figure 3.4. Non-Linear RC battery proposed for estimation of SOC (Vasebi A, 2008)

In this model we have 2 capacitors, surface and bulk, in series with the respective resistances which are parallel to each other. This combination is in series with the terminal resistance. The equivalent circuit model is used to estimate the dynamic performance of the battery. Battery open circuit voltage is estimated based on the variable loads of charging and discharging current.4

As shown in Figure 3.4, V_t is the terminal voltage or open circuit voltage, R_t , R_s and R_e are terminal resistance, surface resistance and bulk resistance respectively, C_s and C_b are surface capacitor and bulk capacitor respectively. In this battery model, the SOC is predicted from the voltage on the bulk capacitor. The value of the surface capacitor is constant. This type of RC model can be used for lithium ion as well lead acid batteries in conjunction with extended kalman filters (Vasebi A, 2008). The energy stored in bulk capacitor is determined by the open circuit voltage (OCV) and the initial parametric value

of surface capacitor is dependent on high frequency excitation. The time constant of the surface capacitor is given by the associated resistance and surface capacitance.

With extended kalman filters, even though the accuracy for measuring SOC increases but problems like SOC drift due to overcharging or ambient temperature fluctuations still persist. In 2009, to address this issue, Gould C.R. et al (C.R. Gould, 2009) proposed a remapped RC model to perform improved modeling capacities and accurately estimate the dynamic model parameters.

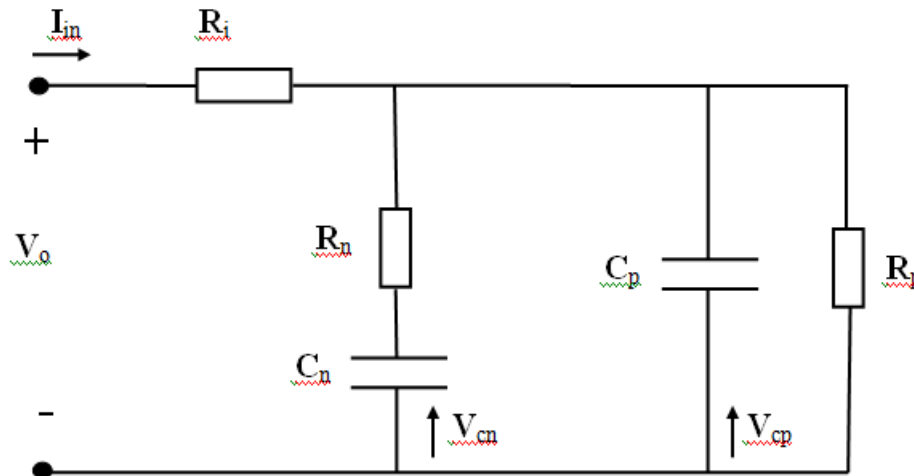


Figure 3.5. Remapped battery model (C.R. Gould, 2009)

For the remapped battery model shown in Figure 3.5, R_p is the self-discharge resistance which is very large compared to the overall resistance of the battery. C_n and R_n are capacitor and resistor in series in the model. The change in C_p over a considerable period of time will be the representation of the state of health (SoH) for the battery. R_i is the resistance of the battery terminals and inter-cell connections. C_p and R_p are capacitor and resistors in parallel.

This battery model has R_n and C_n are the surface resistance and capacitance which are in series. These series resistors and capacitors capture the dynamic behavior of the battery when the battery is in operating condition. The battery tends to drain when it is kept idle for long periods. This physical symptom is captured by the bulk resistor and capacitor in the battery model. Bulk resistance is connected in parallel to the bulk capacitor. The surface resistance and capacitance is connected in parallel to the bulk capacitance and resistance. The whole circuit is connected in series with the terminal resistance. This model is used to estimate the internal resistances with the sub-space state space estimation. The results from state space sub space identification are compared to sliding mode observer and Kalman filter. It is concluded that the state space sub space identification technique is more accurate and robust in identification of state parameters.

3.3.4 Battery Internal Resistance

The most important factor in modeling any type of batteries is the internal resistance of the cells/modules. The internal resistance is highly variable for each module in the battery pack. Internal resistance of the battery cells/modules varies with the temperature it is exposed during its operation. Also, it is observed that the battery performance deteriorates with increasing number of charging and discharging cycles.

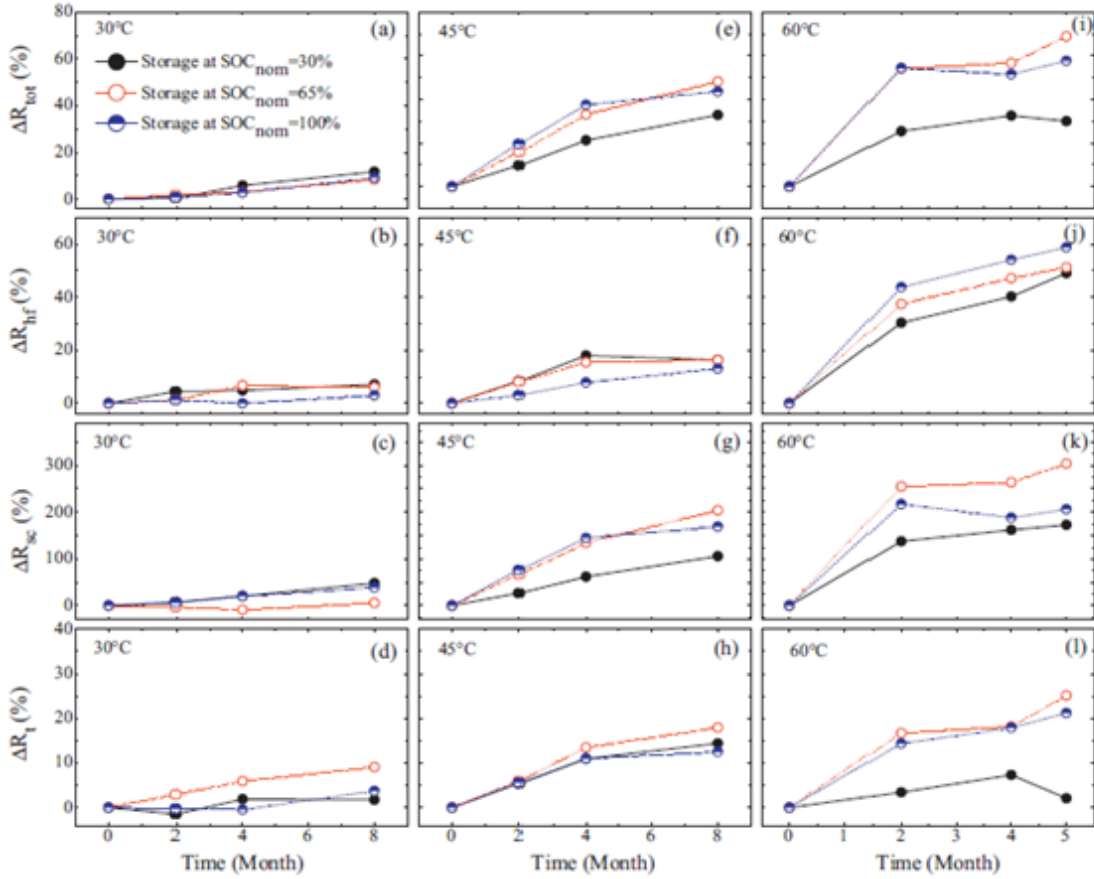


Figure 3.6. Total resistance R_{tot} , Ohmic resistance R_{hf} , Semicircle resistance R_c and Tail resistance R_t (M. Kassem, 2012)

In Figure 3.6, the change in resistance values are plotted with respect to the change in temperature for 0-8 months of battery life. The impedance spectrograph is not shown, but this resistance contributes to the impedance of the battery. In Figure 3.6 R_{hf} is the high frequency intercept with the real axis that is related to the electrolyte resistance and resistance from the external leads and connections, R_{sc} is the resistance related to the charge transfer kinetics and other interfacial contributions like passivating films, R_t is the tail resistance at low frequency featuring transport limitations in solid and liquid phases and R_{tot} is the cumulative resistance of the 3 resistances ($R_{hf} + R_{sc} + R_t$). We can clearly observe

that higher the operational temperature of the battery, higher is the value of internal resistance. This means that the battery performance is lower and degraded.

Kassem et al (M. Kassem, 2012) studied the effect of temperature on the battery chemistry. Similar, study was carried out to study the effect of temperature on the internal resistance of the battery in the circuit based model by Ecker et al (M. Ecker, 2012).

The circuit model of the battery is advantageous over the chemistry based model. A second order model is used to estimate the resistance of the lithium ion battery and the temperature effect on the battery. The temperature of the battery also affects the battery performance. To observe the change in internal resistance of the battery over its life span is given in the following explanation.

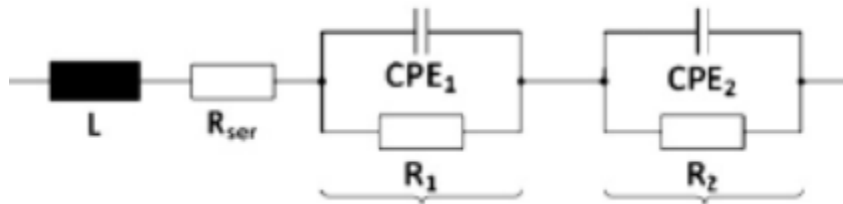


Figure 3.7. The electric circuit model of lithium ion battery (M. Ecker, 2012)

The resistances in Figure 3.7 are R_{ser} , R_1 and R_2 . The battery drain with no-load condition is represented by the resistor R_{ser} and L inductor. The capacitor CPE_1 and resistor R_1 model the behavior of the lithium ion battery under specific load. The parameter values for internal resistance R_2 and capacitor CPE_2 are very small so the change in this resistance affects the system performance minutely as compared to resistance R_1 .

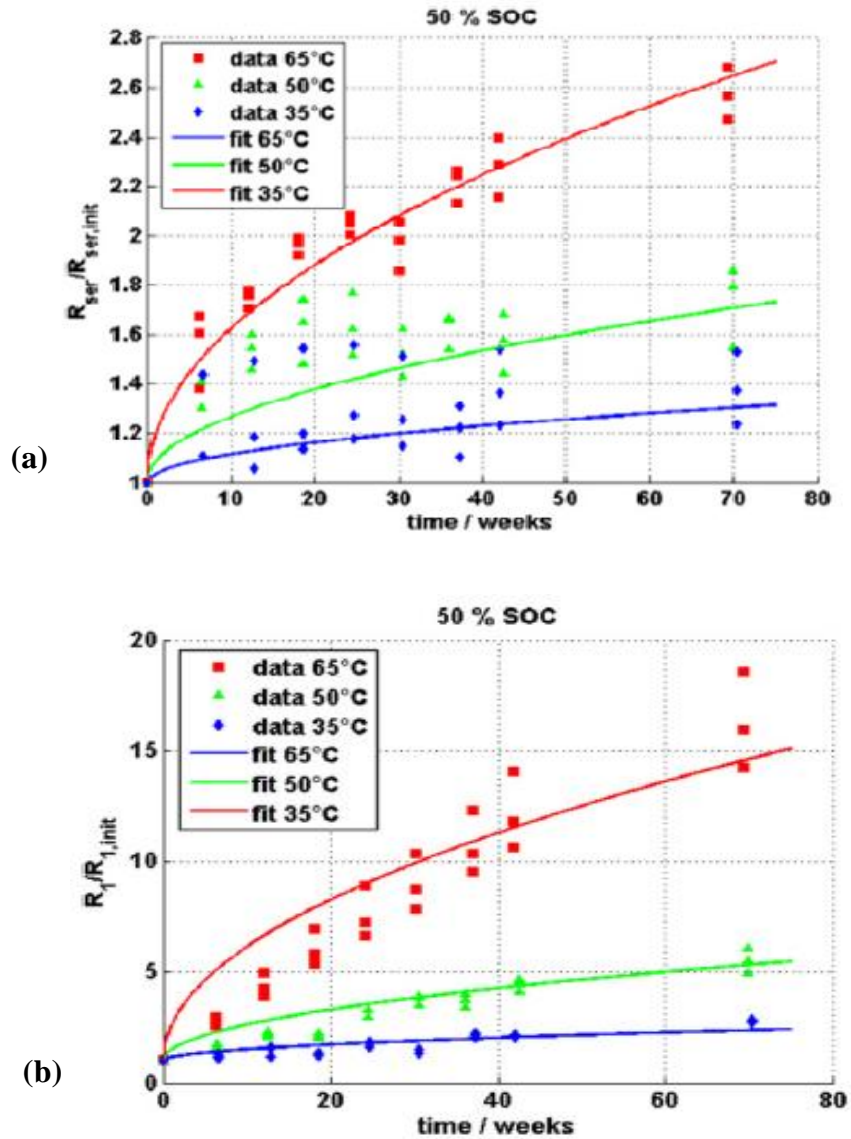


Figure 3.8. (a) & (b) Internal resistance with variation in temperature (M. Ecker, 2012)

The battery performance is also dependent on the operational temperature. In Figure 3.8, we observe the internal resistance of the batteries for a specific number of times in the week. These batteries are operated at three temperatures i.e. at 35°C, 50°C and 65°C. The internal resistance R_{ser} is almost 2-3 times its initial value and R_l increases to 5-15 times of its original value. Resistance R_l is affected by the dynamics of the battery in the operating

condition. Thus we conclude that there is a drastic change in the performance of each cell/module (Madeleine Ecker, 2012). There are various strategies suggested for charging which result in lower degradation of the battery and degradation costs of the battery (S. Bashash, 2011).

3.3.5 Battery Charging Strategies

The charging strategies are dependent on the infrastructure provided by the grid to charge the batteries. Also, it is greatly dependent on the output requirements. An overview of the charging infrastructure in a current single family-multifamily residential and commercial situation is given below.

Table 3-4. U.S. standard electric vehicle charging levels

	Voltage	Current	Power	Phase
Level-1	120	12	1.44	Single
Level-2	208/240	32	6.7/7.7	Single
Level-3	240	70	16.8	Three

The level 1 charging facility includes the single phase 120-V outlet which is most common in the United States. This is the three pronged grounded household outlet connection. The current receivers for these households are between 15 and 20 Amps. The charging time for a typical battery, depending on the battery size, is 3-20 hours. The level 1 charging can be applied to overnight charging.

The level 2 battery charging facility provides 208 to 240 V. This type is described as primary for private and standard for public charging facilities. A typical peak current would be 32 amps AC with a branch circuit breaker rated at 40 amps circuit breaker.

The level 3 charging reduces the charging time significantly. They are supposed to act as the gasoline charging stations. The charging current is 70 amps and the three-phase circuit voltage is 240 V.

The charging time required by electric vehicles depends on two factors, first the infrastructure used for charging and the second is the type and size of the battery. To schedule the charging and discharging strategies we require the knowledge of the charging time for batteries.

Table 3-5. Typical electric vehicle charging time

EV Configuration	Battery Size (kWh)	120 V	240 V	480 V
		12 Amps	32 Amps	100 Amps
PHEV-10	4	3h 5m	35m	n/a
PHEV-20	8	6h 10m	1h 10m	n/a
PHEV-30	16	12h 20m	2h 20m	63m
BEV	24	18h 30m	3h 30m	1h 34m
PHEV Bus	50	n/a	5h 50m	3h 17m

In the Table 3-5, we have PHEV-10 the power capacity is 830 W/kg and energy density is 100 Wh/kg. The cost estimate for the batteries are from \$200~\$300/kWh. There are many tradeoffs between the main categories of the batteries (Wencong S, 2012).

1. High power density (W/kg) is subject to higher voltage
2. High voltage reduces longevity
3. High voltage decreases safety of the battery
4. High voltage increases cost of the battery
5. Increasing energy density (Wh/kg) decreases power density (W/kg)

The two options with high power density and energy density are NiMh and Lithium Ion batteries.

3.3.6 Battery Equalization

A serious problem which affects battery performance is the variable voltage across each battery. Electric vehicle consists of more than 80-100 cells in each battery. The cells have varying internal properties which results in variation in the open circuit voltage. Since SOC is based on the open circuit voltage, if there are errors present in the open circuit voltage measurement, there will be errors in SOC measurements. Also, the battery performance is degraded if wrong measurements for SOC are considered for the battery. To avoid uneven performance of large group of batteries, they are forced to exhaust energy in the heat sink. This results in loss of energy and increases the cost of travelling and utilizing batteries.

The cell voltage imbalance in the series connected batteries is caused by the cell internal resistance, imbalanced state of charge between cell, degradation and the gradients of ambient temperature of the battery pack during charging and discharging. The imbalanced cell voltage causes overcharge or over-discharge and decrease the total storage capacity and total battery cycle life. Hence, equalization is very important to improve the battery life. There are two methods for equalization

- Passive Equalization
- Active Equalization

3.3.6.1 Passive Equalization

In this type of equalization the SOC of each cell/module are equalized based on their voltage difference. The cells/modules are charged to its maximum capacity and the variation in voltage for each cell/module is checked for all modules. The current is depleted from the higher energy module which is converted to heat energy before starting the driving cycle. Thus this operation is termed as passive equalization (Zhenli Zhang, 2013).

3.3.6.2 Active Balancing

In the process of active balancing, the batteries are closely monitored during their operation. The energy from higher energy cell is transferred to lower energy cell. This process saves energy dumped in the heat sink. To address the problem of variation of voltage in series connected cells for electric vehicles, many techniques have been developed. To make the equalization process implementable, cost effective and to keep the voltage and current stresses low, modular charge equalization process was developed by H. Park et al (Park H.S, 2009). In this technique, the battery pack is divided into many small modules and then intra-module equalizer and outer module equalizer are designed.

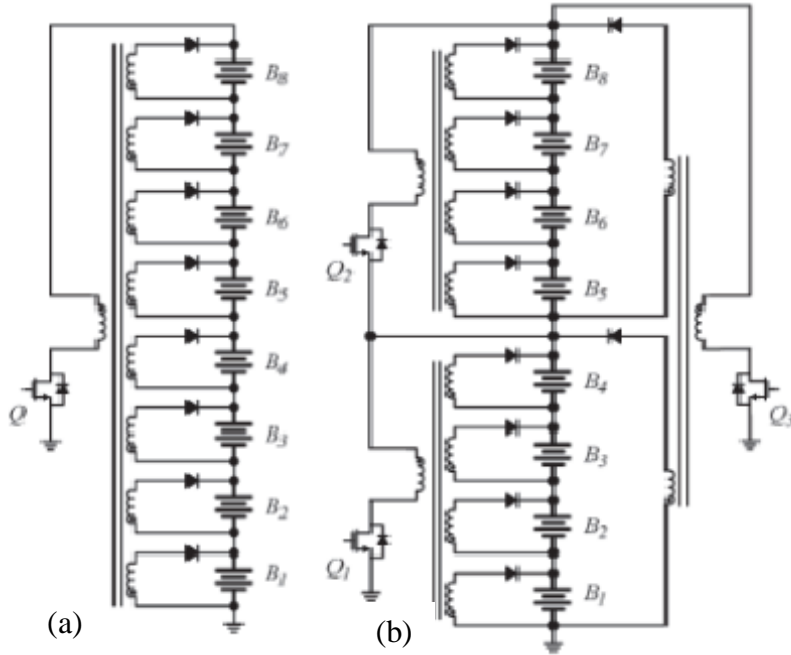


Figure 3.9. Multiwinding transformer (a) Conventional Approach (b) Modularized Approach (Park H.S, 2009)

A battery pack with series connected cells is shown in Figure 3.9 (a). The same battery pack with modularized design pattern is shown in Figure 3.9 (b). The battery pack is divided into maximum number of 8-10 cells per module, many modules in series form a battery pack. With the formation of modules, we overcome problem of mismatched inductance leakage. This inductance leakage is due to the self-inductance of the series connected inductance.

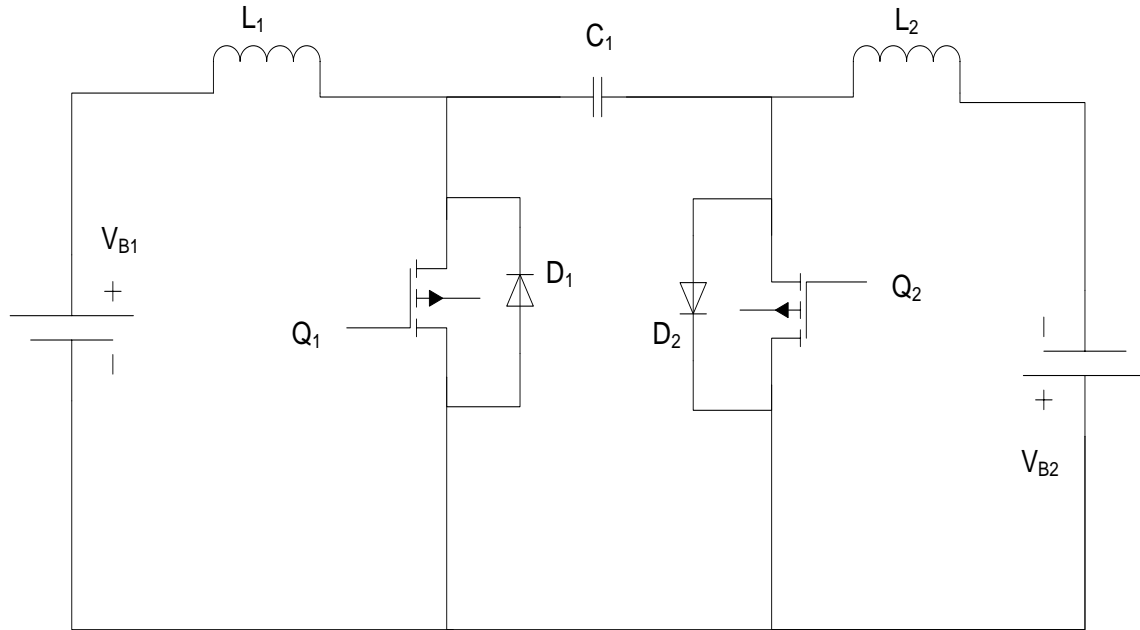


Figure 3.10. Battery Equalization Circuit (Cheng, 2005)

An active method of equalization is modeled by (Cheng, 2005) where energy is transferred from a higher energy module to lower energy module. The voltage equalization scheme by Lee and Cheng (Cheng, 2005) is explained in detail with a two module situation shown in Figure 3.10. The voltage of each module determines the direction of energy transfer between the two modules with proper operation of the MOSFET switches Q_1 and Q_2 . L_1 and L_2 are two uncoupled inductors, while C_1 is an energy transferring capacitor. V_{B1} and V_{B2} are battery voltages for modules (or cells) 1 and 2, respectively.

For normal condition, $V_{C1} = V_{B1} + V_{B2}$. The ideal condition is $V_{B1} = V_{B2}$, although this can seldom be the case in realistic operation. The operational scenario for a pulse width modulation (PWM) is shown below.

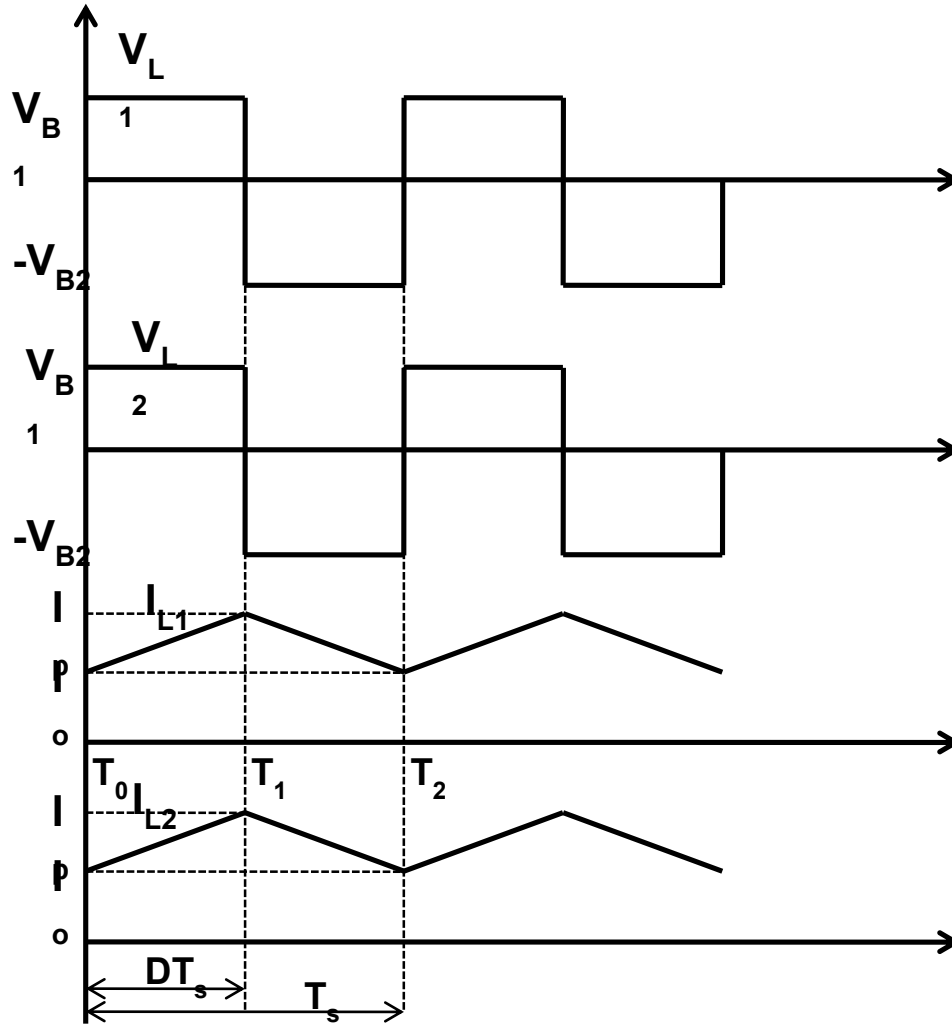


Figure 3.11. Typical switching waveform of the battery equalizer when $V_{B1} > V_{B2}$

(Cheng, 2005)

- 1) $V_{B1} > V_{B2}$: For duration DT_s , where D is the duty ratio of cycle time T_s . Q_1 is turned on, and capacitor C_1 transfers energy to V_{B2} during the same period inductor L_1 stores energy. For duration $(T_s - DT_s)$, Q_1 is turned off, D_2 turns on and the capacitor energy stores energy from V_{B1} and L_2 charges V_{B2} . In the switching duty cycle (T_s), as shown in Figure 3.11, $T_1 - T_0 = DT_s$, while $T_2 - T_1 = (T_s - DT_s)$. The operation can be described by the following equations.

a) For $t \in [T_0, T_1]$, Q_1 is turned on, which implies

$$V_{B1}(t) = L_1 \frac{di_{L1}(t)}{dt} \quad i_{L1}(T_0) = I_0 \quad (3.8)$$

$$V_{B2}(t) = -L_2 \frac{di_{L2}}{dt} + \frac{1}{C_1} \int_{T_0}^t i_{L2}(\tau) d\tau \quad i_{L2}(T_0) = I_0 \quad (3.9)$$

b) For $t \in [T_1, T_2]$, Q_1 is turned off and Q_2 is turned on, which implies

$$V_{B1}(t) = L_1 \frac{di_{L2}(t)}{dt} + \frac{1}{C_1} \int_{T_1}^{T_2} i_{L1}(\tau) d\tau \quad i_{L1}(T_1) = I_p \quad (3.10)$$

$$V_{B2}(t) = -L_2 \frac{di_{L2}(t)}{dt} \quad i_{L2}(T_2) = I_p \quad (3.11)$$

Equations (3.8) through (3.11) describe the voltages V_{B1} and V_{B2} dynamics during one duty cycle of PWM operation. “ D ” is the duty ratio of the switching cycle. I_p is the peak current during the operation cycle DT_s . The currents in the inductors I_{L1} and I_{L2} are given by

$$I_{L1} = \left[\frac{1}{2} \left(\frac{V_{B1}}{L_1} D^2 + \frac{V_{c1} - V_{B1}}{L_1} (1 - D)^2 \right) \right] T_s \quad (3.12)$$

$$I_{L2} = \left[\frac{1}{2} \left(\frac{V_{c1} - V_{B2}}{L_2} D^2 + \frac{V_{B2}}{L_2} (1 - D)^2 \right) \right] T_s \quad (3.13)$$

By varying the switching frequency, the equalization scheme can be implemented in continuous current or discontinuous inductor current mode. During the equalization process, the weak cell is charged by a strong cell to balance the energy level of both the cells. In our study, battery 1 is at higher energy level than battery 2.

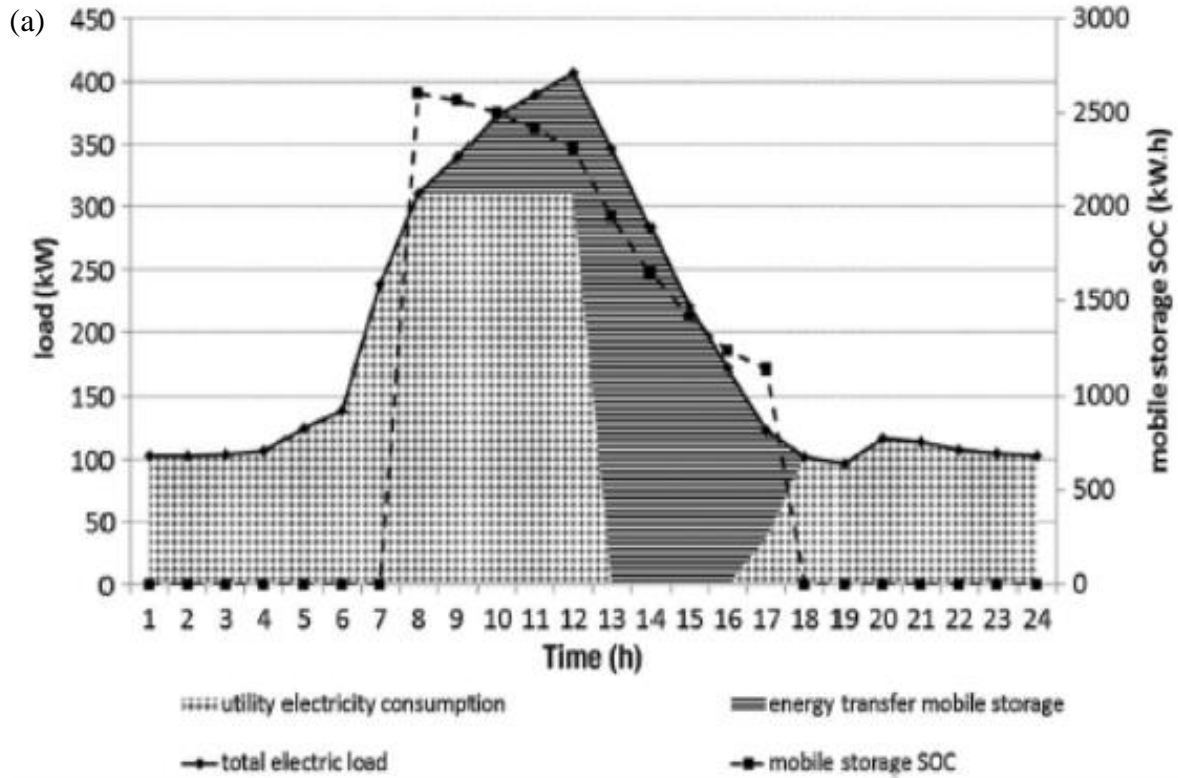
2) $V_{B1} < V_{B2}$: The operation is controlled by the switching Q_2 and D_1 in similar fashion as case 1, and similar equations would apply.

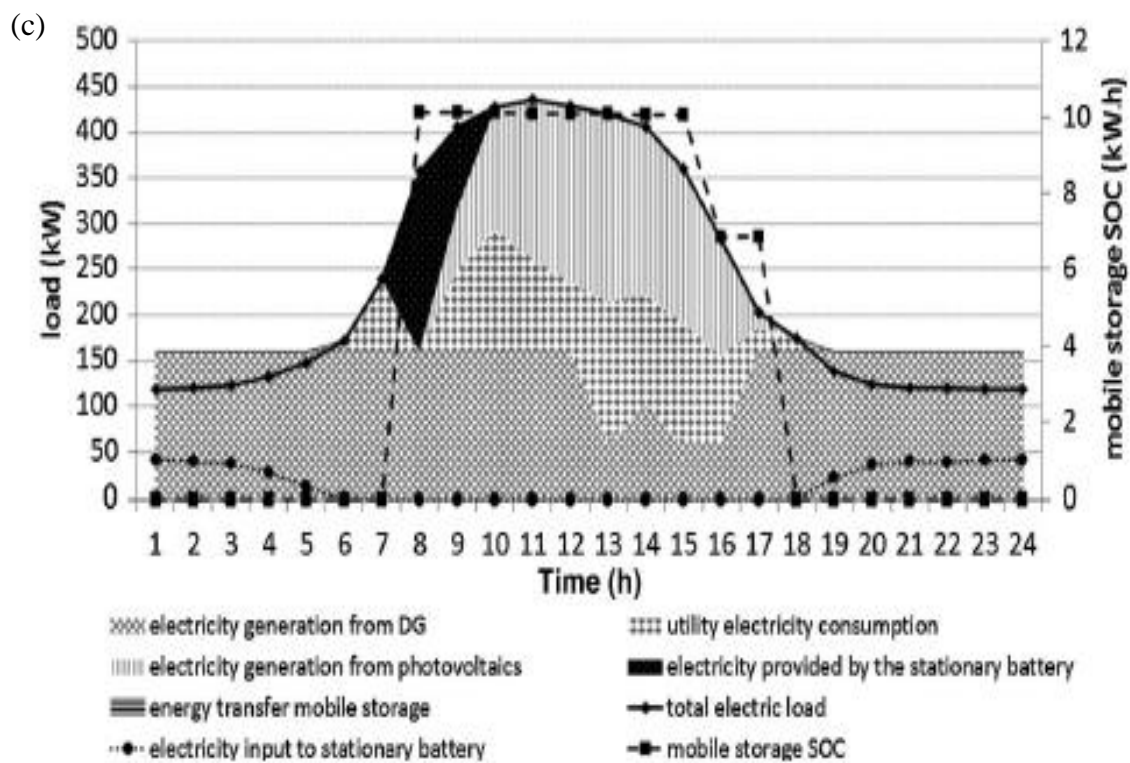
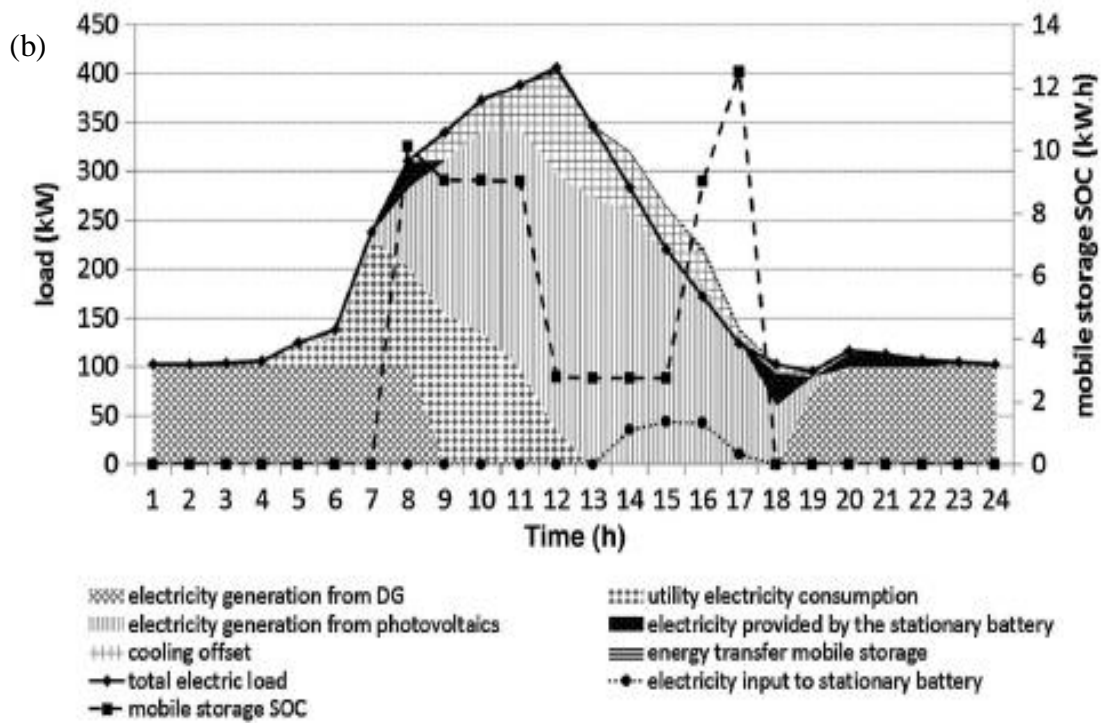
3.4 Smart Grid

The success of implementing hybrids into the market largely depends on the infrastructure of charging the vehicles from the grid (J.G.Lozano, 2012). To build a strong grid network, renewable energy sources like wind energy, solar energy, batteries etc are used along with the conventional sources of energy. Continuous effort is made to lower the cost of energy generation to support the grid (A.Y. Saber, 2012). This has led to novel concepts of smart grid where there could be energy exchange from the grid to the end user and from the end user to the grid (P.Finn, 2012) (A.S. Masoum, 2011). It is possible not only to predict the load and price of the energy for the next day, but also the source of power during a specific time of the day. This concept could be very beneficial for setting up the charging algorithms for electric vehicles (G.Gross, 2009).

The concept of smart grid has motivated researchers to optimize the cost of operation of the grid and its maintenance. The cost of producing and supplying electricity from various sources is minimized using the available renewable and non-renewable sources of energy and the nature of load which is applied on the grid. The load on the grid is time dependent, so does the cost of energy which varies with time, season and many other factors (J. Kiviluoma, 2011). It is widely known, that the load on the grid falls during nights, which brings down the price of electricity whereas the load during the day time increases, this increases the unit price to its maximum values (K.C.Nyns, 2010).

The following study will help us better understand the performance of the smart grid systems (M. Stadler, 2012).





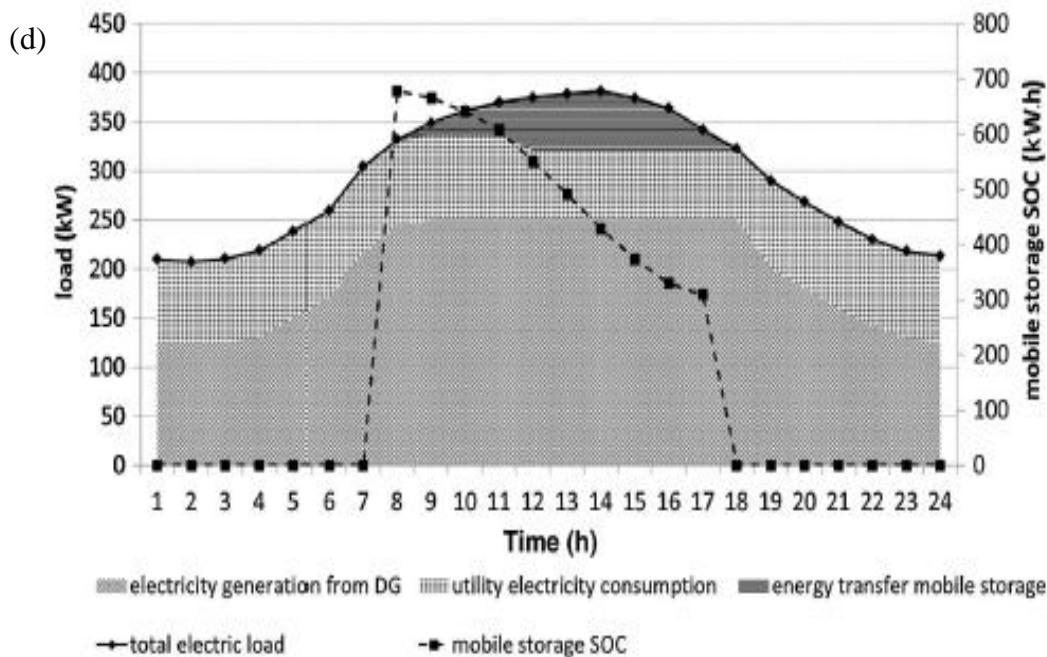


Figure 3.12. a) Diurnal electric pattern on July workday for large school in San Francisco
 b) Diurnal electric pattern for S2 on January workday for large school in San Francisco c)
 Diurnal electric pattern for point S3 on a January workday for large school in San Francisco
 d) Diurnal electric pattern on a July workday for minimal costs for healthcare facility. (M. Stadler, 2012)

In Figure 3.12 A, diurnal grid load in the month of July by a large school in San Francisco is observed. Also, nodes S2 and S3 are observed for the month of January. Nodes are the points of reference used to account of load on the grid and price of the energy on the grid. The seasonal variation is also studied by observing the load in July and January workday at the school. Also, to cover a range of load on electric grid, large schools and health care facilities are studied.

We can clearly observe the daily load during the specific months and specific area. The power requirement during the 24 hour span is known which is supported by the sources like diesel generator, stationary batteries, mobile batteries, photovoltaic cells etc. It is to be noted that the load from 6:00 pm to 6:00 am is low compared to the load during the day time.

To study the behavior of the grid systems we need to know the load on the grid. Typical load on the grid in California is given as below (Christophe Guille, 2009).

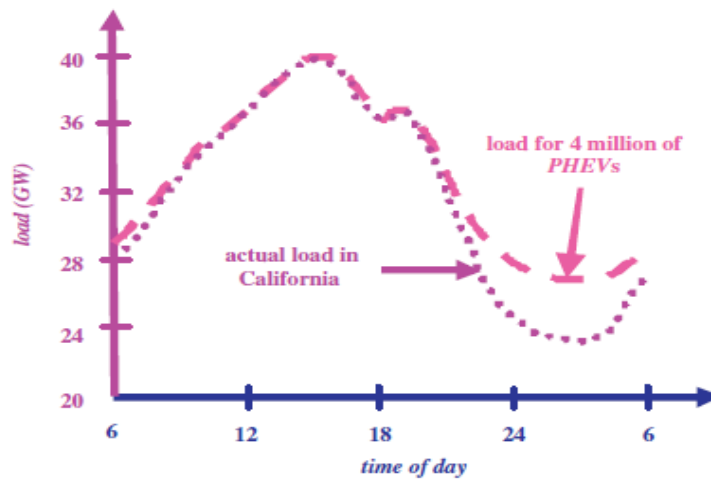


Figure 3.13. California daily load with PHEV and without PHEV load (Christophe Guille, 2009)

In Figure 3.13 we observe that the load on grid rises from 6:00 am 6:00 pm and then decreases from 6:00 pm. The lowest load is during the nights. This indicates that the best time to charge vehicles to balance the grid load is during the nights.

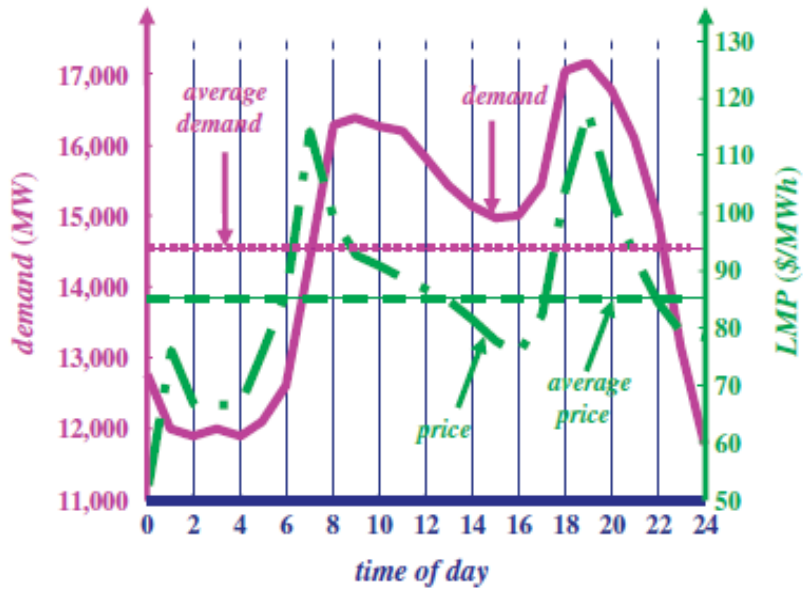


Figure 3.14. Load and price for a day in winter (Christophe Guille, 2009)

The demand and price graph in Figure 3.14 distinctly denote that charging the electric vehicles from 12:00am to 6:00 am would benefit the user charging the electric vehicles. It can be observed that the demand and price of the grid during the night is significantly smaller than the average demand and price.

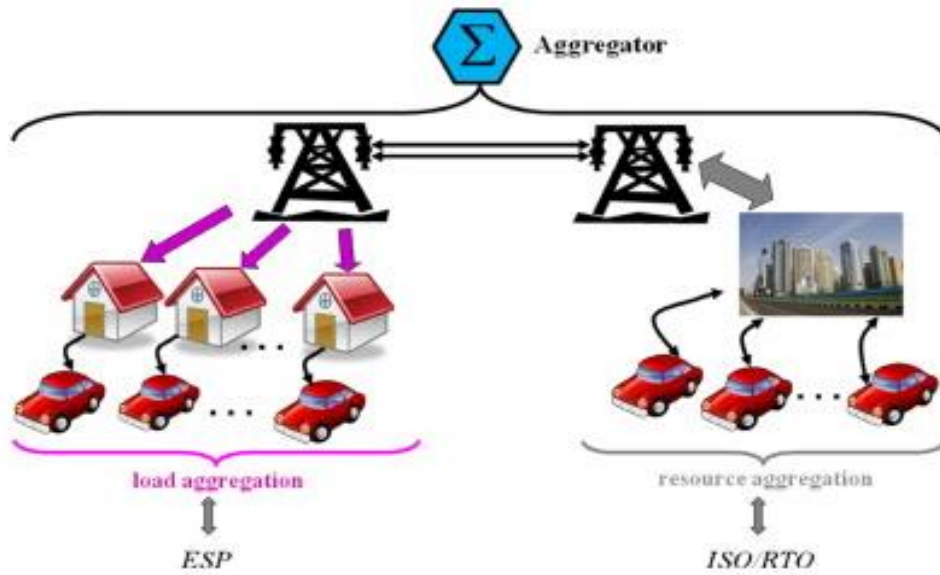


Figure 3.15. Battery vehicle as controlled load and storage (Christophe Guille, 2009)

The batteries can be charged at home from the grid as shown in Figure 3.15. The batteries are a source of energy to the grid when they are connected in a group. The aggregator can act as intermediary between the grid and the battery vehicle owners.

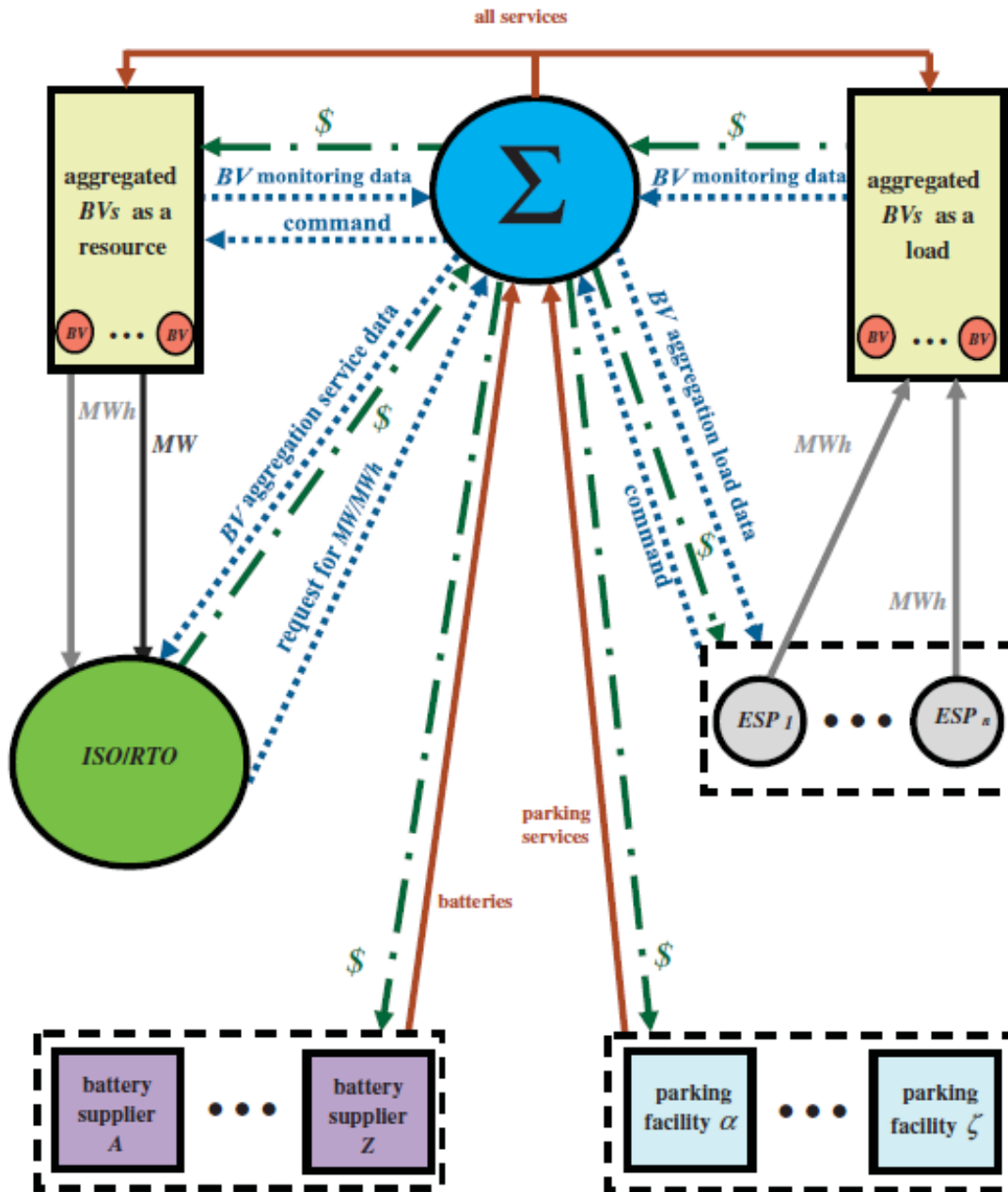


Figure 3.16. The vehicle to grid implementation framework (Christophe Guille, 2009)

In Figure 3.16, we see the network for energy flow to the electric vehicle batteries in various scenarios. The batteries can be charged at home or at charging stations. They can

be used as energy resource to the grid at work places, public parking spots or charging stations.

Electric and plug-in hybrid vehicles use large battery packs, containing batteries in series and parallel arrangement to obtain required battery configuration. Electric vehicles can now-a-days travel more than 100 miles with one complete charging cycle which is significantly more than daily commuting distance from home to office and back home. This allows us to look at the electric vehicles as the potential supplier of energy to the grid.

Increase in the number of electric vehicles in the market will compel the grid to support the additional load. The charging time for electric vehicles is mostly during the nights. The grids have lower loads during nights as compared during the day. Also, the price of electricity during the night is low which helps to minimize the charging cost (H. Khayyam, 2012) . Hence, the grid load and electricity price could be regulated.

The batteries have independent cell/module properties because of their manufacturing process and variability in the processes they undergo (M. Ecker, 2012). Also, they degrade and respond independently to different conditions to which they are exposed. Batteries deteriorate with age and their performance drops down significantly (Benedikt Lutz, 2012). The knowledge of the trip to be travelled, the age of the battery and the time required for charging will help us identify the amount of energy available with any vehicle selected at random. This helps to determine the amount of energy that is available from the batteries that can be exchanged with the grid.

3.4.1 Smart Grid Optimization

In the smart grid scenario, optimizing the performance of charging and discharging the electric vehicles is of prime importance. Sustainable ground transportation is highly dependent on electric vehicles and renewable power sources. The charging process for electric vehicles is controllable. This is advantageous as we can interrupt the charging process and lower the cost of charging and also shift the load on the grid. Charging electric vehicles and power exchange from vehicle to grid can be coordinated to reduce the cost of trip travelled. This will also result in reduced carbon dioxide emissions (Changsun Ahn, 2011).

We should not waste the energy available on the grid and also the energy stored on the batteries. A study has been performed to plan the optimum location of the charging stations with respect to the traffic. In this study, the multi-objective optimization was performed to maximize the profit implementing the electric vehicles in the system. The authors have specified the optimal electric vehicle charging stations, sizing and locations (Guibin Wang, 2013). They have also worked on minimizing the power losses, voltage deviations and also the electric vehicle traveling distance.

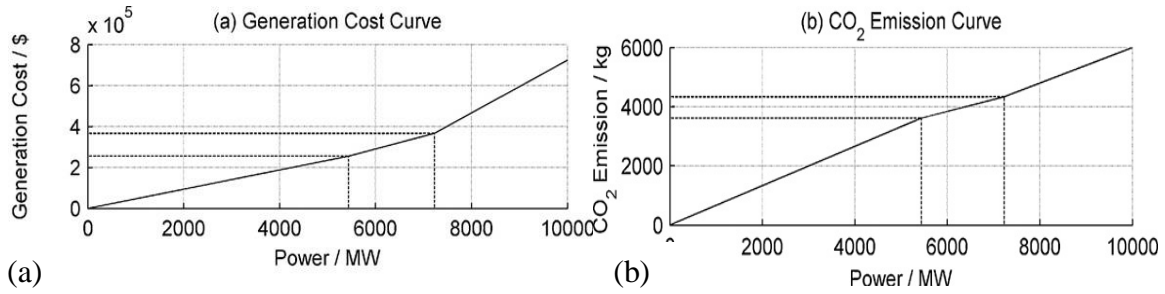


Figure 3.17. (a) Power generation cost curve (b) CO₂ emission curve (Changsun Ahn, 2011)

The price of energy on grid and CO₂ emissions cost are given in

Figure 3.17. These are predominant costs to be considered during the smart grid operation.

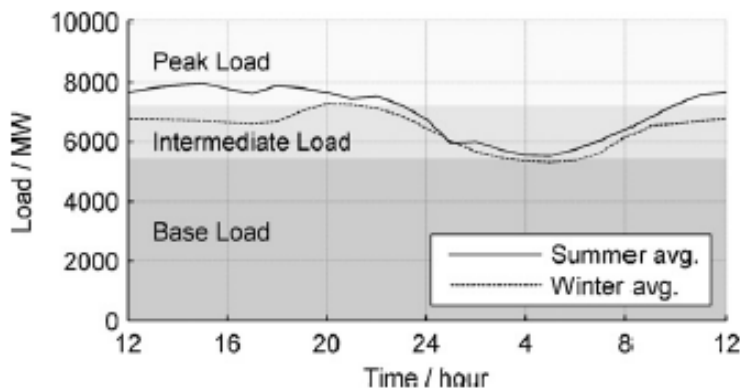


Figure 3.18. Average Non-EV power demand in DTE service area (Changsun Ahn, 2011)

In Figure 3.18 we see the variation in average load during summer and winter. It can be observed that there is a considerable amount of energy difference between the base load and peak load. There is also seasonal variation in the grid load and variation with the geographical locations.

Control over the load on the grid and ability to exchange extra energy available on the electric vehicle can minimize the cost of operation of the grid. It also proves beneficial to the electric vehicle owners. Hence, the overall solution is cost effective.

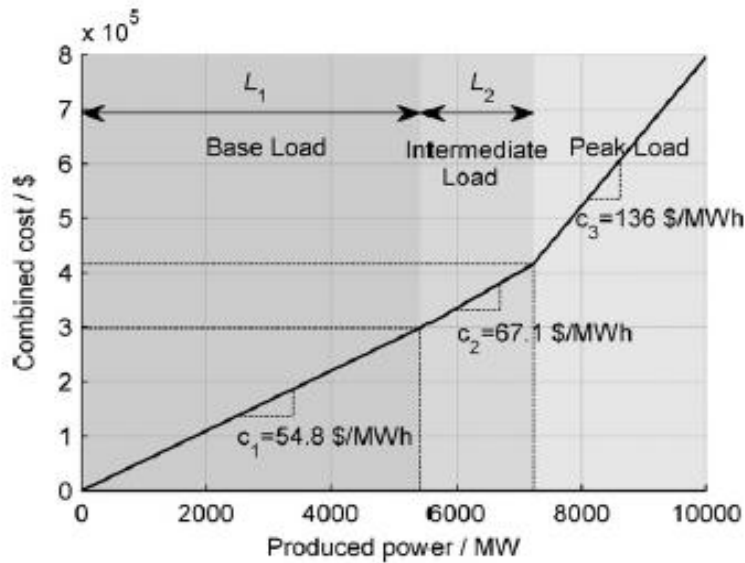


Figure 3.19. Generation cost and CO₂ emission, the carbon tax of \$12/t CO₂ is used.

(Changsun Ahn, 2011)

The cost curve in Figure 3.19 is used to optimize the cost of charging electric vehicles with the linear programming techniques. In this technique, Ahn et al (Changsun Ahn, 2011) control the load on the grid with the electric vehicle charging at lower loads on the grid. Also, the electric vehicles are used to support the load on the grid. Thus the authors use forecasting based load profile, estimated number of plugged vehicles, estimated plug off time and battery SOC of vehicle being charged to optimize the operation of electric vehicles.

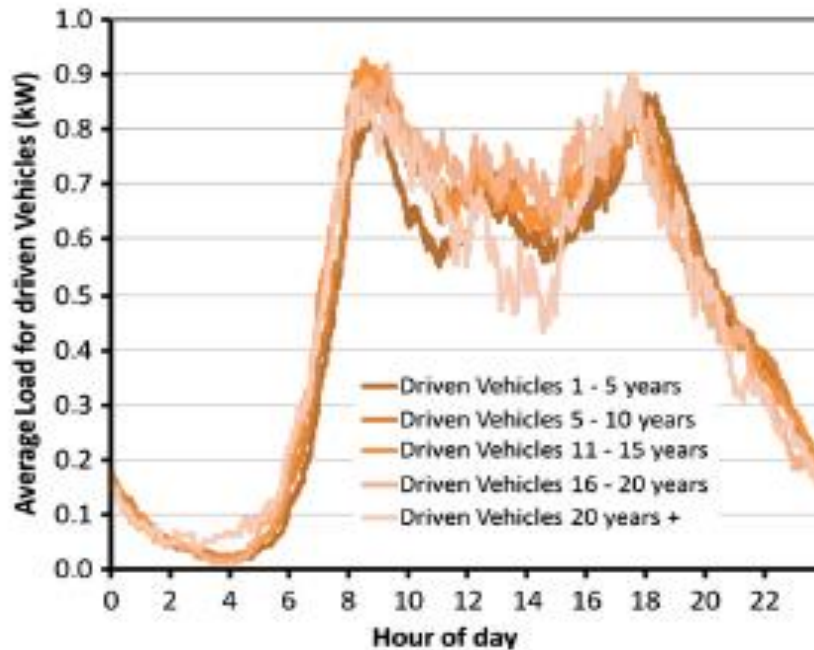


Figure 3.20. PHEV load sensitivity to vehicle age (Changsun Ahn, 2011)

The average driving performance should be considered for optimizing the performance of the electric vehicles. C. Ahn et al have observed in their research study that in the first 20 years, the vehicle is driven on an average of 14000 miles per year and after 20 years it is driven less than 6000 miles. This clearly indicates the driven load classified based on the age of the battery. In Figure 3.20, we observe the electric energy used by electric vehicles over the span of 20 years. The hourly energy spent by the electric vehicles peaks at 8:00 am and 6:00 pm i.e. while going to office and coming back home from the office.

It is also suggested that the average earnings from supporting the grid with electric vehicles is approximately US \$140-\$250 per year over the battery life of the battery. If the battery degradation cost is considered in the operation cost of the electric vehicles (~\$5000 for 16 KWh battery) then the amount earned is approximately US \$10-\$120.

In summary, we can conclude that the batteries can be charged during the off peak hours and if we know the amount of time required for charging the batteries we can minimize the cost for charging the batteries. Finn et al (P. Finn, 2012) conducted the research to optimize the charging time.

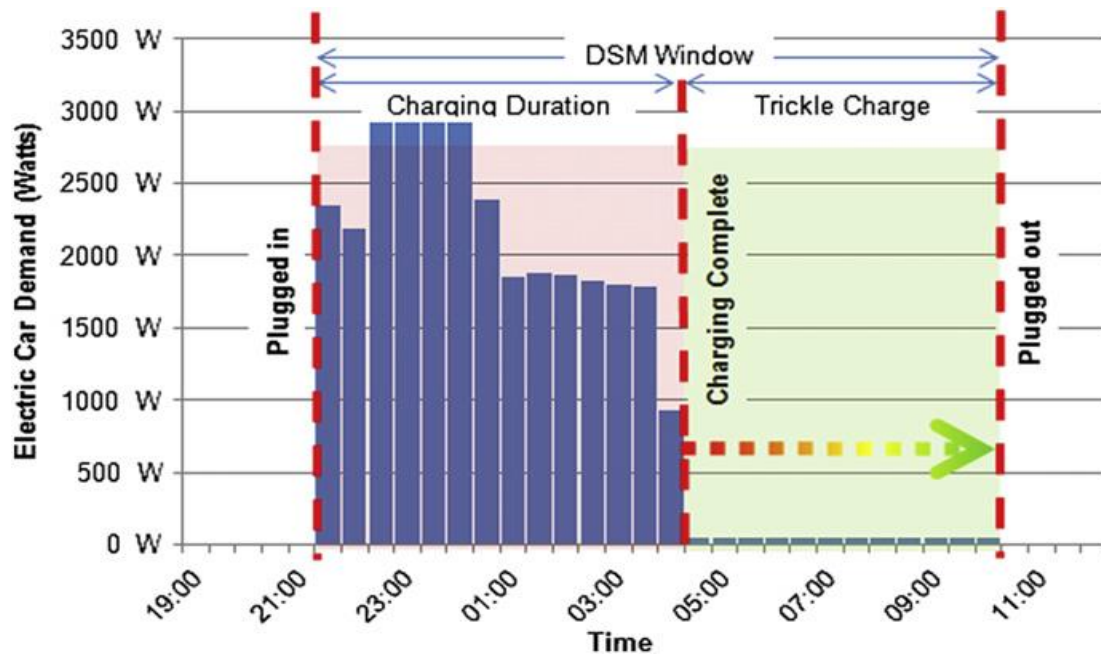


Figure 3.21. Electric car load profile (P. Finn, 2012)

A new battery usually is charged within 4-5 hours depending on the size of the battery as shown in Figure 3.21. Typically a 16 kWh battery is charged in 4-5 hours (P. Finn, 2012). It is to the advantage to both the user and the grid to charge the battery at night during the off peak hours.

3.5 Summary

In this chapter we reviewed modeling techniques of electric vehicle. Battery models are also studied in this chapter. The circuit models are studied to estimate the performance of

the battery during the driving cycle. Voltage based equalization process is discussed in brief to overcome the problem of variable energy batteries in a battery pack. Various parameter estimation techniques from the literature are discussed. These are required to estimate the internal resistance of the lithium ion batteries.

In this chapter, literature on smart grid systems is also reviewed. The price variation of energy on the grid caused by seasonal changes and variation in the energy requirements from the grid during the day is discussed. Techniques to optimize the resources for the grid and the grid load are mentioned. Charging scenarios like charging the batteries at home or at the battery charging stations are discussed in this chapter.

4 Battery Health and Internal Resistance

In this chapter we will study the methods to determine the health of the batteries and the impact of internal resistance on a battery's health. The relationship between the internal resistance and the performance of the batteries will help us evaluate the battery health.

4.1 Battery Health

Simulating a practical driving situation demands modeling of the parts required for driving the electric vehicle. The major part of the electric vehicle simulation is the battery model and parameters of the battery. The battery model will predict the performance of a real life battery under actual driving conditions. We have access to open circuit voltage, current, internal resistance and SOC remaining on the battery pack. This gives the driver an idea of electric range of the battery.

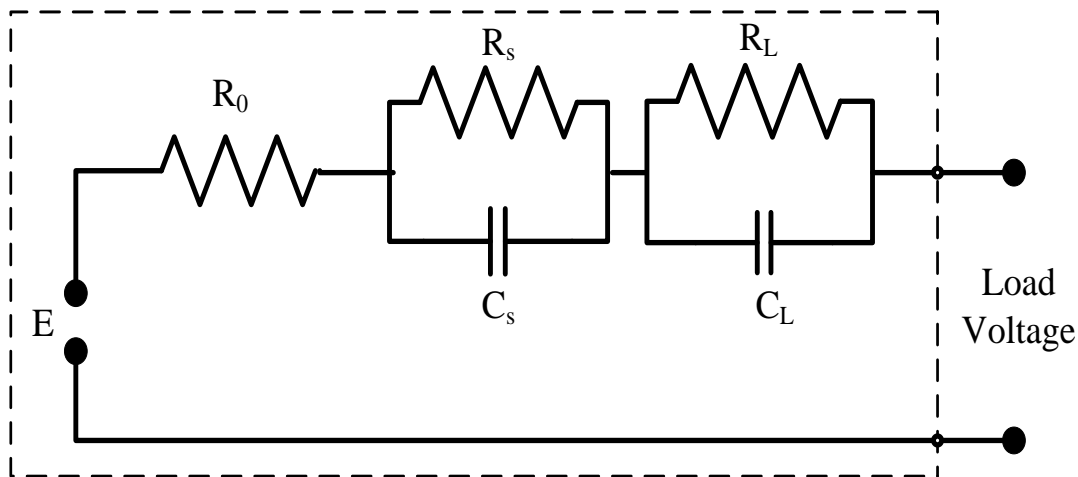


Figure 4.1. The battery equivalent circuit model

An equivalent circuit model of the battery is adopted to identify the internal resistance of the battery. The internal resistance of the battery is used to estimate the performance of the

electric vehicle battery. The advantage of the lithium ion battery circuit model is that it can be used to estimate real time data which is the purpose of our research. In Figure 4.1, the R-C model of the battery is given where C_S and C_L are surface capacitance and bulk capacitance, respectively. R_S , R_L and R_0 are surface resistance, bulk resistance and series resistance, respectively. In general, R_0 and R_S are much smaller than bulk resistance R_L . Similarly, surface capacitance C_S is much smaller than bulk capacitance C_L .

4.1.1 Battery SOC Calibration

Knowledge of the state of charge of a battery in a real-time traffic situation is very important. It is this capacity that determines the range of an electric vehicle. State of charge is also called the “fuel gauge” since it serves a function similar to a fuel gauge in a conventional car. SOC is defined in percentages and the techniques to determine the capacity are very crucial, as battery performances are unpredictable to a large extent and is dependent on many parameter and is difficult to predict accurately.

SOC is defined as the ratio of the electric charge $Q(t)$ which can be delivered by the battery at any instance of time to the nominal capacity of the battery Q_o . Mathematically, the state of charge is given as below

$$SOC(t) = \frac{Q(t)}{Q_o} \quad (4.1)$$

The charge remaining on the battery varies with time and various environmental factors. Also, the aging of the battery should be taken into consideration. The following techniques are used to estimate SOC

1. Specific gravity measurements of chemicals of the battery
2. Internal Impedance of the battery
3. Coulomb counting (current measurement)
4. Open circuit voltage

The deterministic techniques mentioned above can estimate the SOC accurately based on the application. The most efficient and accurate techniques for estimating SOC for electric vehicles are based on open circuit voltage and coulomb counting. Coulomb counting can be used for estimating SOC for a short period of time like during a day or over a span of few months (V Pop, 2008). Open circuit voltage of the battery is an accurate measure for the health of the battery, so the variation of the SOC with the age of the battery is accounted in the open circuit voltage. Thus, we use SOC measurement based on open circuit voltage throughout the life of the battery.

An electric vehicle is driven for a specific driving trip. Changes in the battery of electric vehicle throughout its life are not considered. Coulomb counting an efficient method for estimating the SOC for the vehicle is adopted. Current leaving the battery is positive current, ie when the electric vehicle is driven by the battery. Also it is assumed the current entering the vehicle is negative, i.e. the current when the motor acts as the generator and the battery is charged. The SOC is then calculated depending on the current transfer from the battery every second. The SOC for an electric vehicle under driving condition is given by (S. Bashash, 2011)

$$SOC(k+1) = SOC(k) - \frac{V_{oc} - \sqrt{V_{oc}^2 - 4(R_{eq}) \cdot T_m \cdot \omega_m \cdot \eta_m^{-\text{sgn}(T_m)}}}{2(R_{eq}) \cdot Q_b} \quad (4.2)$$

where,

V_{oc} = Total open circuit Voltage of the battery (Volts)

T_m = Electric motor torque (N.m)

ω_m = Electric motor speed (rad/sec)

η_m = Electric motor efficiency

R_{eq} = Equivalent Internal resistance of the battery (ohms)

Q_b = Battery capacity (Ah)

SOC (k) is the state of charge at the k-th step

Hence, the state of charge of onboard electric vehicle batteries is estimated. This technique to estimate the state of charge will be useful to find the state of charge of the batteries during equalization. The battery state of charge will help to estimate the internal resistance during the specific trip.

4.2 Driving Cycle

We require motor speed and motor torque to study the simulation behavior of the battery. We start the trip at 124 West Freistadt Road in Thiensville, while the destination is 3200 North Cramer Street in Milwaukee. This is a representative of an ideal driving cycle which consists of highways, city roads, stop signs as well as city traffic lights. Since this trip simulates a typical commute for an EV user we have decided to use this driving cycle for our simulations.



Figure 4.2. Route map of the sample trip

The time for driving trip was ~1614sec. The maximum torque during driving is ~140Nm while the maximum torque during braking or negative torque is ~160N.m. The trip includes constant driving speed cycles, constant acceleration cycles and constant deceleration

cycles. This trip includes driving on the city roads as well as on the freeways. It also includes stops at the lights.

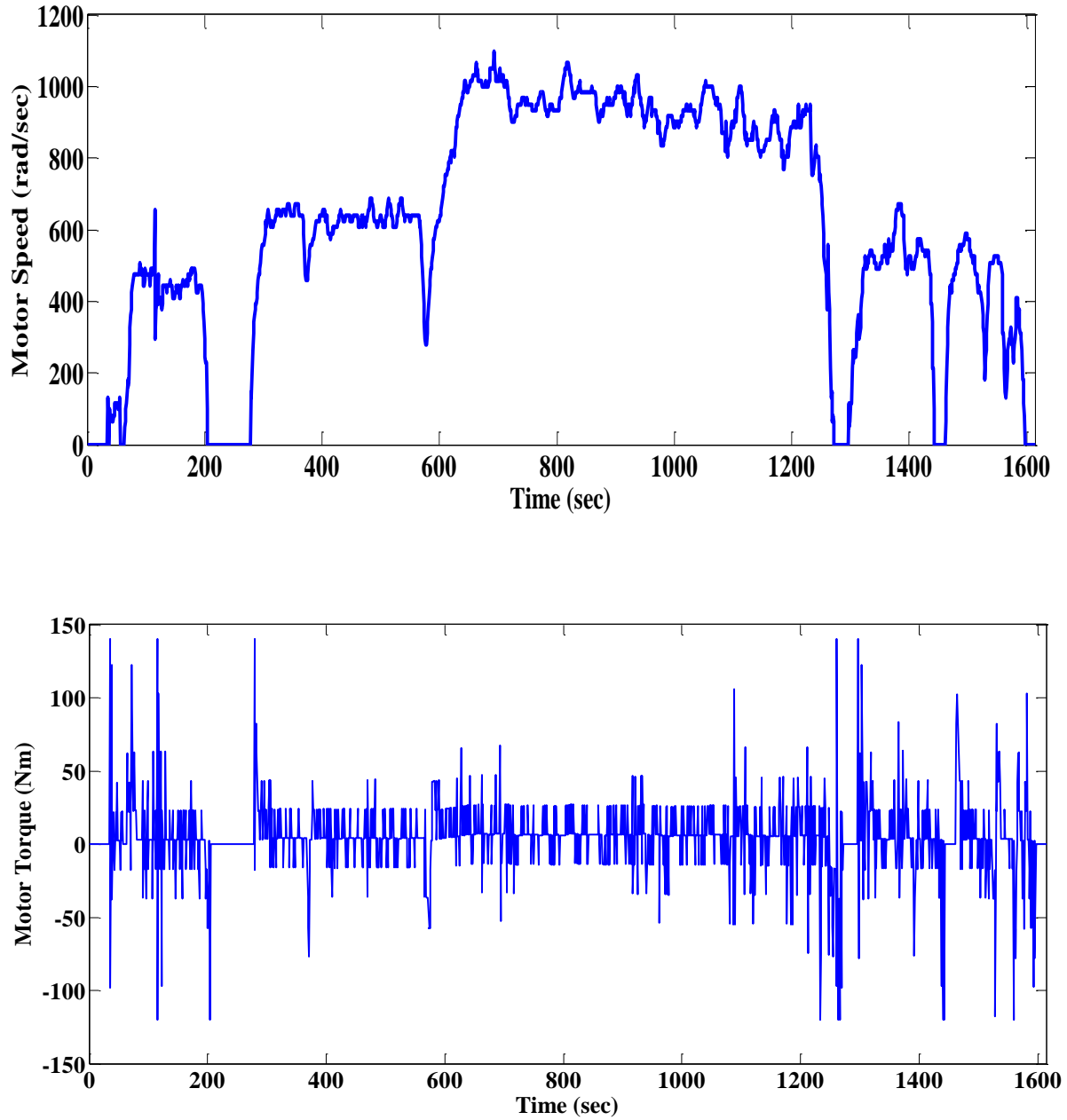


Figure 4.3. (a) Motor speed during driving, (b) Motor torque profile during driving

The following driving speed and torque is used as input to the electric vehicle. The current limits on the battery side were set from -250A to 250A.

4.3 Battery Equalization

The equalization circuit was discussed. The equalization load is applied with the motor load during the operation of electric vehicle.

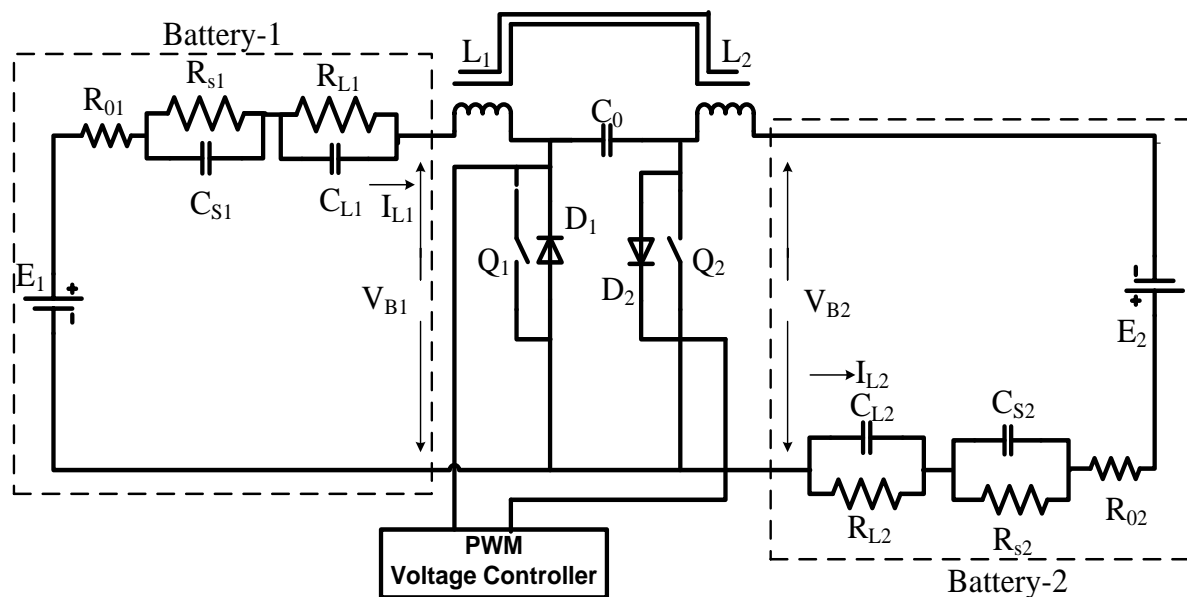


Figure 4.4. Battery with equalization circuit

In Figure 4.4, the whole battery circuit is sectioned in 3 parts, Battery-1, Battery-2 and the equalization circuit. The equalization circuit connects Battery-1 and Battery-2. The pulse width modulation controls the state of charge of the batteries. Each battery circuit has surface capacitor and resistor, bulk capacitor and resistor and a series resistor.

Battery-1 and Battery-2 are connected with the power electronic circuit as shown in Figure 4.4. Battery-1 and Battery-2 together supply power to drive the torque and speed on the electric motor. Also, energy is transferred from Battery-1 to Battery-2 or Battery-2 to Battery-1 to equalize the voltage of the whole battery pack as per the health of the battery. Cases with two modules and three modules are studied.

4.4 Worthiness of Replacement

The concept of worthiness of replacement (WOR) is applied to the battery pack after the battery is equalized and the trip is complete. As mentioned earlier, though equalization is unavoidable, but WOR projects the exact loss of energy in the trip. This analysis would be the decision making factor for projection of completion of the trip as the onboard energy is calculated. The WOR is defined as

$$WOR = \left[\frac{SOC \text{ Change of Current Battery Pack}}{Battery \text{ Pack SOC Change with Certain Module(s) Replaced}} \right] \quad (4.3)$$

In Eq 4.3, “*Certain Module Replaced*” means the SOC change in the ideal case with lowest internal resistance module battery pack and “*Current Battery Pack*” means the SOC change with the modules which have uneven internal resistance and one or more than one modules having high internal resistance.

4.4.1 Two Module Equalization

The module equalization is exactly the same scenario as in Figure 4.4. We will assume that Battery-1 is healthier than Battery-2. This means that the internal resistance of Battery-1 is lower than Battery-2.

Table 4-1. Initial conditions of the two module simulation study

Case No.	Battery No.	Voltage (V)	Capacity (Ah)	SOC (%)	Internal Resistance (Ω)
1	B-1	100.8	20	80	0.075
	B-2	100.8	20	80	0.075
2	B-1	100.8	20	80	0.075
	B-2	100.8	20	65	0.30

Electric vehicle battery will be simulated with the two modules which are at initial conditions mentioned in Table 4-1. The batteries in Case-1 are ideal and are assumed to be healthy batteries. The batteries in Case-2 have same open circuit conditions but different internal resistances. Battery B-2 is unhealthy battery and has higher internal resistance than battery B-1. SOC for battery B-1 and B-2 is observed. The difference in SOC for the same trip would be the additional energy wasted because of the poor energy module. Hence, we can find the exact cost associated with holding a poor module in the battery pack. Results for equalization are shown with case-1 and case-2.

Case 1:

Both modules are in the nominal condition, i.e. having internal resistance of 0.075Ω .

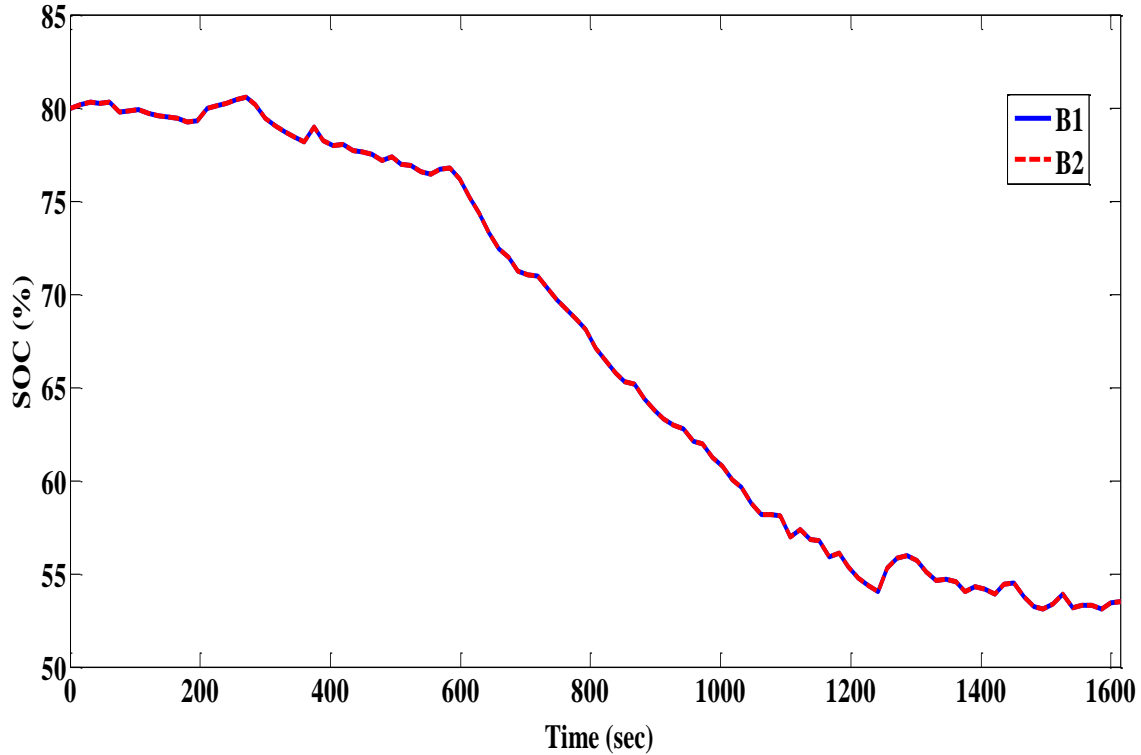


Figure 4.5 Battery module SOC trajectories with Case 1 example driving cycle

Starting from 80% SOC, both modules follow the same discharging trajectory as shown in Figure 4.5. The final SOC for both batteries is 53.52%.

Both batteries have the same internal resistance which is 0.075Ω . The batteries are connected in series which resemble 2 modules. The batteries start discharging at 80% SOC at the beginning of the trip and end at 53.52% SOC at the end of the trip. The electric vehicle travels ~27.5 kilometers in 1614 sec. The battery of the vehicle consumes 26.48% SOC to complete the trip.

Case 2

Battery-1 is in nominal condition, while Battery2 is degraded with internal resistance of $\sim 0.30\Omega$.

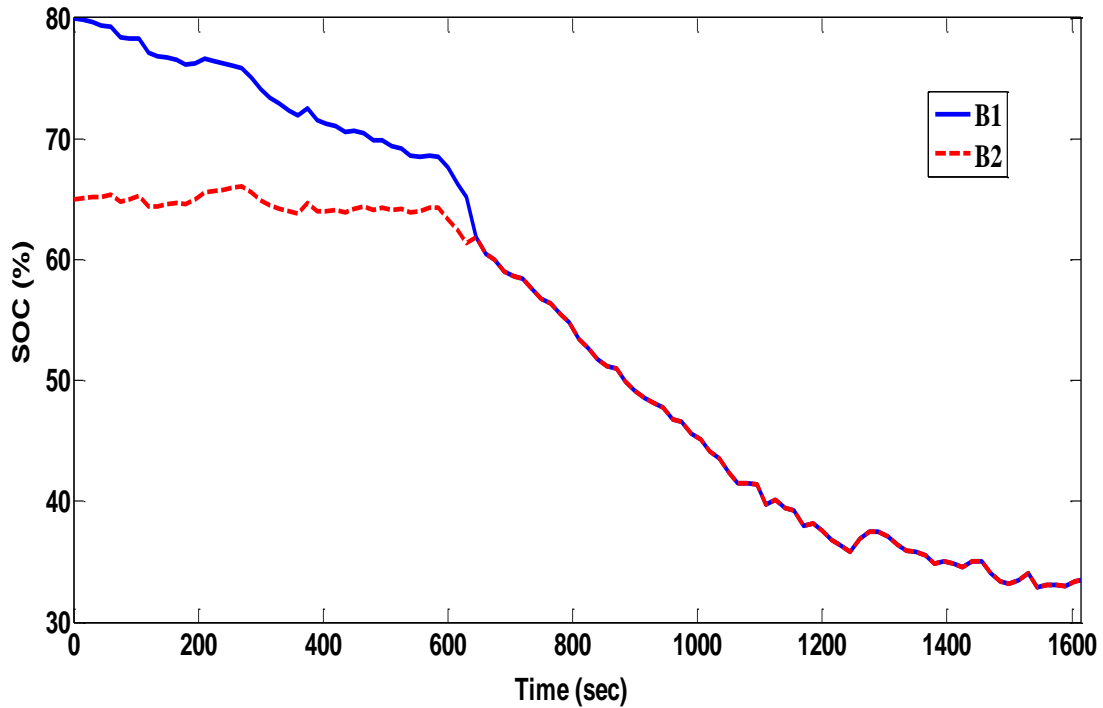


Figure 4.6 Two module battery SOC for example driving cycle for Case-2

In Figure 4.6 the two modules are equalized to 61.8% SOC, and then both modules discharged in identical fashion down to 33.45% SOC by the end of the driving cycle. Though the driving cycle is complete in case-2, there is a considerable amount of energy loss from B-1 supplied to B-2 so as to equalize which could have been used for driving. For case-2 in particular, it can be observed in Figure 4.6 that, due to the relatively large internal resistance of B-2, there is significant amount of energy loss during the equalization from B-1 to B-2. The battery-pack SOC changes by 26.48% in case-1 (both modules

healthy), while it changes by 39.05% in case-2. This is the average of the SOC consumed from both the modules of the electric vehicle battery. Such difference leads to the WOR of 1.47 for B-2.

4.4.2 Three Module Equalization

We intend to generalize the concept of equalization. Now that we have equalized the battery with two modules, we can apply the same concept to a battery with three modules.

Table 4-2. Initial conditions of individual battery modules for simulation study

Case	Battery	Volt (V)	Capacity (Ah)	SOC (%)	Internal Resistance (Ω)
1	B-1	64.8	20	80	0.054
	B-2	64.8	20	80	0.054
	B3	64.8	20	80	0.054
2	B-1	64.8	20	80	0.054
	B-2	64.8	20	72.5	0.081
	B-3	64.8	20	65	0.108
3	B-1	64.8	20	80	0.054
	B-2	64.8	20	80	0.081
	B-3	64.8	20	80	0.108

In the three module case we will assume that internal resistance for battery $B1 > B2 > B3$.

The voltage across each module is 64.8 V and all the batteries have same capacities. The

overall voltage across the battery pack is 194.4V. The internal resistance for ideal module is assumed to be 0.054Ω . Three cases are studied for simulation.

Case 1

All the battery modules are at equal SOC 80% and internal resistance 0.054Ω .

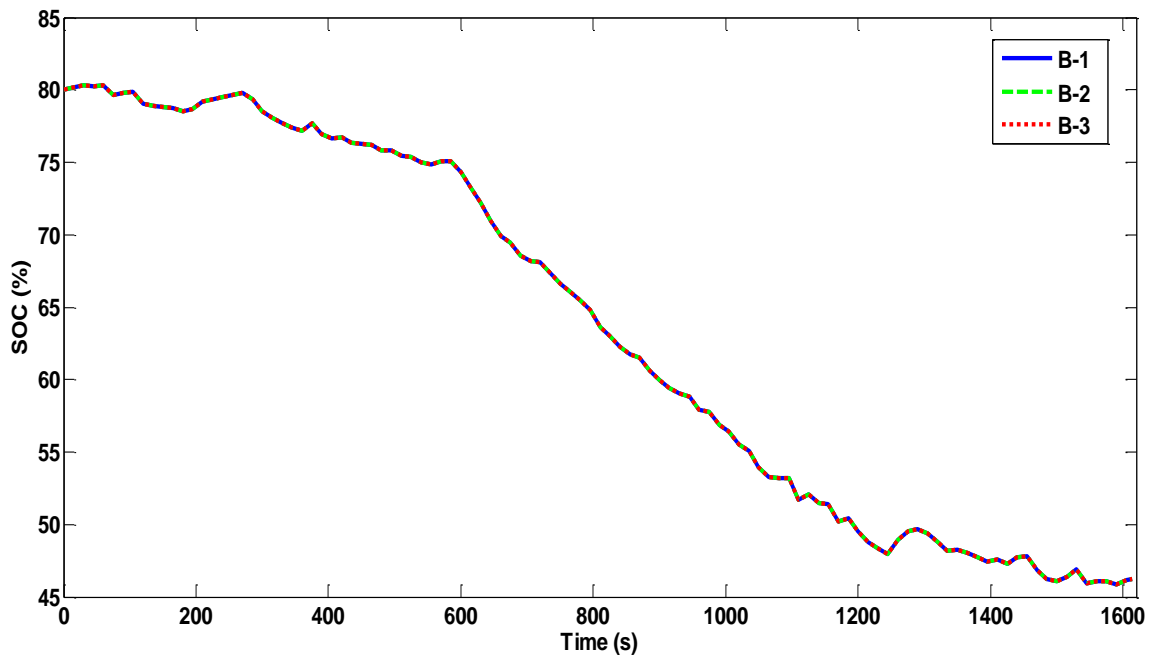


Figure 4.7. SOC trajectory for case1 of three-module battery pack

All the modules demonstrate identical discharging trajectories as shown in Figure 4.7 with the final SOC of 46.26%.

Case 2

B-1 has ideal SOC 80% and internal resistance 0.054Ω , B-2 has 72.5% initial SOC and internal resistance of 0.081Ω and B-3 has internal resistance of 0.108Ω and SOC of 65%.

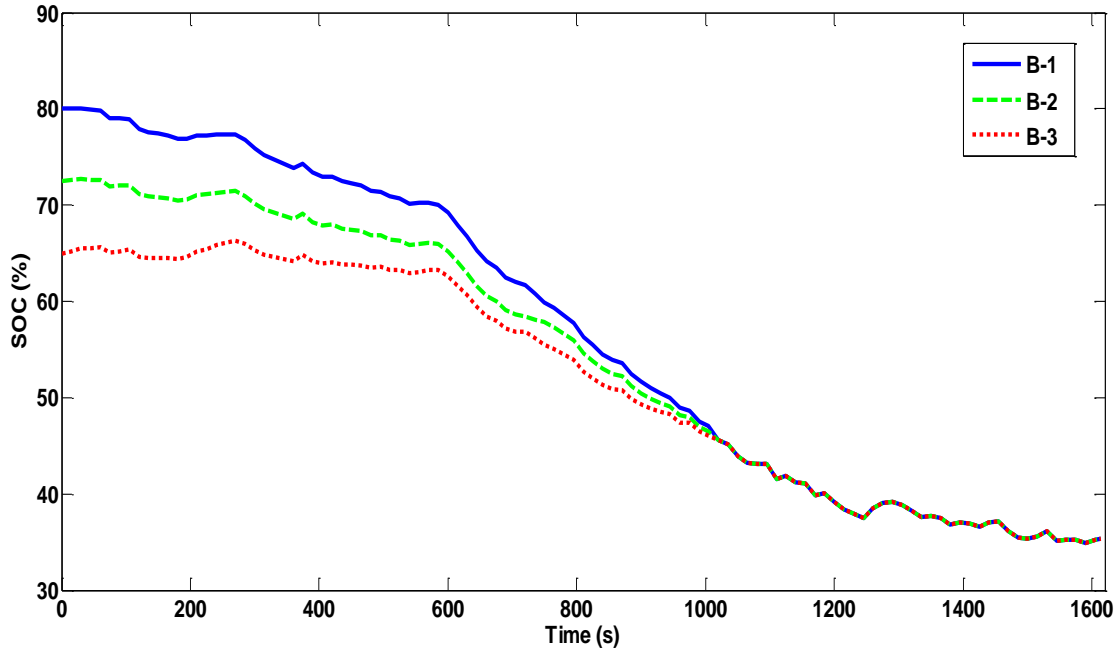


Figure 4.8. SOC trajectory for case 2 of three-module battery pack

During the equalization process, current is discharged from B-1 to B-2, and current is discharged from B-2 into B-3. All the modules equalize their SOC to 45.57%. Afterwards, the three modules jointly discharge to 35.34% SOC by the end of the driving cycle. Although in Case2, the driving cycle can be completed with the onboard battery power, there is a considerable amount of SOC from B-1 supplied to B-2, and that from B-2 supplied to B-3. Further, more due to the relatively higher internal resistances of B-2 and B-3, there is significant amount of energy loss during the aforementioned equalization processes. To complete the same trip, the average SOC drops by 33.74% in Case1, while in Case2, by 37.16%. The corresponding WOR is 1.102.

Case 3

All the battery modules have equal SOC but different internal resistance. The three module case will help us generalize the concept of equalization of battery modules and also give us an idea of practical implementation of such an algorithm.

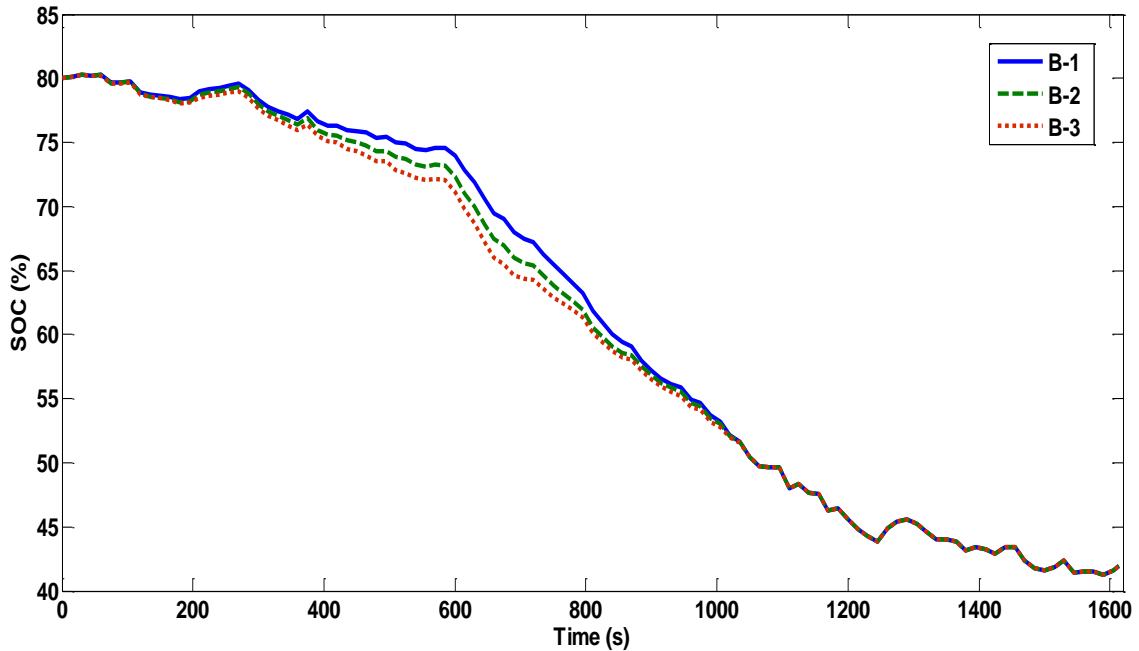


Figure 4.9. Battery SOC trajectories for three modules for Case3 for intermediate equalization

Simulation has also been performed to the situation when battery module equalization occurs not from the start of the trip, but rather in the middle of the trip as the SOC difference increases. For this purpose, we consider the same battery configuration as in Table 4-2, while all the modules have equal starting SOC, i.e. 80%. The SOC deviates for each module during the first 645 seconds, and then after the equalization process starts. We can clearly, observe the state of charge deviation amongst the battery modules. At that point, the SOC

difference between Battery-1 and Battery-2 was 2.05% and that between Battery-2 and Battery 3 was 1.53%, respectively. With the equalization process, the modules are equalized to 50.45% by 1050 seconds. Then the whole battery pack completes the driving cycle at SOC 41.95%. The total energy required for travel trip was 38.05%, and the WOR for the trip was 1.105 in this case as shown in Figure 4.9.

The above simulation results show that equalization can handle the presence of degraded module during vehicle's operation, however, there is a considerable amount of SOC loss during equalization. Highly degraded modules have significantly high internal resistance, which would waste the battery energy and in turn lead to uneconomical operation. If the module-specific internal resistance can be identified online, the vehicle owners can perform the economic analysis based on their preferred trips, and make reasonable decision on module replacement.

4.5 Estimation of Battery Parameters

This section will deal with estimation of parameters of the battery models during the process of equalization. During driving, there is an ongoing process of battery module equalization. There are two modes of operation for the equalization circuit shown in Figure 4.4. The duty ratio of operation for switch ON is δ and $1-\delta$ is time period for switch off. The first is when the switch Q_1 is on and the switch is conducting. The second is when the diode D_2 is conducting. The parameters are estimated after averaging the performance of the switching circuits.

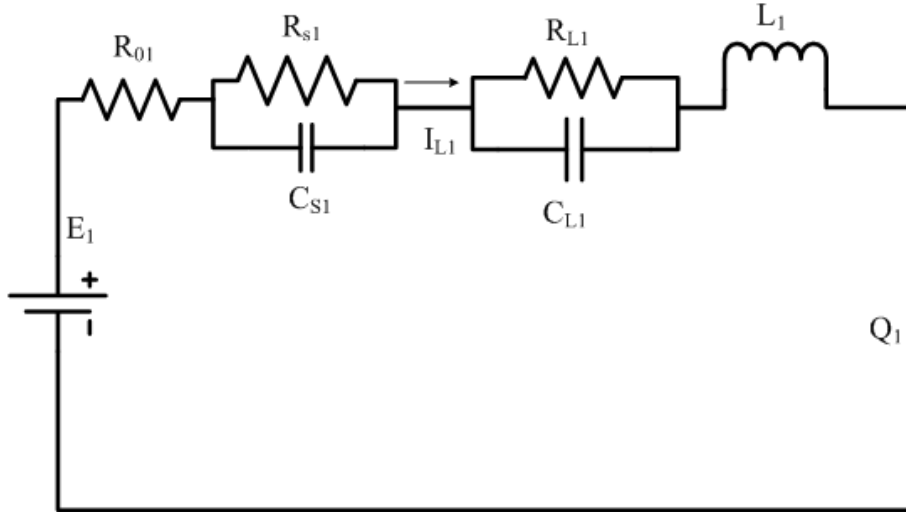


Figure 4.10. Switch Q_1 as conductor

The first part is when the switch Q_1 is on and the circuit is complete. During the time period δ , switch is turned “ON” the inductor is charged as shown in the Figure 4.10. Resistances R_{01} , R_{S1} and R_{L1} will be estimated for time period δ . The second part is when the switch D_2 is on and the circuit is complete.

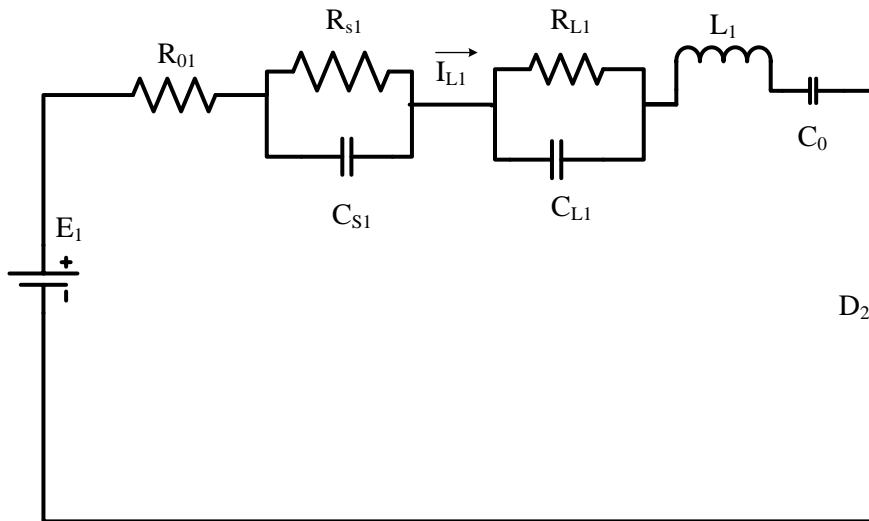


Figure 4.11. Diode D_2 as conductor

During the time period $1 - \delta$, diode is turned *ON*, the inductor charges the capacitor C_0 as shown in the Figure 4.11. Resistances R_{01} , R_{S1} and R_{L1} will be estimated for time period “ $1 - \delta$ ”.

After solving the circuit model we will estimate the parameters for the batteries. The models are averaged for switching between the switch Q_1 and D_2 . The estimation of the parameters will be dependent on the two switching circuits. Proper estimation technique will be applied to estimate the required battery internal resistances.

4.5.1 Subspace Estimation of Internal Resistance Map of EV Battery Pack

In order to obtain the module-wise internal resistance map of battery pack for WOR evaluation and online monitoring, we propose to estimate the internal resistance with the battery equalization signals, i.e. the associated voltage and current measurements, during the actual trip (i.e. with the driving cycle input).

In this study, the subspace identification (Ljung, 1998) method is applied for the relevant parameter estimation based on the current and voltage measurements in the equalization circuit. Based on a state-space battery model, subspace parameter estimation permits estimation of static battery parameters based on input-output data (I_{in} and V_o). The process can be carried out online during the vehicle operation so that actual change of battery characteristics can be identified (Juang, 1994).

The subspace identification theory is briefly reviewed next. For the m -input, p -output, n^{th} order system with discrete-time model

$$x(t+1) = Ax(t) + Bu(t) + w(t) \quad (4.3a)$$

$$y(t) = Cx(t) + Du(t) + v(t) \quad (4.3b)$$

where $x(t)$ are states, $u(t)$ and $y(t)$ are input and output, respectively, $w(t)$ is the process noise or disturbance, and $v(t)$ is the measurement noise. System (4.3a and 4.3b) can be diagonalized via similarity transformation as

$$\tilde{x}(t+1) = T^{-1}AT\tilde{x}(t) + T^{-1}Bu(t) + \tilde{w}(t) \quad (4.4a)$$

$$y(t) = CT\tilde{x}(t) + Du(t) + v(t) \quad (4.4b)$$

where T is invertible and defined by

$$\tilde{x}(t) = T^{-1}x(t) \quad (4.5)$$

The output can be estimated by assuming that \hat{A} and \hat{C} are fixed, i.e.

$$y(t | B, D) = \hat{C}(qI - \hat{A})^{-1}Bu(t) + Du(t) \quad (4.6)$$

is linear in B and D . The predictor is formed from past inputs, and Eq. (4.5) is an output error model. Therefore, if the system operates in open loop, one can consistently estimate B and D .

$$y(t | B, D, x_0) = \hat{C}(qI - \hat{A})^{-1}x_0\delta(t) + \hat{C}(qI - \hat{A})^{-1}Bu(t) + Du(t) \quad (4.7)$$

Equation (4.5) is linear in $x_0 = x(0)$ and $\delta(t)$ is the unit pulse at time $t = 0$.

Matrices A and C are estimated from extended observability matrix for r observable rows, i.e.

$$G = \begin{pmatrix} C \\ CA \\ \vdots \\ CA^{r-1} \end{pmatrix} \quad (4.8)$$

G has dimensions $(pr) \times n$. C can be estimated by

$$\hat{C} = G(1:p, 1:n) \quad (4.9)$$

Similarly, A is estimated by

$$G(p+1:pr, 1:n) = G(1:p(r-1), 1:n) \hat{A} \quad (4.10)$$

After estimating the initial state, the prediction error minimization method can be used to determine the unknown parameters in the state space model. In this study, the target parameter is the internal resistances for the respective batteries. The estimation quality can be evaluated with the prediction error

$$\varepsilon(t, \theta_*) = y(t) - \hat{y}(t | \theta_*) \quad (4.11)$$

for $1 \leq t \leq N$ error sequence is filtered by

$$\varepsilon_F(t, \theta) = L(q)\varepsilon(t, \theta) \quad (4.12)$$

The filter is used to filter out the error from the original estimation.

where, $L(q) \equiv 1$ in this case.

For parameter estimation, the cost function is defined as

$$V_N(\theta, Z^N) = \frac{1}{N} \sum_{t=1}^N l[\varepsilon_F(t, \theta)] \quad (4.13)$$

where, $l(\cdot)$ is a quadratic function, $Z^N = [y(1), u(1), y(2), u(2), \dots, y(N), u(N)]$ is the vector of the input-output data pairs. The least-square method is applied for parameter estimation:

$$\hat{\theta}_N = \hat{\theta}_N(Z^N) = \arg \min_{\theta \in D_M} V_N(\theta, Z^N) \quad (4.14)$$

where, $\theta \in D_M \subset R^N$, and D_M is the set of parameter vectors. This procedure of estimating the required parameter θ is prediction-error identification method.

In order to apply the foregoing prediction-error identification method to battery equalization process, the associated state-space model is obtained as follows. Based on the two operational modes described in Section 4.5, the averaged state-space model was derived. When battery 1 is at higher energy level, battery 1 charges battery 2. Referring to

Figure 4.10 and

Figure 4.11 the average state space model for battery is as given below.

$$\begin{bmatrix} \dot{x}_1 \\ \dot{x}_2 \\ \dot{x}_3 \\ \dot{x}_4 \end{bmatrix} = \begin{bmatrix} -\frac{1}{R_{cs1}C_{cs1}} & 0 & \frac{1}{C_{cs1}} & 0 \\ 0 & -\frac{1}{R_{cL1}C_{cL1}} & \frac{1}{C_{cL1}} & 0 \\ \frac{-1}{L_1} & \frac{-1}{L_1} & \frac{-R_{01}}{L_1} & 0 \\ 0 & 0 & \left(\frac{1}{C_0} - \frac{x}{C_0}\right) & 0 \end{bmatrix} \begin{bmatrix} x_1 \\ x_2 \\ x_3 \\ x_4 \end{bmatrix} + \begin{bmatrix} 0 \\ 0 \\ -\frac{x}{C_0} \\ 0 \end{bmatrix} d \quad (4.15)$$

$$E_1 = \begin{bmatrix} -2 & -2 & \frac{R_{01}}{L_1} & 0 \end{bmatrix} \begin{bmatrix} x_1 \\ x_2 \\ x_3 \\ x_4 \end{bmatrix} \quad (4.16)$$

where, x_1 is the voltage across capacitor C_{s1} , x_2 is the voltage across capacitor C_{L1} , x_3 is the current through inductor L_1 and x_4 is the voltage across capacitor C_0 . Similarly, the state-space model for battery 2 is as below

$$\begin{bmatrix} \dot{x}_1 \\ \dot{x}_2 \\ \dot{x}_3 \\ \dot{x}_4 \end{bmatrix} = \begin{bmatrix} -\frac{1}{R_{cs2}C_{cs2}} & 0 & \frac{1}{C_{cs2}} & 0 \\ 0 & -\frac{1}{R_{cl2}C_{cl2}} & \frac{1}{C_{cl2}} & 0 \\ \frac{-1}{L_2} & \frac{-1}{L_2} & \frac{-R_{02}}{L_2} & 0 \\ 0 & 0 & \left(\frac{1}{C_0} - \frac{x}{C_0}\right) & 0 \end{bmatrix} \begin{bmatrix} x_1 \\ x_2 \\ x_3 \\ x_4 \end{bmatrix} + \begin{bmatrix} 0 \\ 0 \\ -\frac{x}{C_0} \\ 0 \end{bmatrix} d \quad (4.17)$$

$$E_2 = [-2 \quad -2 \quad \frac{R_{02}}{L_2} \quad 0] \begin{bmatrix} x_1 \\ x_2 \\ x_3 \\ x_4 \end{bmatrix} \quad (4.18)$$

where, the states are same as those in Eq. (4.15)

After obtaining the values for the parameters from the subspace state space estimation, we calculate the values for each of the resistances. R_{CS1} , R_{CL1} and R_{01} are identified internal resistances for battery 1 and R_{CS2} , R_{CL2} , and R_{02} are internal resistances for battery 2. Thus the internal resistances of individual modules can be estimated throughout a specific trip.

4.5.2 Results with Subspace State Space Parameter Estimation

The subspace identification scheme described in Section 4.5.1 is applied to the two-module case for estimating the battery internal resistances. As described earlier in battery modeling section, surface internal resistance, load resistance and terminal resistance appear in the state-space model of battery equalization. This study mainly considers the following parameters: surface capacitance (C_s), bulk capacitance (C_i), inductors (L_1 and L_2) in the equalization circuit, capacitors (C_0) from the equalization circuit, surface internal resistance R_s , and bulk internal resistance R_i . The nominal values for the capacitance and

inductance parameters in the two-module simulation case are set as: $C_1= 90000$ Farads, $C_s= 9000$ Farads, $L_1=L_2=13$ mH and $C_0= 12\mu$ F.

In order to assure the unique solution or convergence of the parameter estimation, the condition of persistent excitation (PE) is evaluated for the input signals (K. J. Aström, 1994). The PE order of is n if

$$C_n = \lim_{t \rightarrow \infty} \frac{1}{t} \phi^T \phi = \begin{bmatrix} c(0) & c(1) & \cdots & c(n-1) \\ c(1) & c(0) & \cdots & c(n-2) \\ \vdots & \vdots & \ddots & \vdots \\ c(n-1) & c(n-2) & \cdots & c(0) \end{bmatrix} \quad (4.19)$$

is nonsingular, where the covariance of input is given by

$$c(k) = \lim_{t \rightarrow \infty} \frac{1}{t} \sum_{i=1}^t u(i)u(i-k) \quad (4.20)$$

Determination of PE order is based on the evaluation of the covariance matrix and checking if it is of full rank. The number of parameters to be estimated should not higher than the order of PE that can be achieved for the given input-output data. Using eigen values is a more reliable method to check the matrix singularity. The condition number, i.e. the ratio of largest eigen value magnitude to the smallest, is a more trustworthy index to test if a matrix is full rank even though all eigen values are non-zero. If the condition number is very large, the full rank condition is not practically valid.

The internal resistances for battery1 (R_{cs1} , R_{cl1} and R_{01}) and battery 2 (R_{cs2} , R_{cl2} and R_{02}) are estimated using the subspace identification method described earlier.

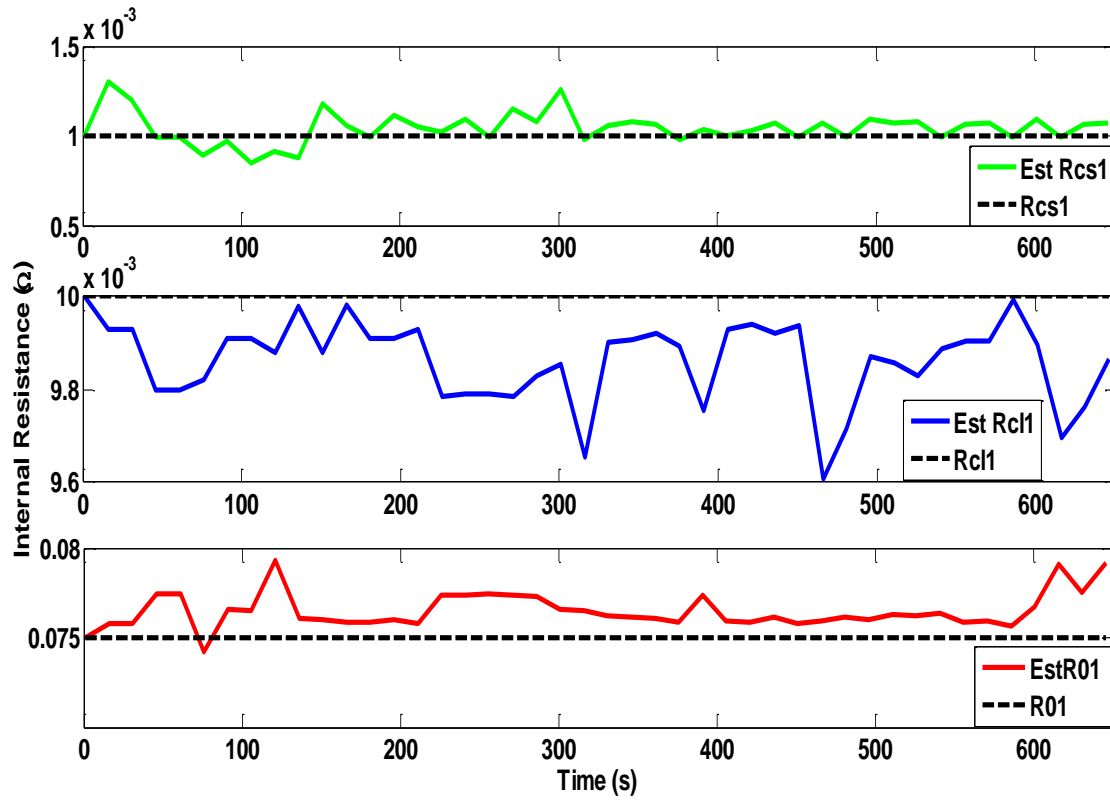


Figure 4.12. Online estimation of Battery-1 internal resistance for the 2-module case.

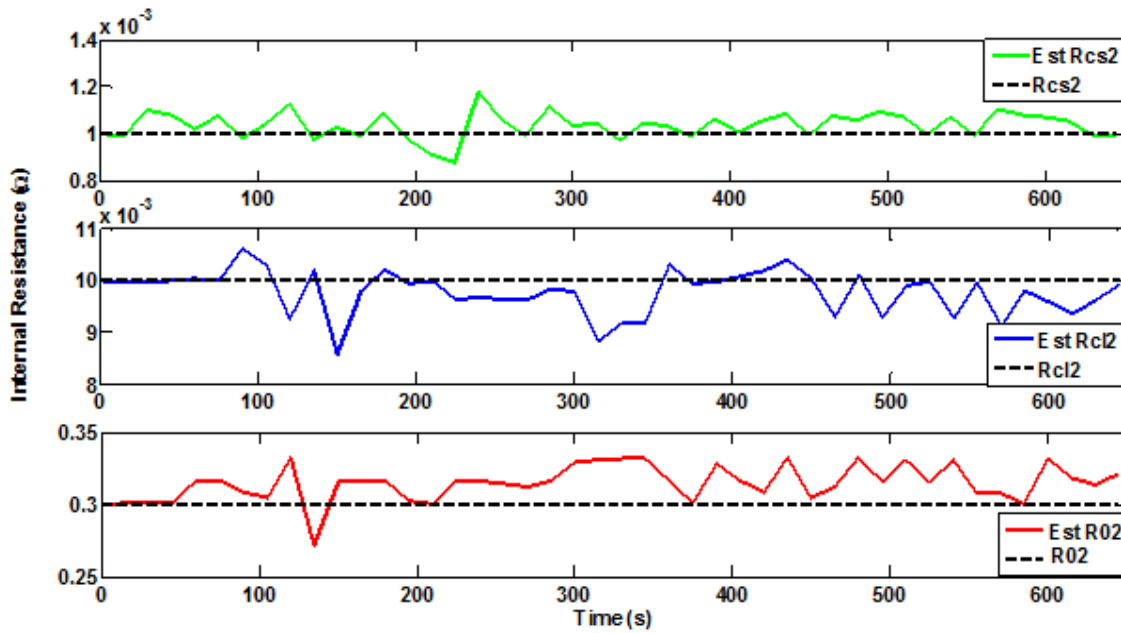


Figure 4.13. Online estimation of Battery-2 internal resistance for the 2-module case.

The online estimation of the internal resistances of batteries 1 and 2 are shown in Figure 4.12 and Figure 4.13, respectively.

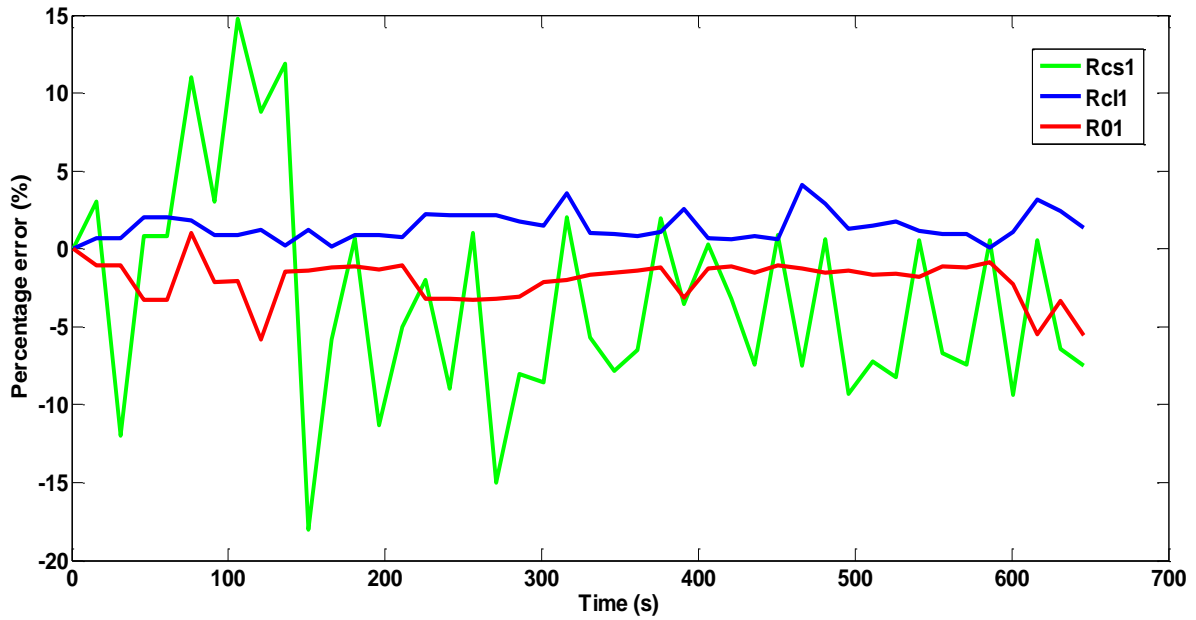


Figure 4.14. Relative error in estimating Battery-1 internal resistance for the two-module case.

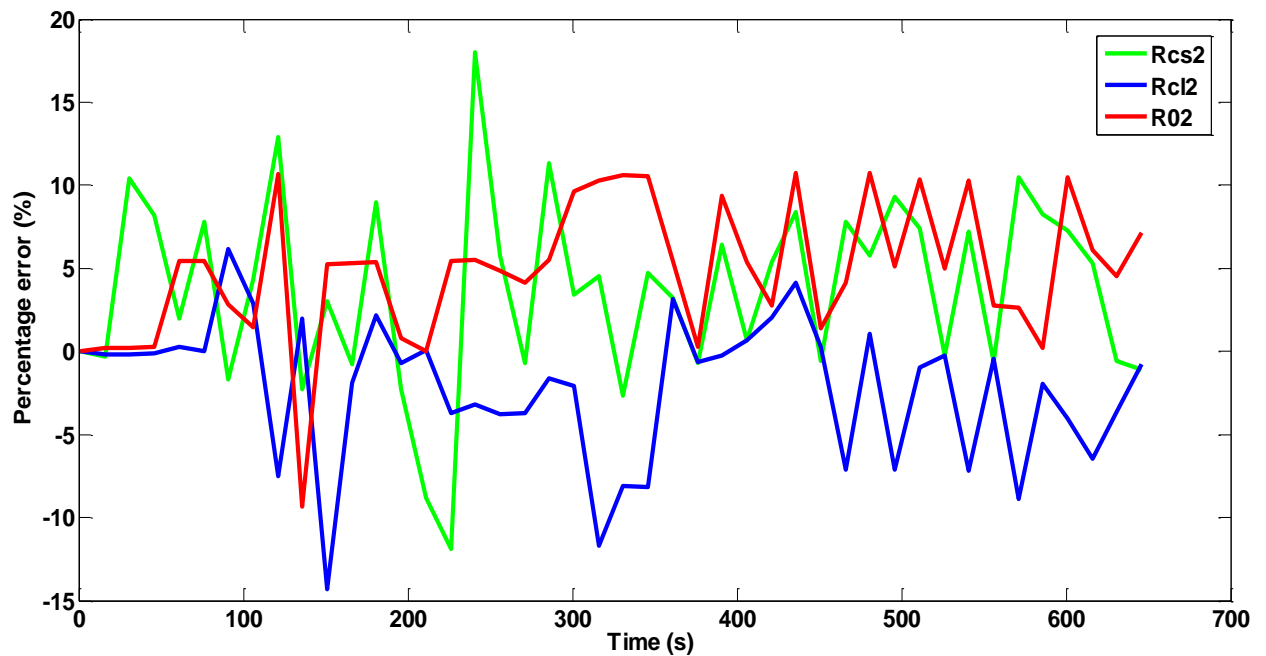


Figure 4.15. Relative error in estimating Battery-2 internal resistance for the two-module case.

The relative errors in estimating the internal resistances are plotted in Figure 4.14 and Figure 4.15 for battery1 and 2, respectively, which are within 18%. Such accuracy is generally acceptable for fault detection and WOR evaluation purpose.

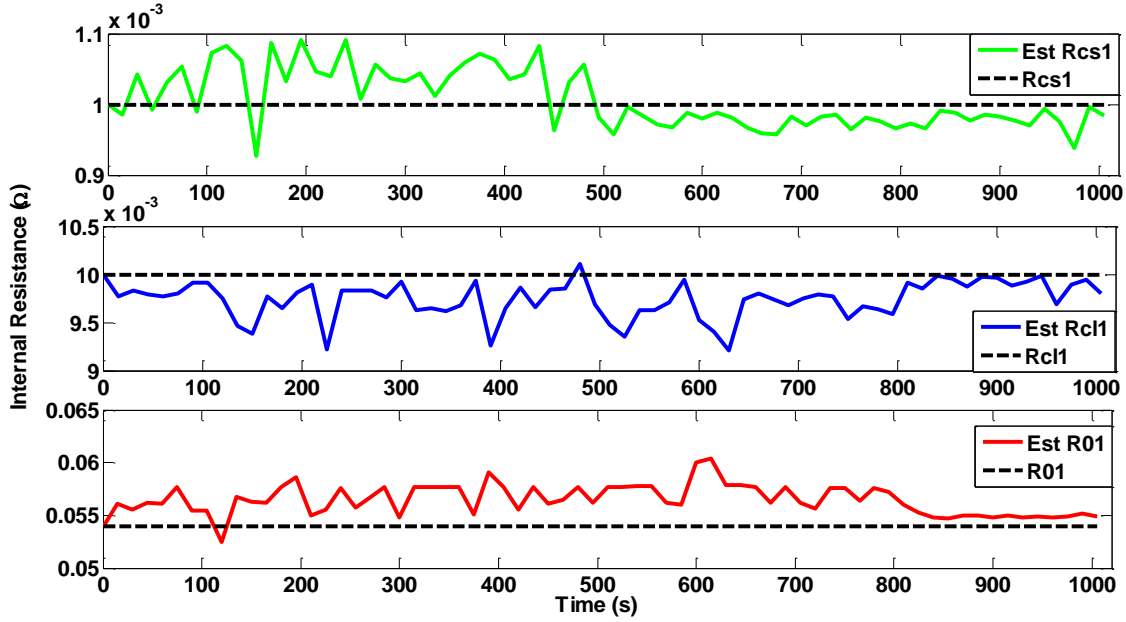


Figure 4.16. Estimation of Battery-1 internal resistance for the 3-module case.

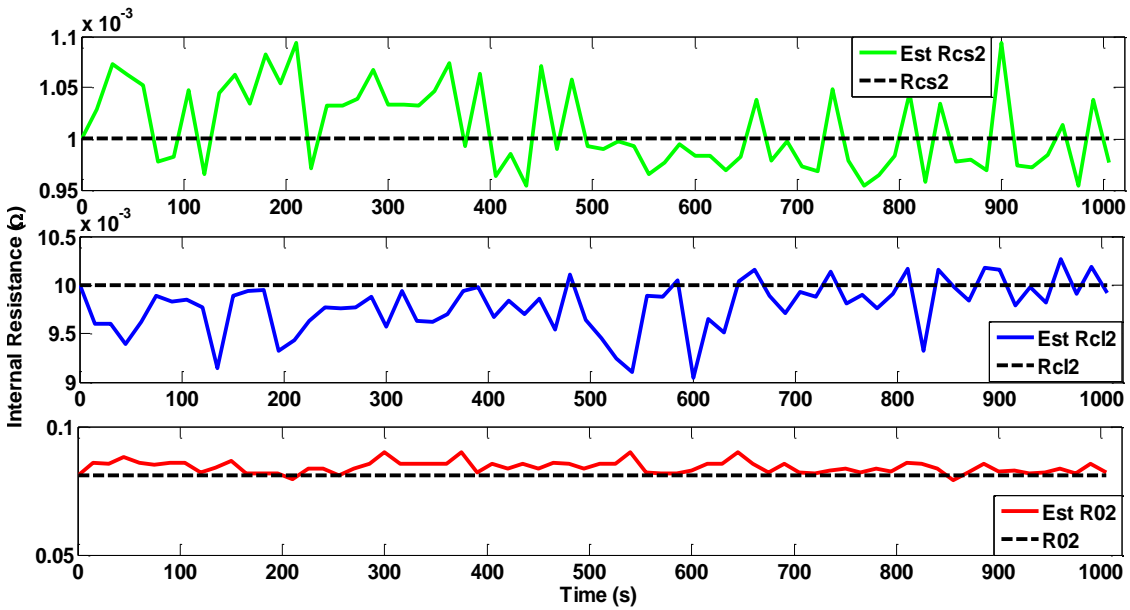


Figure 4.17. Estimation of Battery-2 internal resistance for the 3-module case

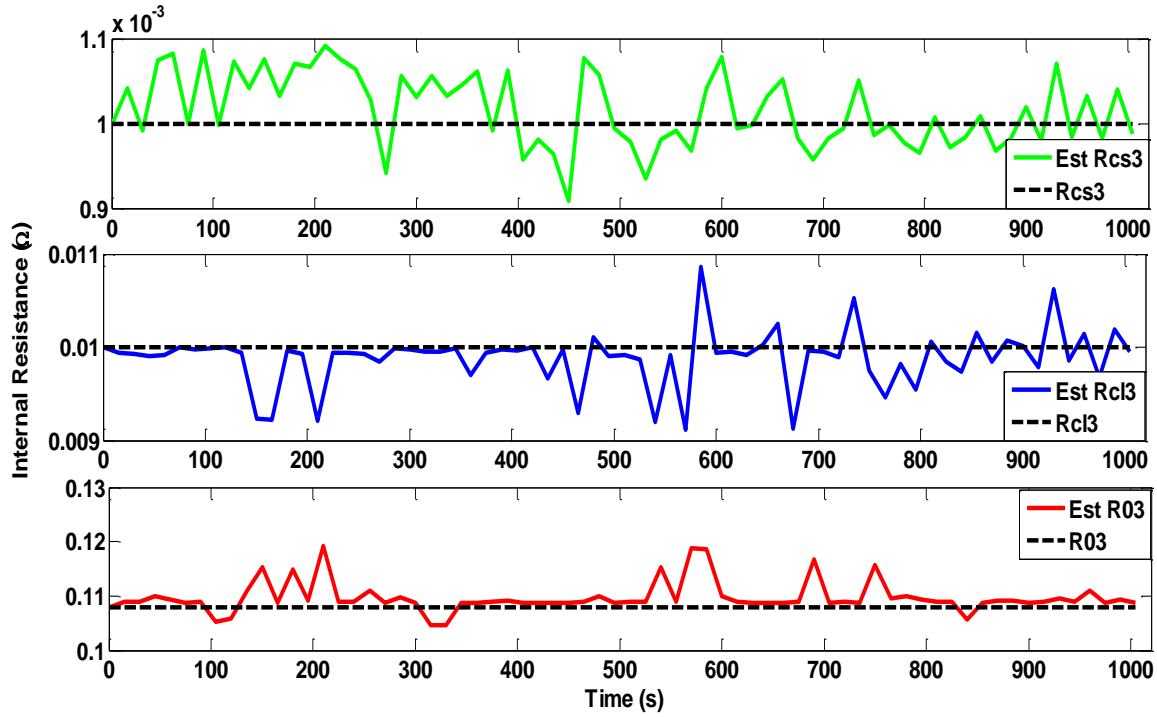


Figure 4.18. Estimation of Battery-3 internal resistance for the 3-module case.

The parameters R_{cs} and R_{cl} are 0.001Ω and 0.01Ω whereas $R_{01}=0.054\Omega$, $R_{02}=0.081\Omega$ and $R_{03}=0.108\Omega$.

Similar simulation study is then performed for the 3-module equalization process. In this case, the parameters we identify are R_{cs1} , R_{cl1} and R_{01} for Battery 1, R_{cs2} , R_{cl2} and R_{02} for Battery 2, and R_{cs3} , R_{cl3} and R_{03} for Battery 3. Figure 4.16 - Figure 4.19 illustrate the estimation of the parameters for the three batteries.

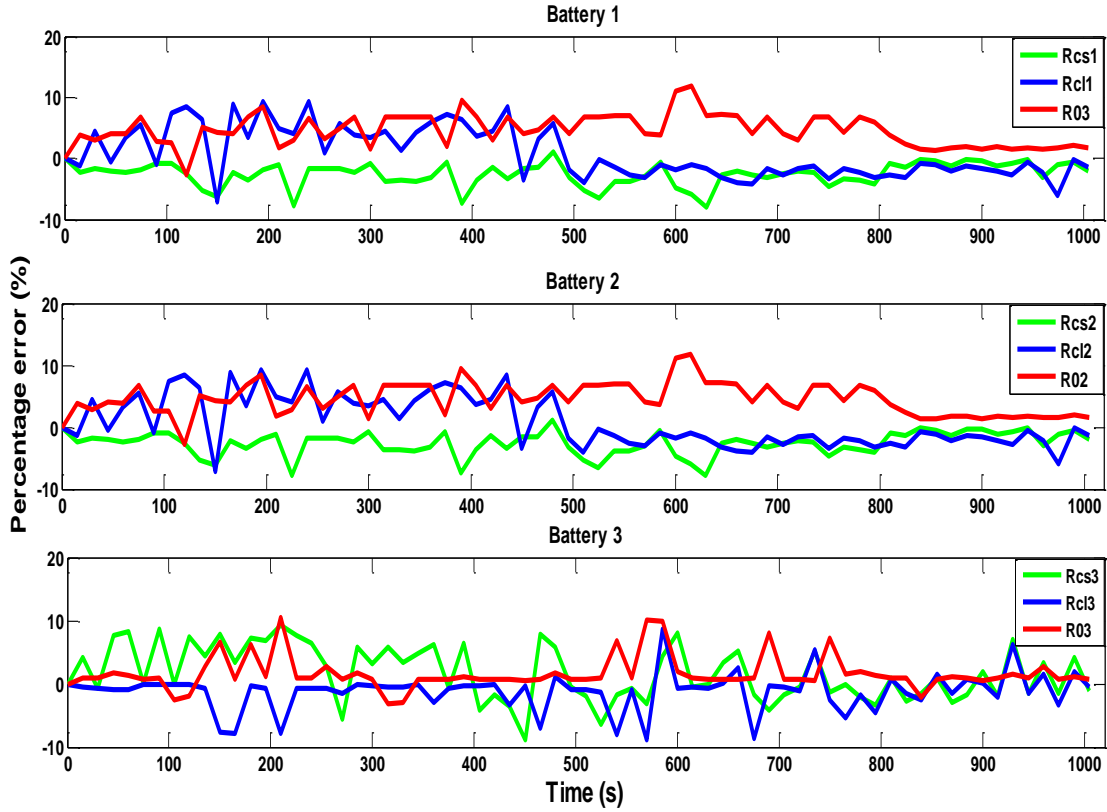


Figure 4.19. Relative error in estimating the Battery-1, Battery-2 and Battery-3 internal resistance for 3-module case.

Figure 4.19 shows the relative errors for these estimations for the three battery modules. For Battery 1, R_{cs1} has mean deviation of 0.8% with variation from -7.8 to 9.25%, R_{cl1} has a mean deviation of -2.5% with a variation from -7.8 to 1% and R_{01} has mean deviation of 4.5% with variation from -2.75 to 11.75%. For Battery 2, R_{cs2} has mean deviation of 1% with variation from -4.6 to 9.4%, R_{cl2} has a mean deviation of -2.2% with a variation from -9.6 to 2.66% and R_{02} has mean deviation 3.9% with variation from -2.4 to 11.15%. For Battery 3 R_{cs3} has mean deviation of 1.7% with variation from -8.9 to 9.32%, R_{cl3} has a mean deviation of -1.15% with a variation from -8.6 to 8.8% and R_{03} has mean deviation of 1.6% with variation from -3.0 to 10.45%.

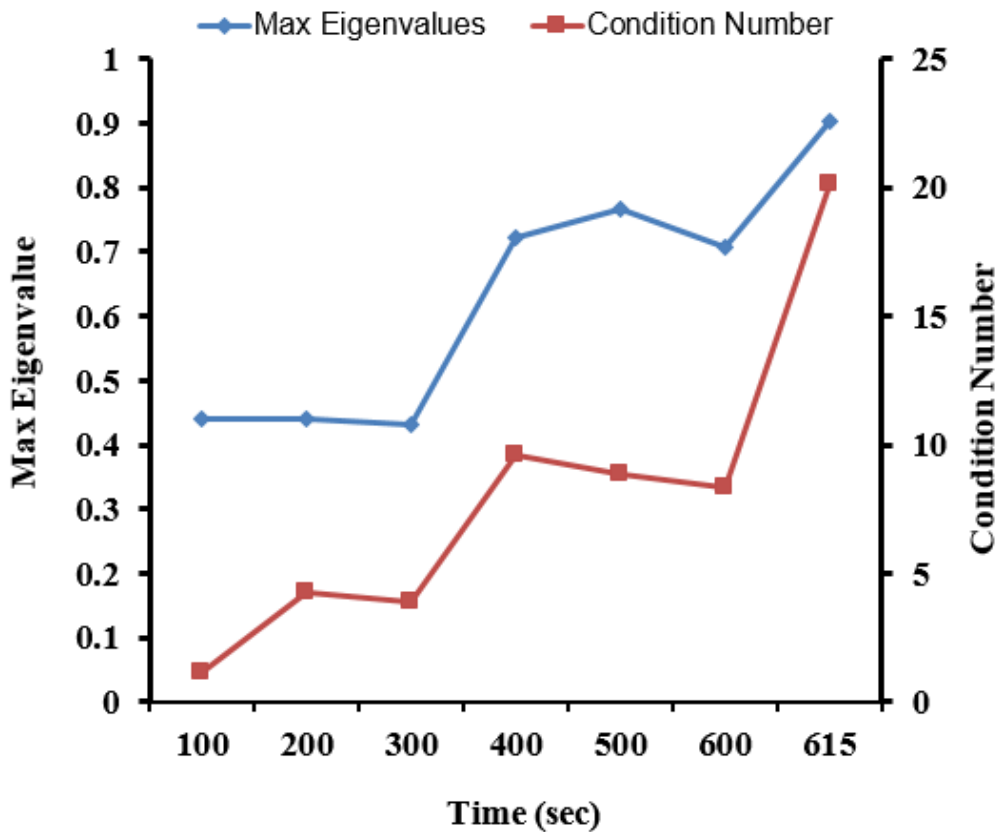


Figure 4.20. Maximum eigenvalue and condition number for the input signal throughout the trip.

In this study, the input is the duty ratio of the equalization circuit. The input data segment for every 100 seconds is used to evaluate if the 4th order PE is valid. The condition numbers and the maximum magnitude eigen-values are shown in Figure 4.20 to validate the 4th order PE condition.

4.6 Summary

In this chapter we proposed a circuit model which estimates the internal resistance of lithium ion battery. A typical driving cycle that includes mix of freeway, city streets and stop-n-go driving conditions was simulated. We accurately estimated the state of charge

and internal resistance of onboard lithium ion batteries. We estimated the internal resistance was estimated using a sub-space-state-space identification technique. We also checked the estimated model for persisted excitation condition which assures us of the unique solution or convergence of the parameter estimation. The energy loss during the process of equalization. The amount of energy loss from higher energy module to lower energy module controls the decision making of replacement of the batteries. Based on the modeling and simulating results it was evident that the internal resistance of the batteries dictates the worthiness of replacement of the onboard lithium ion batteries.

5 Optimizing the Trip Cost

The internal resistance of electric vehicle batteries or large pack of batteries does not increase overnight, but increases gradually with regular usage. The battery internal resistance rises with its age and the pattern of usage. There are many factors that contribute to the increase in the internal resistance such as usage over a period of time, deep discharge cycles, variable current input and output requirements etc. The internal resistance values in this research study are approximately equivalent to the lithium ion batteries of a Chevrolet Volt. We assume that the increase in the internal resistance is over the life time of the battery. Table 5.1 includes battery internal resistance as a function of its life. The batteries are divided into 4 groups.

Table 5.1. Battery internal resistance as per the age of battery

Name	Battery Age (years)	Internal Resistance (Ω)
Group 1	0-1.5	0.104
Group 2	1.5-3.0	0.156
Group 3	3.0-4.5	0.313
Group 4	4.5-6.0	0.521

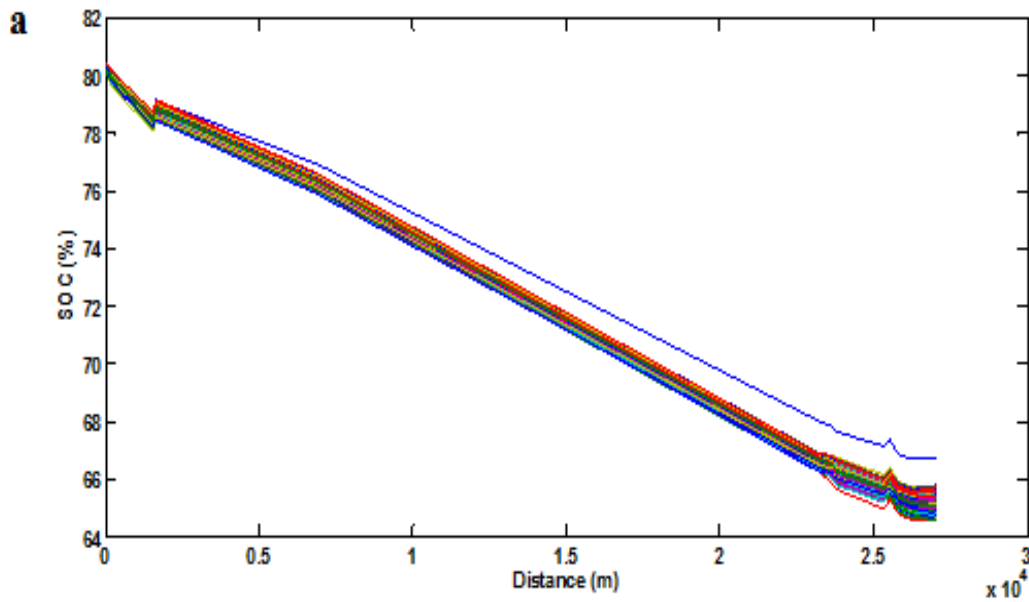
The assumption in this study is that the battery life is 6 years. This does not imply that the battery is not usable after 6 years. We just intend to study its performance through its working life. The batteries are charged from 30% to 80% SOC on a daily basis. The batteries are at 80% SOC at the beginning of the day i.e. at 7:00AM and it returns to 30%

at the end of the day i.e. at 7:00 PM. The battery starts charging from 7:00 PM and is completely charged by 7:00 AM the next morning.

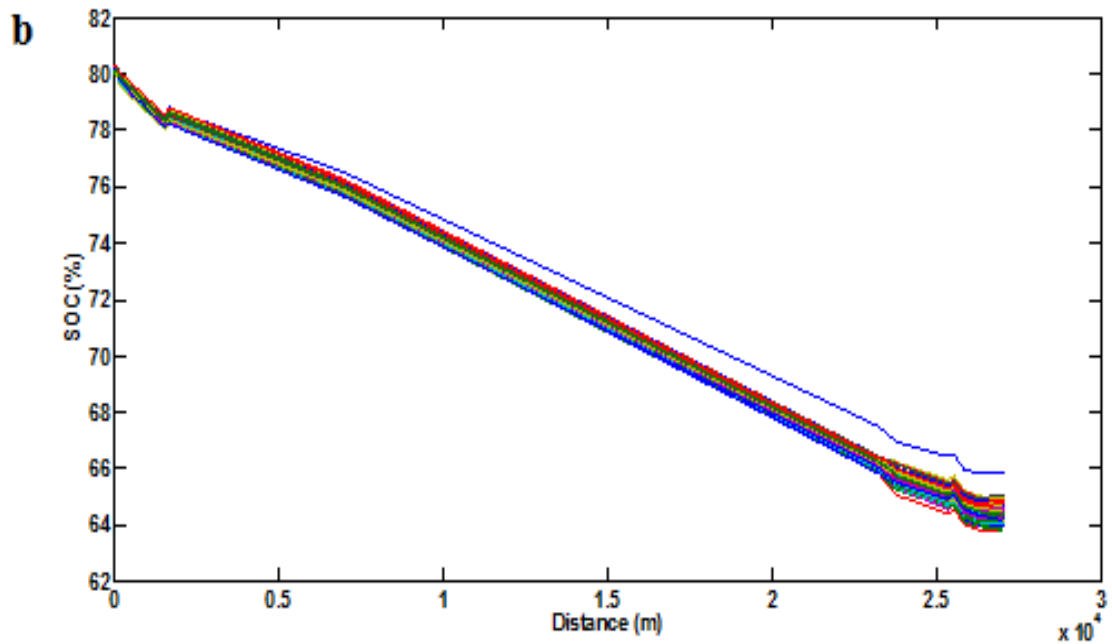
The charging times for electric vehicle batteries change with their age. The charging times for electric vehicle battery depend on battery internal resistance. We use the battery models mentioned in Figure 4.1, and Eq. 4.2 gives the SOC of the battery during charging.

5.1 Battery Discharging

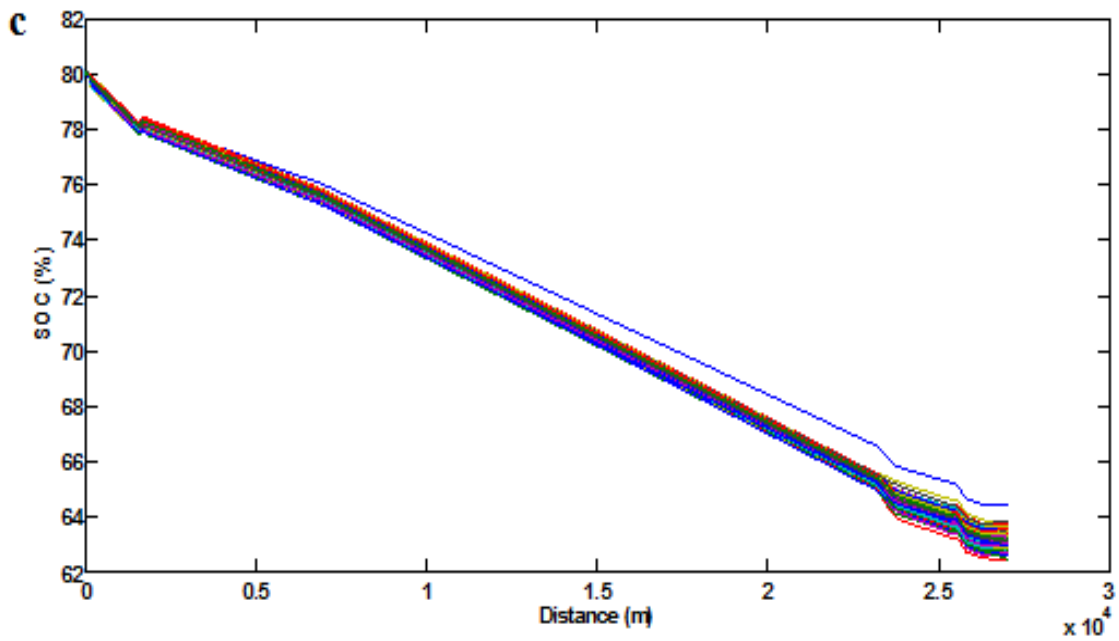
The motor speed and motor torque profiles for the trip used for simulation are as given in Figure 4.3. The whole driving cycle is converted into spatial mode as different segments take a different amount of time but the distance remains constant. We simulate 100 driving cycles with 4 battery configurations as mentioned in Table 5.1.



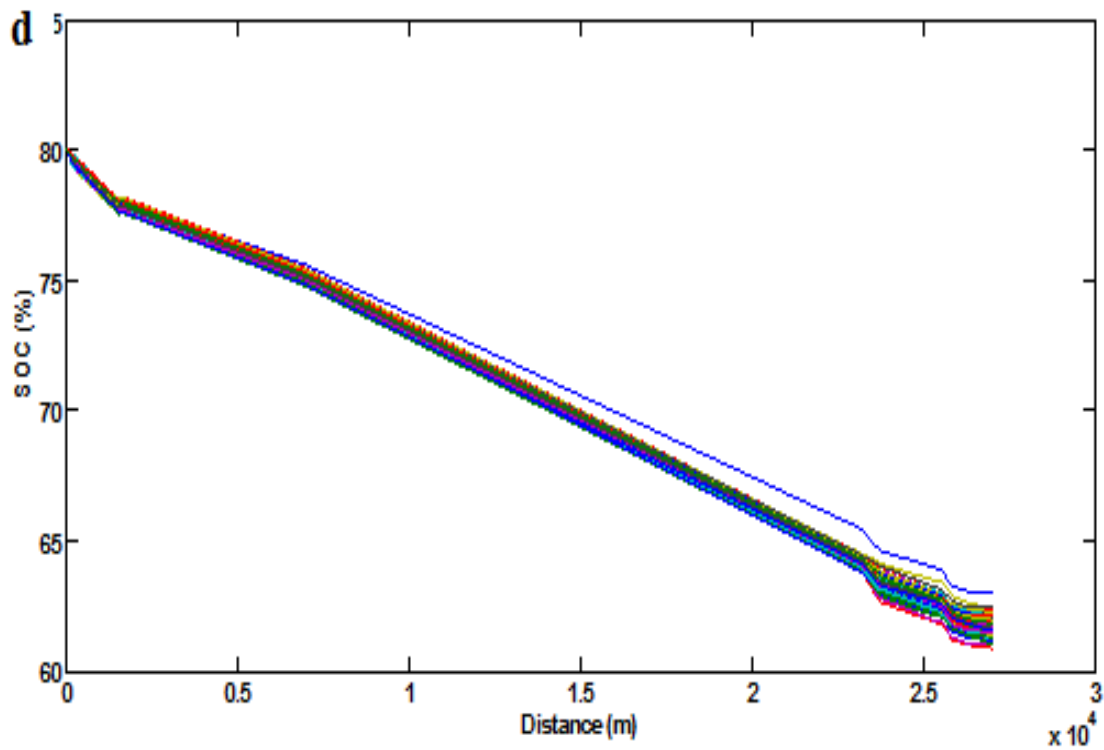
Battery performance during 0-1.5 years



Battery performance during 1.5-3.0 years



Battery performance 3.0-4.5 years



Battery performance 4.5-6.0 years

Figure 5.1. Battery performance for 100 vehicles on a given driving torque and speed

The driving distance for all the batteries is same but the energy required is different as the battery performance changes with the driving pattern. The energy consumption of batteries with higher internal resistance is greater than the energy consumption of the lower internal resistance batteries. We see that group-1 batteries require an average of 14.79% SOC with a standard deviation 0.325, group-2 batteries require an average of 15.55% SOC with a standard deviation of 0.31, group-3 batteries require average of 16.8% SOC with a standard deviation of 0.31, group-4 batteries require average of 18.28% SOC with a standard deviation of 0.34.

5.2 Charging the Battery

We assume that batteries are at 30% SOC at the beginning of the charging cycle, which is also the lowest point of the operational range. The battery is at 80% SOC when it is fully charged.

Table 5-2. Battery internal resistance as per the age of battery during charging

Name	Battery Age (years)	Internal Resistance (Ω)
Group 1	0-1.5	0.032
Group 2	1.5-3.0	0.049
Group 3	3.0-4.5	0.098
Group 4	4.5-6.0	0.160

The internal resistance for charging primarily varies with its age. The nominal internal resistance for various battery groups is as shown in Table 5-2.

The internal resistance of the batteries is variable. The variation in the internal resistance is from the ageing effect of the battery. As the battery ages the internal resistance of the battery increases compared to its initial value.

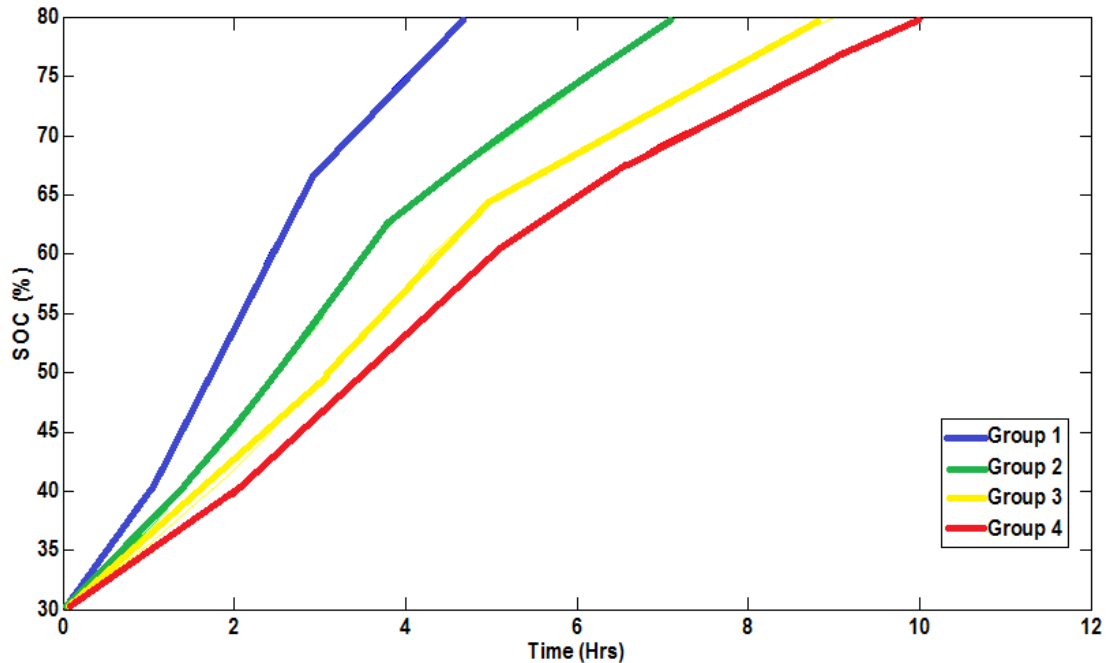


Figure 5.2. Charging time for batteries in all the groups

The charging process for all group batteries is shown in Figure 5.2. The charging time increases as there is a rise in the internal resistance of the battery. The batteries are charged with 240V and 30A current until 60% SOC and then at 120V and 15A till 80%. The charging pattern is selected to maintain battery health and performance. It can be seen that group-1 battery charges in 4.74 hours, group-2 requires 7.15 hours, group-3 requires 9.0 hours and group-4 requires 10.05 hours of charging.

From the driving cycle and the time required for charging of batteries, we can conclude that group-4 batteries require the maximum amount of charging time. This results in increased cost of charging. Additionally, group-4 batteries require the maximum amount of energy to complete a given trip. On the other hand the group-1 batteries require the minimum amount of time for charging and require the minimum percentage of SOC on the

battery to complete the trip. Hence, the cost for the trip would be minimized if we charge the battery at the cheapest hour price.

Now, with the day-ahead prediction of energy prices on the grid, we can minimize the cost of charging the electric vehicles. We know the amount of energy required by our vehicle to complete a trip and the price of energy available on the grid. This helps us to initiate charging only at the lowest prices.

In the smart grid scenario, we can not only minimize the charging costs of the electric vehicles but also minimize the travel cost by exchanging excess energy in the battery with the grid at times where the per unit energy costs are the highest and earning a revenue to minimize the cost of the trip traveled.

5.3 Cost Function for the Trip

We will consider day-ahead prices for charging the electric vehicles, the power supplied and power available for exchange from the electric vehicles is known. There are 100 vehicles in each of the four battery groups for charging and exchanging energy with the grid, so total number of vehicles used in the simulation study is 400. Each group batteries has two operations charging battery using energy from the grid and supplying excess energy to the grid. Charging energy from the grid is represented by group $pb1_i$, $pb2_i$, $pb3_i$ and $pb4_i$. Discharging energy to the grid is represented by group $pb5_i$, $pb6_i$, $pb7_i$ and $pb8_i$. The optimum cost during the charging and discharging is the hourly summation of the energy supplied by the grid at its hourly price and the energy supplied to the grid at its hourly price. Battery charging using from the grid and discharging to the grid is explained by the objective function

$$Cost = Max \sum_{i=1}^{i=24} [(pb5_i * C_i * x_5 + pb6_i * C_i * x_6 + pb7_i * C_i * x_7 + pb8_i * C_i * x_8) - (pb1_i * C_i * x_1 + pb2_i * C_i * x_2 + pb3_i * C_i * x_3 + pb4_i * C_i * x_4)] \quad (5.1)$$

where,

C_i : is the energy cost per hour

$pb1_i$: is the energy supplied to battery during any specific hour from Group-1

$pb2_i$: is the energy supplied to battery during any specific hour from Group-2

$pb3_i$: is the energy supplied to battery during any specific hour from Group-3

$pb4_i$: is the energy supplied to battery during any specific hour from Group-4

$pb5_i$: is the battery energy exchanged with the grid at any specific hour from Group-1

$pb6_i$: is the battery energy exchanged with the grid at any specific hour from Group-2

$pb7_i$: is the battery energy exchanged with the grid at any specific hour from Group-3

$pb8_i$: is the battery energy exchanged with the grid at any specific hour from Group-4

$x_5 - x_8$: is the number of batteries from each of the 4 group at any specific hour

$x_1 - x_4$: is the number of batteries connected to the grid from group 1 to 4 respectively

The charging cost is dependent on the hourly price fixed by the grid. Also the vehicle to grid price is fixed by the grid but the vehicle to grid energy exchange will be the profit of the integrator and the user.

The charging and discharging process have their own limitations. The charging process is constrained with the infrastructure and the maximum power which can be supplied to the battery during an hour. It is assumed that the maximum number of batteries connected to the grid for charging from a single group is 100. In vehicle to grid scenario, the energy available for exchange is dependent on the health of the battery. Batteries with higher internal resistance have lower energy available for exchange whereas batteries with small internal resistance have greater amount of energy available for exchange. The energy capacity for all the group batteries during exchange to the grid is variable.

5.4 Opportunity Cost

We assume that we have the knowledge of the cost of charging and cost of discharging on a specific day of the week. This knowledge provides us the cost of energy on the specific day from which we estimate the charging and discharging pattern. We define opportunity cost as

$$\text{Opportunity Cost} = \frac{\text{Money Spent on Charging (\$/ KWh)}}{\text{Money Earned from Exchanging (\$/ KWh)}} \quad (5.2)$$

To derive the opportunity cost, we require the average cost for charging of batteries from group 1 to group 4 and money earned by exchanging energy with the grid from group 5 to group 8 batteries. Batteries from group 1 to group 4 are assumed to have 16.5KWh of on-board energy when they are completely charged. Batteries from group 5 to group 8 have varied energy for exchange. Opportunity cost would be a measure to evaluate the performance of a particular group of batteries on a specific day for which we have access to forecast price of charging and have knowledge of the trip we are planning to travel.

The opportunity cost gives the exact profit percentage of the electric vehicle for daily operation. If the opportunity cost is greater than 1, then we incur loss in the transaction. The alternative charging and discharging patterns will be suggested to avoid loss. One of the methods will be to limit the charging state of charge of the electric vehicle. Smaller the opportunity cost greater is the profit on diurnal basis. Hence, the opportunity cost will be used to specify the charging hours and discharging hour for optimum performance of the batteries.

5.5 Optimization Problem

In near future, there will be rise in the number of electric vehicles on the road. The rise will force us to move towards battery charging stations instead of charging the batteries on the household grid. The operational cost for the integrators is dependent on the charging times and opportunity to exchange energy with the grid. The integrator has the knowledge of the next day's price of the electricity on the grid, knowledge of the age of the batteries and knowledge of the daily driving trip. The integrator's operational profits will be from minimizing the charging costs and gaining maximum profit by exchanging energy to the grid.

The grid declares its hourly price a day prior in advance. An optimization problem can be formulated as below.

$$G_{price} = \{X_1, X_2, X_3, \dots, X_{24}\} \quad (5.3)$$

where, G_{price} : Hourly strategy of the grid price

X_{1-24} : Unit hourly price declared by grid at 12:00 AM to 23:00 PM in \$/MW

The next part of the optimization problem is for the integrator to strategize and minimize the operation cost. The integrator has large set of batteries with variable resistances. The variation in the internal resistance changes the behavior of the battery. As the internal resistance rises the charging time for the battery increases. A battery with high internal resistance more energy in driving compared to lower internal resistance batteries and it will have lesser energy to transfer when we connect vehicle to the grid. Hence, it is important

for integrator to decide on the charging times for each group of the battery. Also, the integrator earns money during the heavy load and high price hours. The strategy by the integrator can be explained as

$$I_{price} = \sum \{Y_1 + Y_2 + Y_3 + \dots Y_{12}\} - \{Z_1 + Z_2 + Z_3 + \dots Z_{12}\} \quad (5.4)$$

where, I_{price} : Hourly strategy of the integrator

Y_1 : Hourly price of charging batteries from grid at 6:00 pm

Y_2 : Hourly price of charging batteries from grid at 7:00 pm

Y_3 :Hourly price of charging batteries from grid at 8:00 pm

Y_4 : Hourly price of charging batteries from grid at 9:00 pm

Y_5 : Hourly price of charging batteries from grid at 10:00 pm

Y_6 : Hourly price of charging batteries from grid at 11:00 pm

Y_7 : Hourly price of charging batteries from grid at 12:00 am

Y_8 : Hourly price of charging batteries from grid at 1:00 am

Y_9 : Hourly price of charging batteries from grid at 2:00 am

Y_{10} : Hourly price of charging batteries from grid at 3:00 am

Y_{11} : Hourly price of charging batteries from grid at 4:00 am

Y_{12} : Hourly price of charging batteries from grid at 5:00 am

Z_1 : Hourly price earned from vehicle to grid 6:00 am

Z_2 : Hourly price earned from vehicle to grid 7:00 am

Z_3 : Hourly price earned from vehicle to grid 8:00 am

Z_4 : Hourly price earned from vehicle to grid 9:00 am

Z_5 : Hourly price earned from vehicle to grid 10:00 am

Z_6 :Hourly price earned from vehicle to grid 11:00 am

Z_7 : Hourly price of charging batteries from grid at 12:00 pm

Z_8 : Hourly price of charging batteries from grid at 1:00 pm

Z_9 : Hourly price of charging batteries from grid at 2:00 pm

Z_{10} : Hourly price of charging batteries from grid at 3:00 pm

Z_{11} : Hourly price of charging batteries from grid at 4:00 pm

Z_{12} : Hourly price of charging batteries from grid at 5:00 pm

The constraints to the problem are given as below

- The energy consumed by each battery should be equal to 16.5 KWh.

- The energy from vehicle to grid is limited the remaining energy on the battery from group 1 to group 4
- Limit on the number of batteries that can be connected to the grid per hour

Thus in this optimization problem formulation, the intention is to find the optimal strategy for a given day by the integrator. The stroky which is based on the energy pricing announced. It is also dependent on the charging and discharging cycle by the grid

5.6 Simulation Results

Our research objective is to maximize our profit by selling extra amount of energy available within the batteries of various groups. We assume there are 400 vehicles in our simulation study. The owners of these vehicles charge the batteries at their residence. We use linear programming technique to solve our problem. We will be considering various cases for optimizing the operation of electric vehicle batteries. In this research study, we start our day at 7.00pm in the day and complete the cycle at 6:00pm the next day to complete a 24-hour cycle (Midwest ISO, n.d.).

5.6.1 Case 1

We charge all the batteries to 80% SOC and use these batteries for the driving cycle. We know the energy required for completing the trip. Thus, we know the energy available from all the groups at any specific hour which could be available for exchange with the grid. All the batteries are available for exchange from the vehicle to the grid (V2G) at any given hour of the day.

Table 5-3. Battery energy capacity available for exchange

Name	Battery Age (years)	Energy (KWh)/EV
Group 5	0-1.5	6.25
Group 6	1.5-3.0	5.88
Group 7	3.0-4.5	4.99
Group 8	4.5-6.0	3.88

The energy available for exchanging with the grid is as shown in Table 5-3. The energy supplied during charging and the time required to charge the battery is shown in Figure 5.2.

We get the optimized cost of the trip with the specific energy used for charging and selling the energy at the highest cost during the day. We use cost for the energy from the Midwest Independent Transmission System Operator. We have access to all the batteries from 6:00 am to 6:00 pm for exchanging energy with the grid. The trip cost for 400 vehicles was \$195.822.

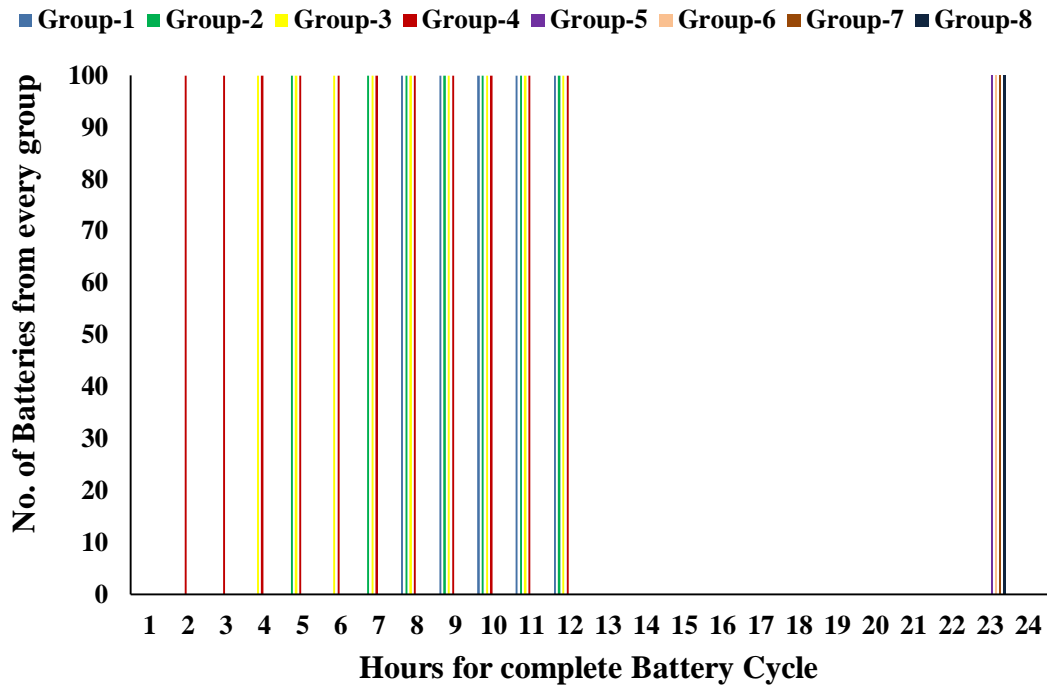


Figure 5.3. Batteries performance during charge from and discharge to grid

5.6.2 Case 2

We assume that we have a limited number of batteries for V2G for every hour from all the groups. We limit the batteries that we can connect to the grid at any point to 15 from each group. We have energy available for exchange as given in Table 5-3.

The performance cost of the batteries under the above specified conditions is \$217.805.

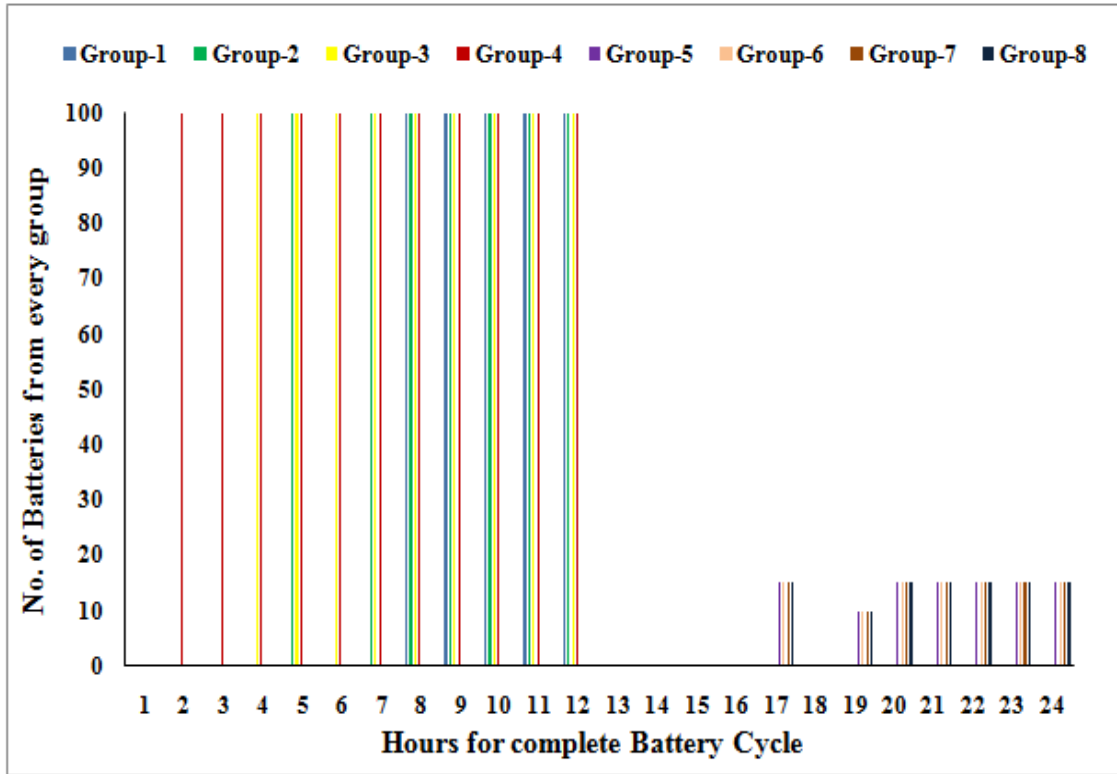


Figure 5.4. Limited batteries performance during charge from and discharge to grid

5.6.3 Summer Battery Cycle

In this case, we limit the maximum energy the user trades with the grid. We assume that the maximum energy requirement of the grid from the batteries is 450KWh at any hour of the day. The data we simulate is for a week in summer i.e. from 7/30/2012 (Monday) to 8/3/2012 (Friday).

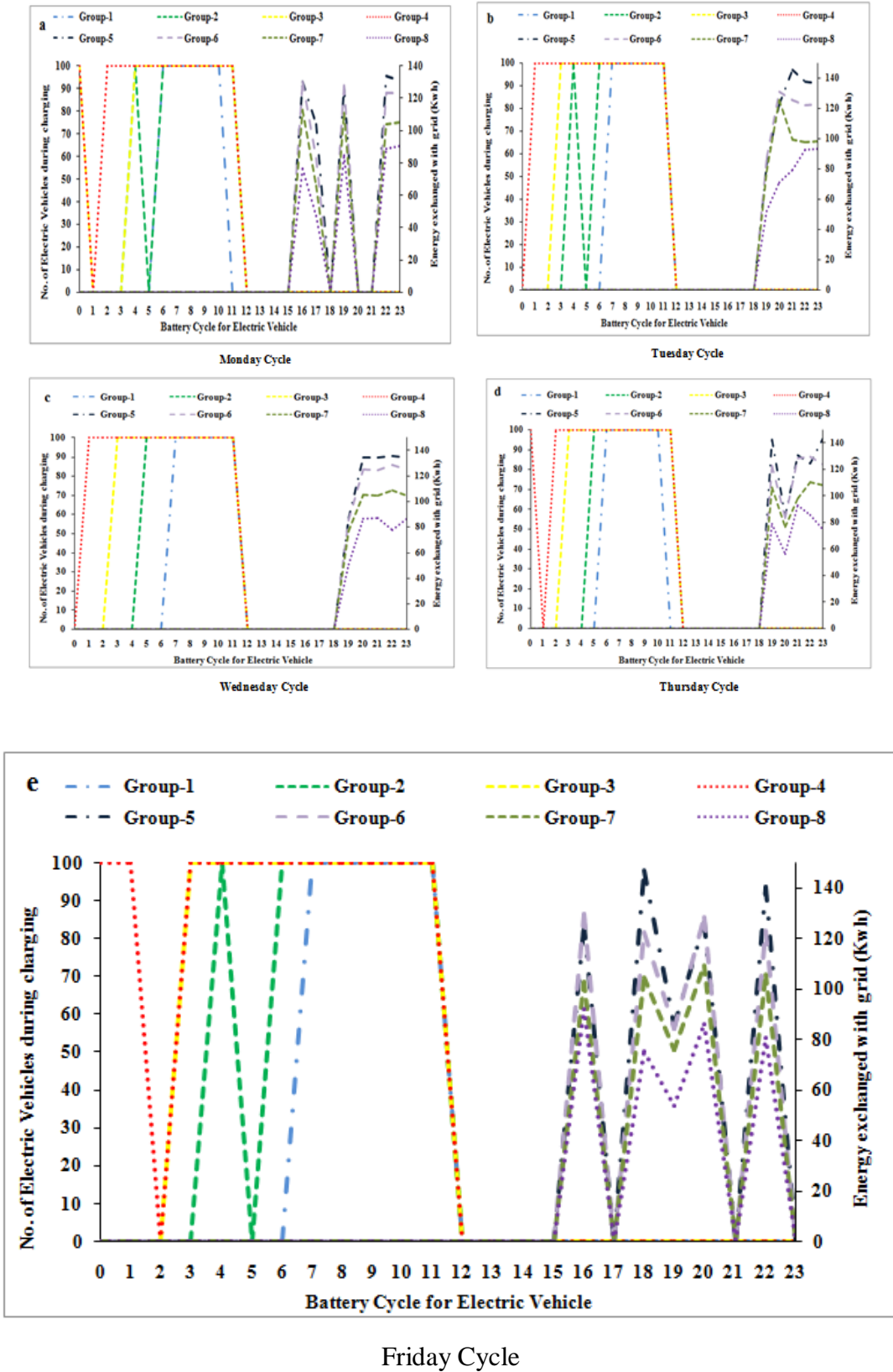


Figure 5.5. Performance of batteries during a week in summer

We use Matlab *Linprog* function to simulate our data and find the optimized cost of charging of the batteries for all the groups. We studied the charging of batteries and discharging of batteries for a week in summer 2012. We assumed that our battery cycle begins at 7:00pm and is completed at 7:00pm the next day. We assumed that the batteries charge from 7:00pm to 7:00am. The batteries are assumed to be at 30% SOC at the beginning of the charging cycle. Total numbers of batteries which are connected for charging from 7:00pm to 7:00 am are represented by Group-1 to Group-4 in Figure 5.5. The amount of energy the batteries exchange with the grid at any hour from 7:00am to 7:00pm is given by group-5 to group-8 in Figure 5.5.

Table 5-4. Cost of battery cycle per day in summer

	Monday	Tuesday	Wednesday	Thursday	Friday
Cost Function	149.03	229.58	158.19	246.40	231.92

The total cost of battery cycle to the user for a weekday is shown as in Table 5-4. This cost includes the cost of charging and exchanging energy to the grid.

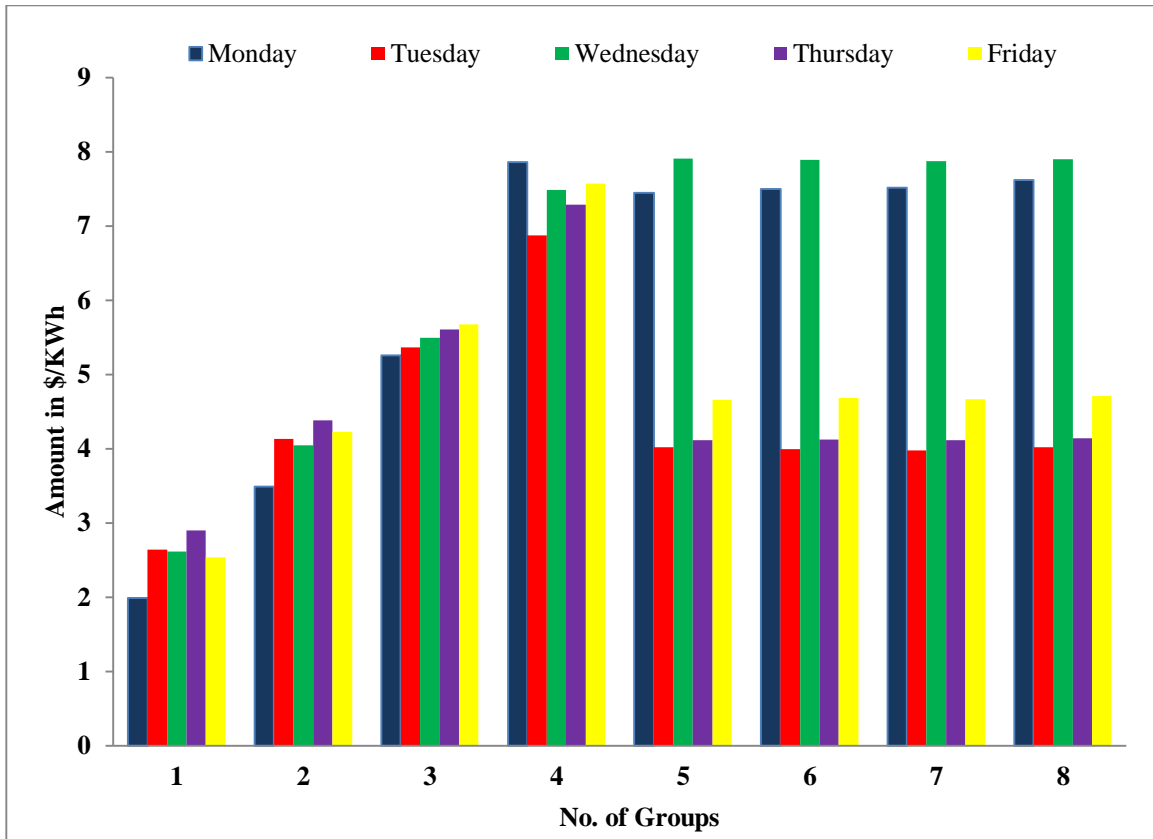


Figure 5.6. The average performance of batteries in summer

We calculate the total cost of charging batteries from group-1 to group-4. Then we calculate the profit earned by exchanging available energy in the batteries with the grid. Thus, we have the estimated costs of energy per kilowatt in charging from G2V and discharging from V2G. The cost for group-1 to group-8 is as shown in Figure 5.6.

In Figure 5.6, we can see that group-1 to group-4 is the average performance of batteries during charging i.e. G2V whereas group-5 to group-8 is the average performance to the batteries during discharging i.e. V2G. Group-5 consists of batteries from group-1 during V2G, group-6 consist batteries from group-2 during V2G, group-7 consists batteries from group-3 during V2G and group-8 consists batteries from group-4 during V2G.

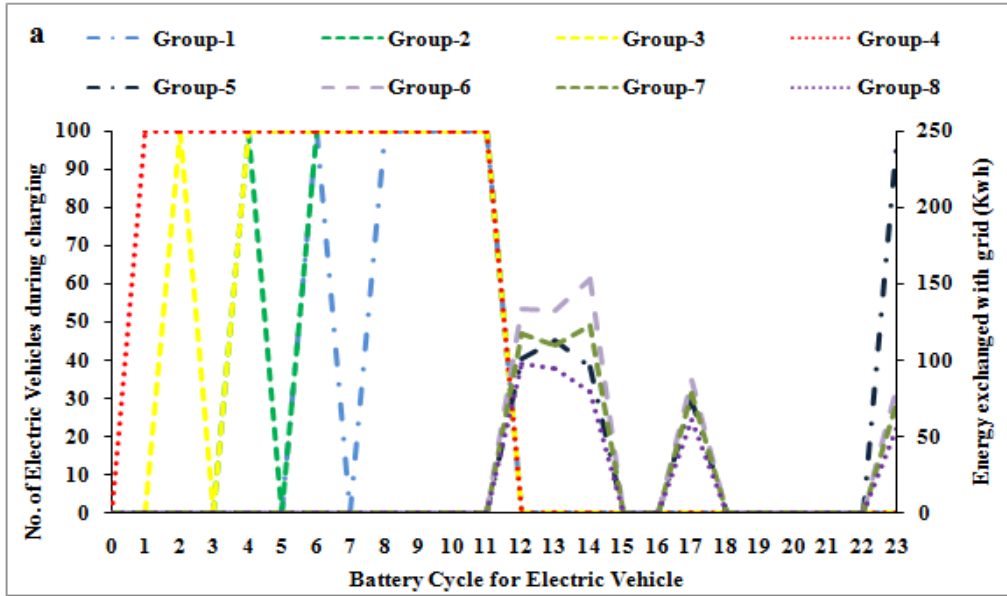
Table 5-5. Opportunity cost for a week in summer

	Monday	Tuesday	Wednesday	Thursday	Friday
OCB-1	0.26	0.65	0.33	0.70	0.54
OCB-2	0.46	1.03	0.51	1.06	0.90
OCB-3	0.69	1.34	0.69	1.36	1.21
OCB-4	1.03	1.71	0.94	1.75	1.60

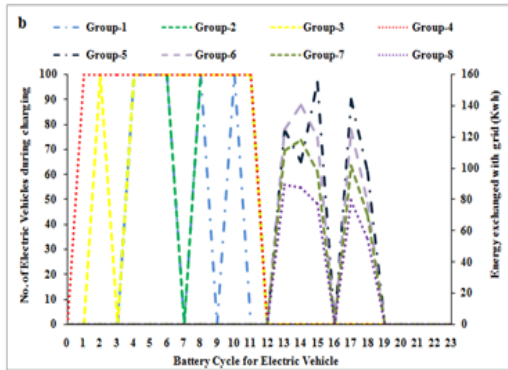
We calculate the opportunity cost from equation 5.2. The opportunity cost is a measure of profit through average exchange with the grid (grid2vehicle and vehicle2grid). It is clear from the opportunity cost function that smaller the opportunity cost, greater is the profit. An opportunity cost greater than 1 indicates that we spent more on charging the batteries than we earned by selling excess energy to the grid.

5.6.4 Winter Battery Cycle

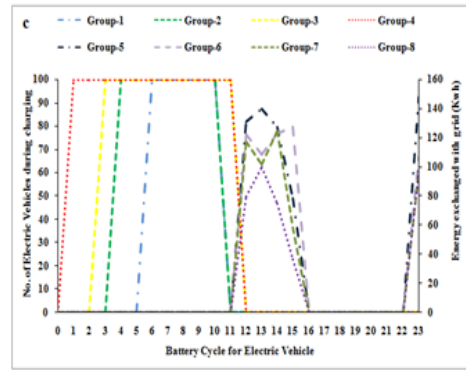
We use a similar analysis as in Case-3 to simulate a week's data during winter i.e. from 01/09/2012 to 01/13/2012 (Monday to Friday). We limit the energy requirement from the grid to 450KWh.



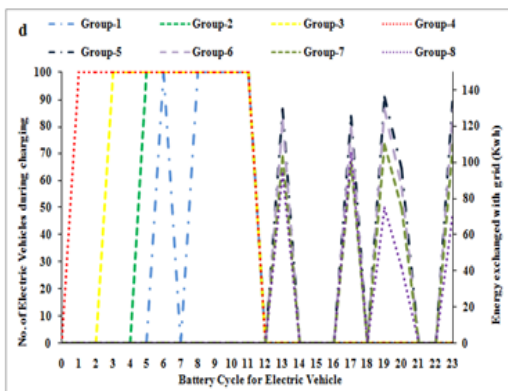
Monday Cycle



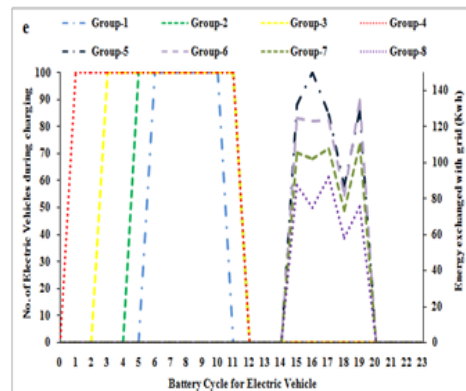
Tuesday Cycle



Wednesday Cycle



Thursday Cycle



Friday Cycle

Figure 5.7. Performance of batteries during a week in winter

The simulation results for a week in winter help us to understand the load distribution of the electric vehicles on the grid. It also helps us to understand the exact period that is beneficial to the user to connect the electric vehicles to support the grid for earning maximum profit. We charge the batteries from 7.00pm to 7.00am. The batteries are available for exchange anytime of the day and the grid requirement is set the maximum to 450KWh.

Table 5-6. Cost of battery cycle per day in winter

	Monday	Tuesday	Wednesday	Thursday	Friday
Cost Function	67.32	229.54	207.57	206.74	278.59

We get the cost functions for weekdays for a period of one week in winter as given in Table 5-6. The cost value comprises of charging cost and the grid exchange cost.

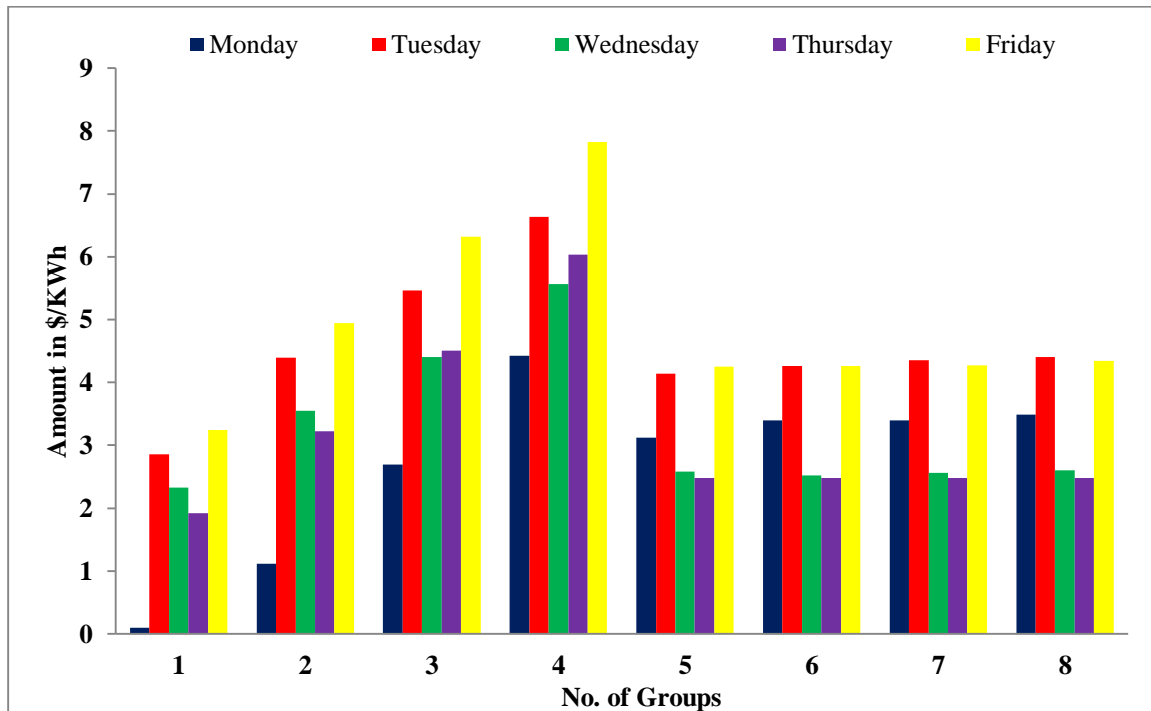


Figure 5.8. Costs incurred and gained during charging and exchanging energy with grid in winter

Figure 5.8, illustrates the cost of charging for group-1 to group-4 batteries during a week. The profit earned by exchanging energy with the grid is known from the values of group-5 to group-8. We calculate the opportunity cost as given in equation 5.2. Group-1 to group-4 is the average performance of batteries during charging per hour whereas group-5 to group-8 is the average performance to the batteries during the exchange to the grid per hour. Group-5 consists of batteries from group-1 which exchange energy to the grid, group-6 consist batteries from group-2 which exchange energy to the grid, group-7 consist batteries from group-3 which exchange energy to the grid and group-8 consist batteries from group-4 which exchange energy to the grid.

Table 5-7. Opportunity Cost for a week in winter

	Monday	Tuesday	Wednesday	Thursday	Friday
OCB-1	0.03	0.69	0.90	0.77	0.76
OCB-2	0.32	1.03	1.40	1.30	1.15
OCB-3	0.79	1.25	1.71	1.82	1.47
OCB-4	1.26	1.50	2.14	2.43	1.80

Looking at the data from Table 5-5 and Table 5-7 and applying the opportunity cost, we can observe that there are cases of loss with the current operation pattern. We intend to reduce the cost of charging by charging the batteries to cater the trip in the cases where losses are registered. Our intention is to reduce the battery cycle cost by reducing the energy level on the battery which facilitates charging batteries to lower energy level.

5.6.5 Summer Battery Cycle - Reducing Charging Time

Based on the opportunity costs for each group of batteries for summer and winter as in Table 5-5 and Table 5-7, we reduce the charging costs for each group of batteries. Drivers charge the batteries to limited SOC which is required to complete our specific driving trip. We do not charge the batteries completely to their full capacities. This reduces the number of hours for charging of the batteries and in turn reduces their charging costs. The charging of electric vehicles from the grid and discharging to the grid for a week in summer varies across the group and the day of the week as shown in Figure 5.5. This results in variation in SOC to which batteries are charged.

Table 5-8. Charging Batteries with variation in SOC during summer

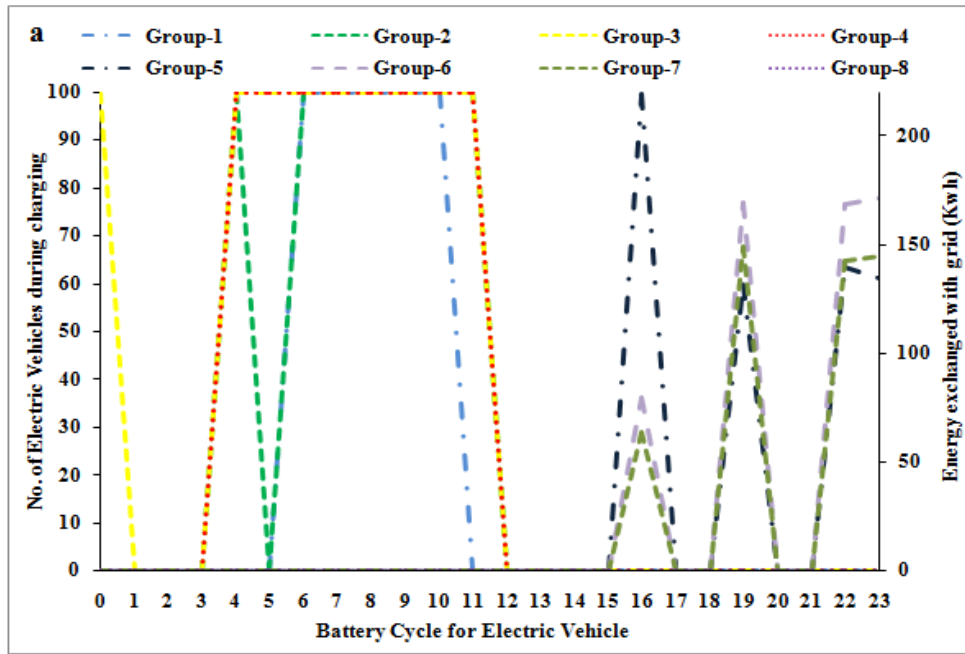
	Monday	Tuesday	Wednesday	Thursday	Friday
Group 1	80%	80%	80%	80%	80%
Group 2	80%	80%	80%	75%	80%
Group 3	80%	65%	80%	65%	65%
Group 4	70%	70%	80%	70%	70%

When batteries from group-3 and group-4 are charged to 65% and 70% respectively it indicates that the batteries from these groups do not take part in the exchange of energy to the grid. The stored energy in these batteries is used only for completing the trip.

We can see from Figure 5.9, the charging times of group-1 to group-4 batteries to the state of charge as shown in Table 5-8. We also see the energy exchanged from the batteries to the grid at different times in a day. The cost breakup for batteries taking part in an exercise during a week in summer is as given below.

Table 5-9. Cost of battery cycle per day for a week in summer with varied SOC

	Monday	Tuesday	Wednesday	Thursday	Friday
Cost Function	104.13	189.35	158.19	189.80	189.67



Monday Cycle

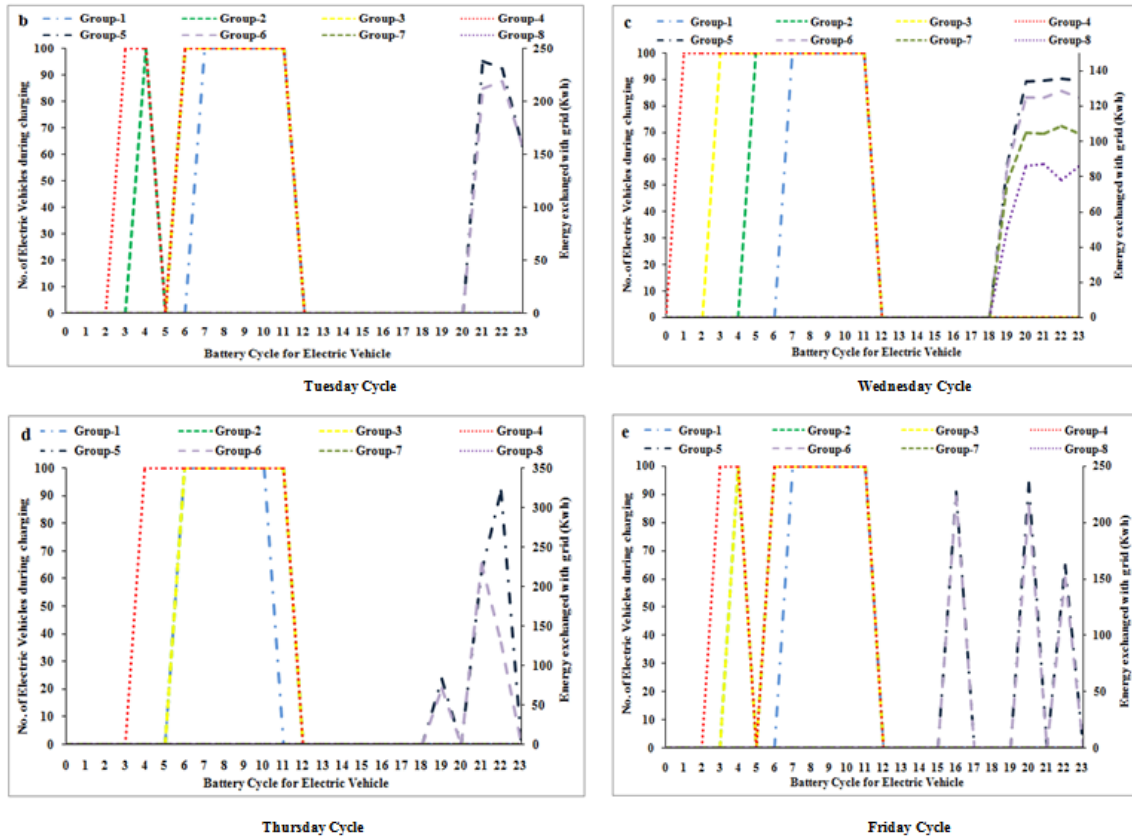


Figure 5.9. Performance of batteries during a week in summer with varied state of charge

We can observe comparing cost functions from Table 5-4 and Table 5-9 that we spend lesser amount for battery cycle for each day. The knowledge of charging and exchange of energy i.e. V2G demonstrates the average charging cost of the battery per day and the average cost of exchanging energy per day. This is shown as in the figure below.

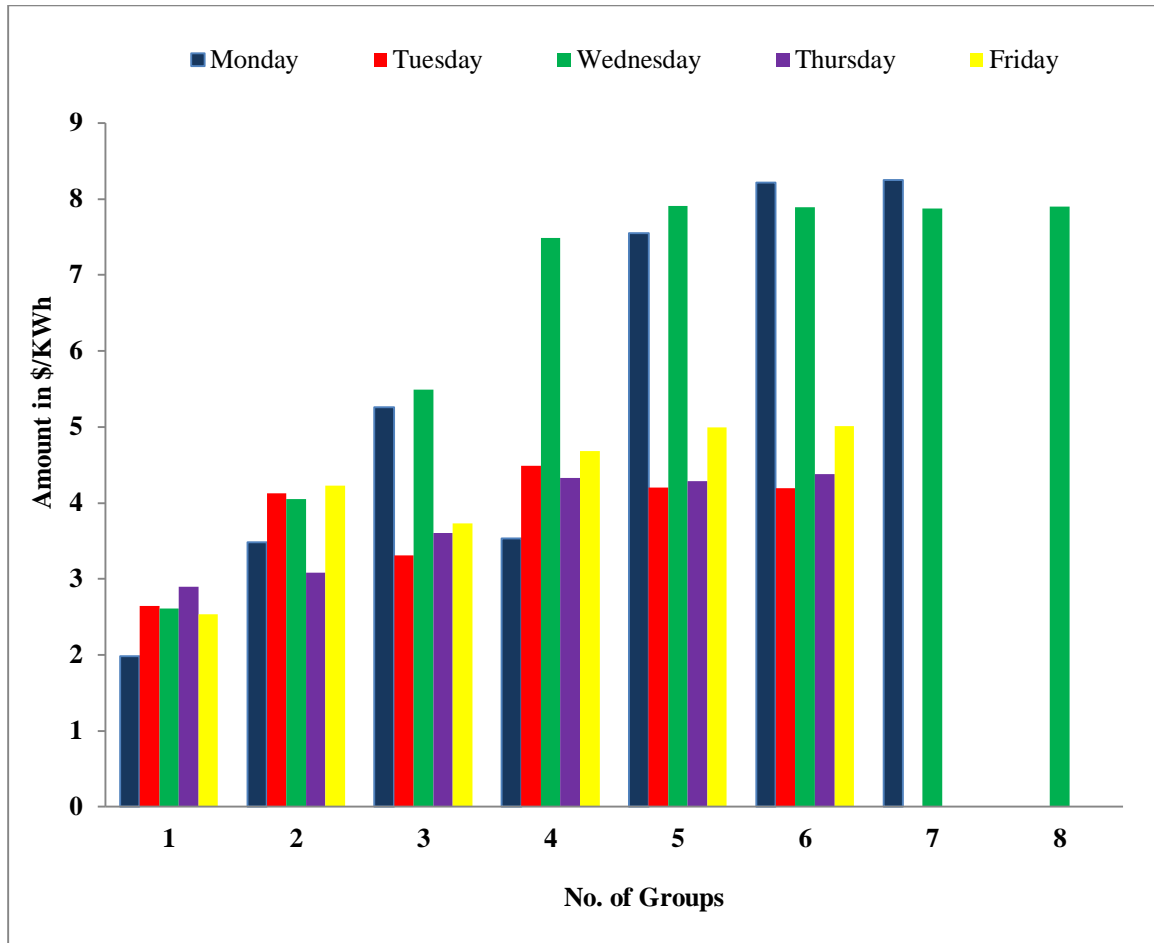


Figure 5.10. Costs incurred and gained during charging and exchanging energy with grid in summer

We can observe from Figure 5.10 that group-8 batteries take part in exchanging energy to the grid on Wednesdays only. Group-8 batteries are batteries from group 4 which are used during V2G. Group-7 batteries are used for exchanging energy to the grid on Mondays and Wednesdays only. The opportunity cost function would be a measure of the profit for batteries taking part in the exercise.

Table 5-10. Opportunity Cost for a week in summer

	Monday	Tuesday	Wednesday	Thursday	Friday
OCB-1	0.26	0.62	0.33	0.67	0.50
OCB-2	0.42	0.98	0.51	0.70	0.84
OCB-3	0.63	NR	0.69	NR	NR
OCB-4	NR	NR	0.94	NR	NR

From the results in Table 5-10, we can clearly observe that opportunity cost for group 1 and group 2 batteries for all the days during summer is below 1.0 which indicates profit for the user. The batteries which just complete the driving trip have their function as “NR” no result as these batteries do not take part in exchanging energy with the grid. In this case, we try to optimize the values by reducing the final state of charge for group 3 and group 4 in cases where we observe that the opportunity cost function is greater than 1.0 in Table 5-5.

5.6.6 Winter Battery Cycle - Reducing Charging Time

Similar to situation discussed in section 5.6.5, we will calculate the cost functions by reducing the charging time for each group of battery. We do not charge the batteries for groups which have their opportunity cost functions greater than 1.0 i.e. to their full capacities. We charge the batteries for all groups as mentioned below.

Table 5-11. Charging Batteries with variation in SOC during winter

	Monday	Tuesday	Wednesday	Thursday	Friday
Group 1	80%	80%	80%	80%	80%
Group 2	80%	80%	75%	75%	75%
Group 3	80%	65%	65%	65%	65%
Group 4	70%	70%	70%	70%	70%

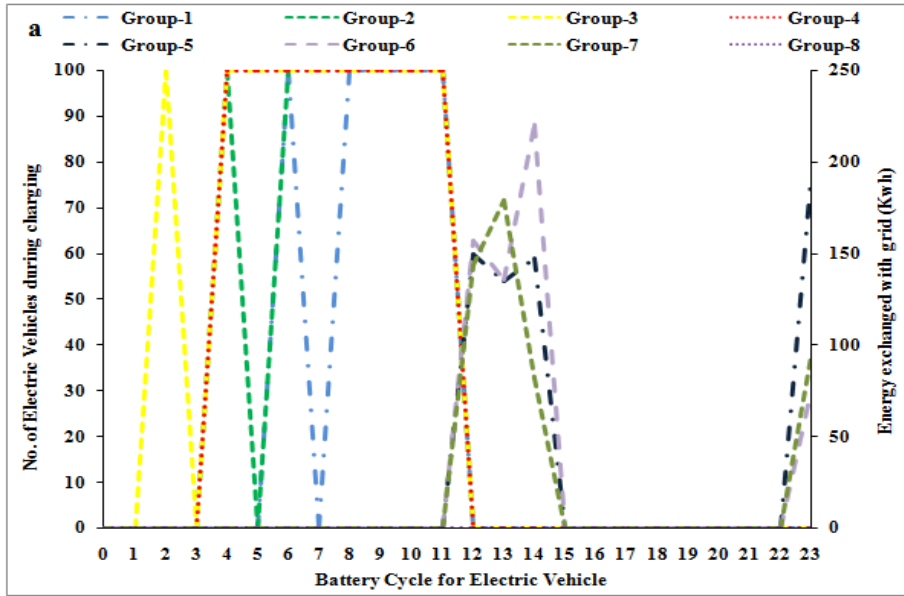
When batteries from group-3 and group-4 are charged to 65% and 70% respectively, it indicates that the batteries from that group do not take part in the exchange of energy with the grid.

The charging and discharging patterns for group-1 to group-8 batteries are demonstrated in Figure 5.11. The cost functions for these batteries are given in the table below.

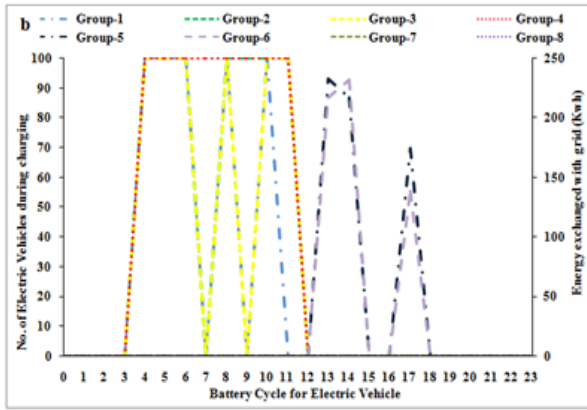
Table 5-12. Cost of battery cycle per day for a week in winter with varied SOC

	Monday	Tuesday	Wednesday	Thursday	Friday
Cost Function	33.68	177.95	161.13	139.71	209.25

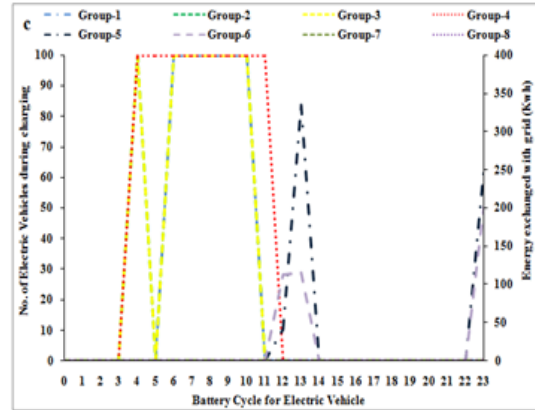
When we compare the cost functions for batteries in Table 5-7 and Table 5-12, we clearly see that the cost functions for battery cycle per day for a week in winter with the varied state of charge is lower than the completely charged batteries. As we calculated the charging and discharging cost for batteries in this exercise during summer, we also calculate the same cost during winter.



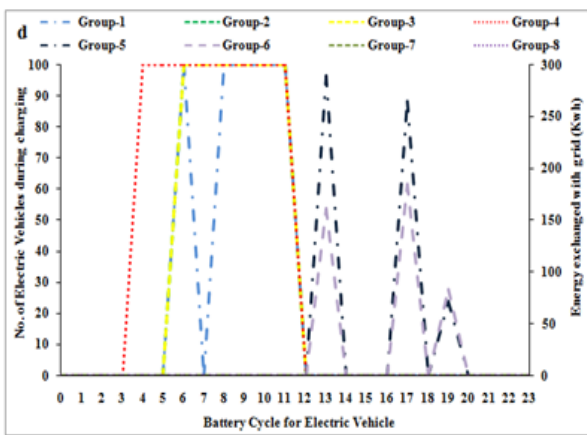
Monday Cycle



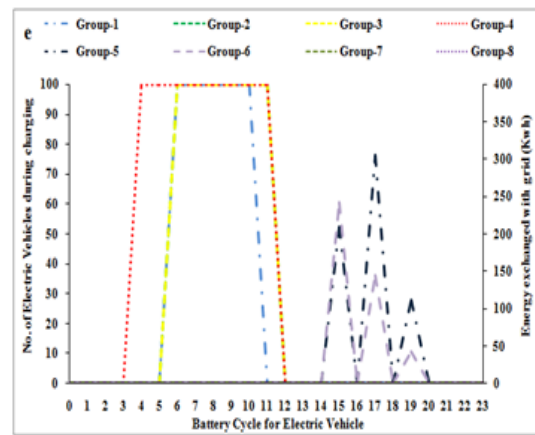
Tuesday Cycle



Wednesday Cycle



Thursday Cycle



Friday Cycle

Figure 5.11. Performance of batteries during a week in winter with varied state of charge

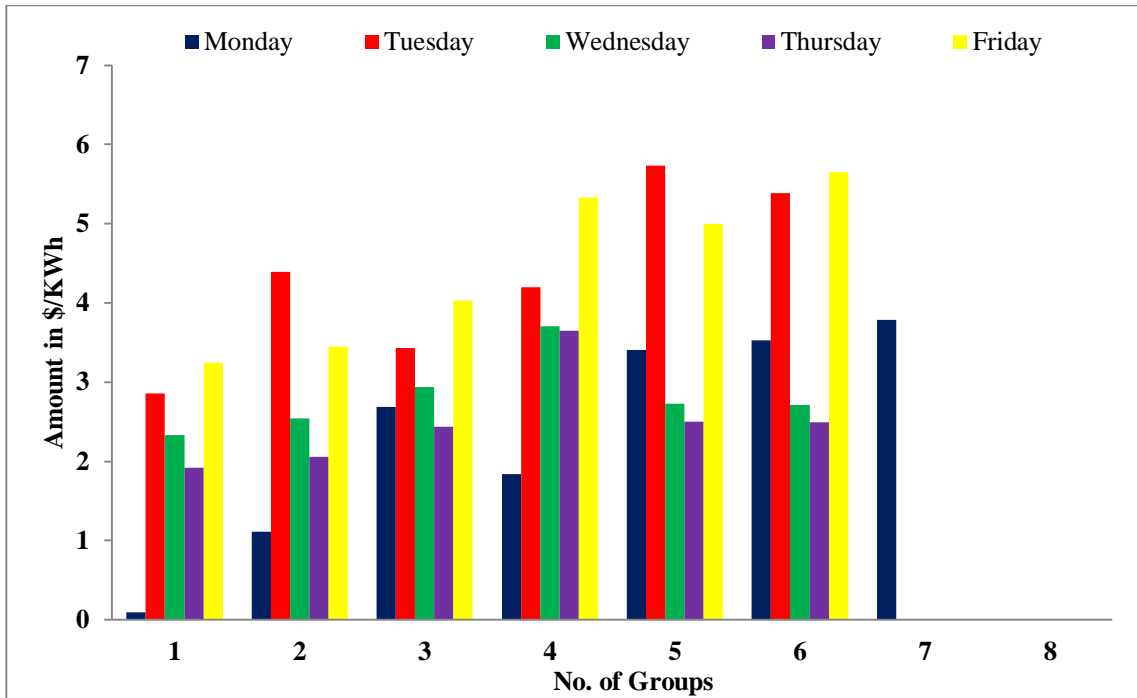


Figure 5.12. Costs incurred and gained during charging and exchanging energy with grid in winter

From Figure 5.12 we observe group-8 batteries only cater the driving trip and do not take part in the exercise for exchanging energy from the electric vehicle battery to the grid. We also observe that group-7 batteries take part in the exchange of energy with the grid on Mondays only and the batteries fulfill the driving trip during the rest of the days of the week

Table 5-13. Opportunity Cost for a week in winter

	Monday	Tuesday	Wednesday	Thursday	Friday
OCB-1	0.02	0.49	0.85	0.76	0.65
OCB-2	0.31	0.81	0.93	0.82	0.61
OCB-3	0.71	NR	NR	NR	NR
OCB-4	NR	NR	NR	NR	NR

From the results in Table 5-13, we can clearly observe that opportunity cost for all the days during winter is less than 1.0 which indicates profit for the user. The batteries which just complete the driving trip have their function as “NR” no result as these batteries do not take part in exchanging energy with the grid. In this case, we try to optimize the values by reducing the final state of charge for group 3 and group 4 in cases where we observe that the opportunity cost function is greater than 1.0 in Table 5-7.

5.7 Summary

In this chapter, we simulated and tested the performance of electric vehicle batteries which vary in age in a spatial scheme. The internal resistance of the batteries throughout their life cycle was estimated. The estimated the energy consumed by each age group battery for the same driving trip was also estimated. We have designed and optimized the performance of the electric vehicle batteries on daily driving cycles. We designed the charging strategies for electric vehicles based on the internal resistance of the batteries. The discharging strategies designed will compensate for minimizing the cost by exchanging energy to smart grid. This process also defined various strategies to minimize the user cost of operation of electric vehicles.

6 Effect of Temperature on Battery Performance

In this chapter we study the effect of battery equalization on the performance of the battery and its operational temperature. The operational battery temperature is very crucial for the battery performance. The internal resistance varies with temperature. During the process of equalization, the battery with higher energy level transfers energy to the battery with lower energy level. It is very important to know the effect of battery equalization on the operational temperature of each module.

6.1 Battery Modeling

The battery used in this study is modeled using COMSOL-Multiphysics Software. The battery will be simulated with the electric load which drives the electric vehicle. The thermal model along with battery modeling will be used to study the behavior of the battery. This will indicate the operational temperature of the battery and the transient behavior of the battery.

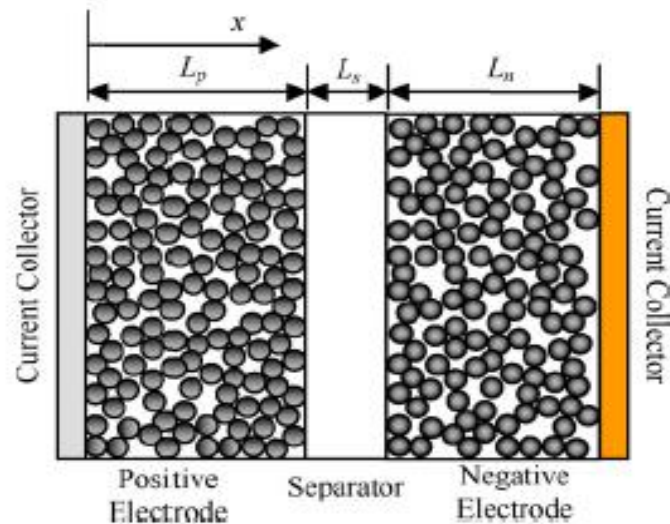


Figure 6.1. Physical model of a lithium ion battery model

A cross section of the Lithium ion cross section is shown in Figure 6.1. The current collector is the outer can for the battery. Aluminum is used as metal for current collector. The positive electrode for the lithium ion battery is LiMn_2O_4 , negative electrode is graphite Li_xC_6 and the liquid electrolyte is LiPF_6 . This lithium ion battery model will be simulated with the driving cycle to learn thermal behavior.

The performance of lithium ion battery is strongly affected by its operational temperature. The operational temperature can be studied on a simulation platform only if a physical model of the battery is studied. A mathematical model of the lithium ion battery is studied to know the thermal behavior of the lithium ion batteries. There is a lithiated organic component which fills in the porous components and serves as the electrolyte.

The following parameters are used to construct lithium ion battery model.

a_s	Specific interfacial area, m^2m^{-3}
c	Concentration of the binary electrolyte, mol m^{-3}
C_p	Specific heat, $\text{J Kg}^{-1}\text{K}^{-1}$
c_s	Concentration of lithium ion in solid mol m^{-3}
D_e	Salt diffusion coefficient m^2s^{-1}
D_s	Diffusion coefficient of lithium ion in solid electrode particles m^2s^{-1}
E_{cell}	Cell Voltage (V)
F	Faraday's constant, 96487 C eq^{-1}
h	Effective heat transfer coefficient $\text{W m}^{-2} \text{K}^{-1}$
I_{app}	Applied current density A m^{-2}

J	Pore wall flux of lithium ions $\text{mol m}^{-2} \text{s}^{-1}$
k	Electrochemical reaction rate constant $\text{m}^{2.5} \text{mol}^{-0.5} \text{s}^{-1}$
L	Thickness of battery component (m)
R	Gas Constant $8.3145 \text{ Jmol}^{-1} \text{ K}^{-1}$
R_s	Radius of electrode particle (m)
t	Time (s)
T	Temperature (K)
t_+	Transference number of lithium ion
U	Open circuit potential (V)
$U_{i,ref}$	Open circuit potential of electrode i under the reference temperature (V)
x	Spatial coordinate
ε	Porosity
ε_f	Volume fraction of fillers
ρ	Density Kg m^{-3}
σ_i	Electronic conductivity of solid matrix S m^{-1}
λ	Thermal conductivity $\text{W m}^{-1} \text{ K}^{-1}$
ϕ_1	Potential in the solid phase (V)
ϕ_2	Potential in the electrolyte phase (V)
max	Maximum
eff	Effective
n	Negative Electrode

p Positive Electrode

s Separator

The material balance for the Li-Ions in an active solid material particle is governed by Fick's second law in spherical coordinates.

$$\frac{\partial c_{s,i}}{\partial t} = D_{s,i} \frac{1}{r^2} \frac{\partial}{\partial r} \left(r^2 \frac{\partial c_{s,i}}{\partial r} \right) \quad (6.1)$$

At the center of the particle there is no flux, "i" will stand for 'p' positive and 'n' negative electrodes respectively is represented as

$$\text{at } r = 0: -D_{s,i} \left(\frac{\partial c_{s,i}}{\partial r} \right) = 0 \quad (6.1.a)$$

At the surface of the particle, the flux is equal to the consumption and production rate of Li ions caused by the electrochemical reaction which takes place at the solid-liquid interface.

$$\text{at } r = R_{s,i}: -D_{s,i} \left(\frac{\partial c_{s,i}}{\partial r} \right) = J_i \quad (6.1.b)$$

J_i is the flux of lithium ions away from the surface of the spherical particles.

The material balance for the binary electrolyte which is in the liquid phase is given by

$$\varepsilon_i \frac{\partial c_i}{\partial t} = \frac{\partial}{\partial x} \left(D_{eff,i} \frac{\partial c_{s,i}}{\partial x} \right) + (1-t_+^0) a_i J_i \quad (6.2)$$

where, i is replaced for positive, negative and separator, a_i is the electrode surface area per unit volume of the electrode. The pore wall flux, J_s in the separator is equal to zero. The mass flux at two boundary conditions for the cell in x -direction is given by

$$-D_{eff,p} \left. \frac{\partial c_p}{\partial x} \right|_{x=0} = 0 \quad (6.2.a)$$

$$-D_{eff,n} \left. \frac{\partial c_n}{\partial x} \right|_{x=L_p+L_s+L_n} = 0 \quad (6.2.b)$$

The concentration of the binary electrolyte and its flux is continuous between the positive electrode and separator and the separator and negative electrode

$$c_p \Big|_{x=L_p^-} = c_p \Big|_{x=L_p^+} \quad (6.2.c)$$

$$c_s \Big|_{x=(L_p+L_s)^-} = c_n \Big|_{x=(L_p+L_s)^+} \quad (6.2.d)$$

$$-D_{eff,p} \left. \frac{\partial c_p}{\partial x} \right|_{x=L_p^-} = -D_{eff,s} \left. \frac{\partial c_s}{\partial x} \right|_{x=L_p^+} \quad (6.2.e)$$

$$-D_{eff,s} \left. \frac{\partial c_s}{\partial x} \right|_{x=(L_p+L_s)^-} = -D_{eff,n} \left. \frac{\partial c_n}{\partial x} \right|_{x=(L_p+L_s)^+} \quad (6.2.f)$$

The effective diffusion coefficient of the binary electrolyte in the liquid phase is corrected by porosity.

$$D_{eff,i} = D_{e,i} \mathcal{E}_i^{brugg_i} \quad (6.2.g)$$

The diffusion coefficient of the binary electrolyte ($D_{e,i}$) is given as

$$D_{e,i} = 10^{-4} \times 10^{-4.43 - \left(\frac{54}{(T-229-5.0 \times 10^{-3} \times c_i)} \right)} - 0.22 \times 10^{-3} c_i \quad (6.3)$$

The charge balance which is governed by Ohm's law in solid state is given by

$$\sigma_{eff,i} \frac{\partial^2 \phi_{1,i}}{\partial x^2} = a_i F J_i \quad (6.4)$$

where, 'i' stands for p and n

The effective conductivity and specific area can be calculated by following formula

$$\sigma_{eff,i} = \sigma_i (1 - \varepsilon_i - \varepsilon_{f,i}) \quad (6.4.a)$$

$$a_i = (3 / R_{s,i}) (1 - \varepsilon_i - \varepsilon_{f,i}) \quad (6.4.b)$$

The charge flux at the interface of the current collector and the positive electrode is equal to the current density applied to the cell.

$$-\sigma_{eff,p} \frac{\partial \phi_{1,p}}{\partial x} \Big|_{x=0} = I_{app} \quad (6.4.c)$$

There is no charge flux at the positive electrode and separator and the separator and negative electrode

$$-\sigma_{eff,p} \frac{\partial \phi_{1,p}}{\partial x} \Big|_{x=L_p} = 0 \quad (6.4.d)$$

$$-\sigma_{eff,p} \left. \frac{\partial \phi_{1,n}}{\partial x} \right|_{x=L_p+L_s} = 0 \quad (6.4.e)$$

The potential of the solid phase along the length of x direction at $x = 0$ and $x = L_p+L_n+L_s$

is given as

$$x=0, \quad \phi_{1,p} \Big|_{x=0} = E_{cell} \quad (6.4.f)$$

$$\phi_{1,n} \Big|_{x=L_p+L_s+L_n} = 0 \quad (6.4.g)$$

Ohm's law defines the charge balance in the liquid phase is given as

$$-\frac{\partial}{\partial x} \left(\kappa_{eff,i} \frac{\partial \phi_{2,i}}{\partial x} \right) + \frac{2RT(1-t_+^0)}{F} \frac{\partial}{\partial x} \left(\kappa_{eff,i} \frac{\partial (\ln c_i)}{\partial x} \right) = a_i F J_i \quad (6.5)$$

The specific conductivity of the binary electrolyte is a function of temperature and concentration.

$$\kappa_{eff,i} = \kappa_{e,i} \mathcal{E}_i^{brugg_i} \quad (6.5.a)$$

The binary electrolyte's ionic conductivity is given as

$$\kappa_i = 10^{-4} \times c_i \left(\begin{array}{l} -10.5 + 0.668 \times 10^{-3} c_i + 0.494 \times 10^{-6} c_i^2 + 0.074T - 1.78 \times 10^{-5} c_i T \\ -8.86 \times 10^{-10} c_i^2 T - 6.96 \times 10^{-5} T^2 + 2.8 \times 10^{-8} c_i T^2 \end{array} \right)^2 \quad (6.5b)$$

The is no charge flux at the two ends of the cell which is given by

$$-\kappa_{eff,p} \frac{\partial \phi_{2,p}}{\partial x} \Big|_{x=0} = 0 \quad (6.6.a)$$

$$-\kappa_{eff,n} \frac{\partial \phi_{2,n}}{\partial x} \Big|_{x=L_p+L_s+L_n} = 0 \quad (6.6.b)$$

At the interfaces of the electrodes and the separator, flux is continuous. Butler-Volmer equation is used to define the flux

$$J_i = k_i (c_{s,i,max} - c_{s,i,surf})^{0.5} c_{s,i,surf}^{0.5} c_i^{0.5} \times \left[\exp\left(\frac{0.5F}{RT} \eta_i\right) - \exp\left(-\frac{0.5F}{RT} \eta_i\right) \right] \quad (6.7)$$

The overpotential of the intercalation reaction is given by

$$\eta_i = \phi_{1,i} - \phi_{2,i} - U_i \quad (6.7a)$$

The energy balance with the boundary conditions determined by Newton's cooling law is given as

$$\rho C_p \frac{dT}{dt} = \lambda \frac{\partial^2 T}{\partial x^2} + Q_{rxn} + Q_{rev} + Q_{ohm} \quad (6.8)$$

$$Q_{rev} = FaJT \frac{\partial U}{\partial T} \quad (6.8.a)$$

$$Q_{ohm} = \sigma_{eff} \left(\frac{\partial \phi_1}{\partial x} \right)^2 + \kappa_{eff} \left(\frac{\partial \phi_2}{\partial x} \right)^2 + \frac{2\kappa_{eff} RT}{F} (1-t_+^0) \frac{\partial(\ln c)}{\partial x} \frac{\partial \phi_2}{\partial x} \quad (6.8.b)$$

where, h is heat transfer coefficient, T_∞ is the environmental temperature.

Q_{rxn} is total reaction heat generation rate, Q_{rev} is total reversible heat generation rate and

Q_{ohm} is total ohmic heat generation rate,

$$Q_{rxn} = FaJ (\phi_1 - \phi_2 - U) \quad (6.9.a)$$

$$Q_{rev} = FaJT \frac{\partial U}{\partial T} \quad (6.9)$$

$$Q_{ohm} = \sigma_{eff} \left(\frac{\partial \phi_1}{\partial x} \right)^2 + \kappa_{eff} \left(\frac{\partial \phi_2}{\partial x} \right)^2 + \frac{2\kappa_{eff}RT}{F} (1-t_+^0) \frac{\partial(\ln c)}{\partial x} \frac{\partial \phi_2}{\partial x} \quad (6.9.c)$$

The temperature which is dependent on the open circuit potential is given by Taylor Series expansion

$$U_i = U_{i,ref} + (T - T_{ref}) \left[\frac{dU}{dT} \right]_i \quad (6.10)$$

6.2 Simulations of Battery Behavior

The lithium ion battery model setup used during our study resembles the "li_battery_drive_cycle" from comsol-multiphysics. The initial conditions for the base battery model are as follows :

Table 6-1. Battery Parameter used for modeling

Parameters	Symbols	Values
Battery capacity	Q_B	16.5 [A*h]
Initial cell voltage	Ecell_init	4.2 [V]
Negative electrode thickness	L_neg	30e-6 [m]
Positive electrode thickness	L_pos	55e-6 [m]
Separator thickness	L_sep	30e-6 [m]
Negative current collector thickness	L_neg_cc	7 [um]
Positive current collector thickness	L_pos_cc	10 [um]
Number of cell layers	n_layers	48
Positive electrode thermal conductivity	kT_pos	1.58 [W/(m*K)]
Negative electrode thermal conductivity	kT_neg	1.04 [W/(m*K)]
Positive current collector thermal conductivity	kT_pos_cc	300 [W/(m*K)]
Negative current collector thermal conductivity	kT_neg_cc	800 [W/(m*K)]
Separator thermal conductivity	kT_sep	2.5 [W/(m*K)]
Positive electrode density	rho_pos	2328.5 [kg/m ³]
Negative electrode density	rho_neg	1347.33 [kg/m ³]
Positive current collector density	rho_pos_cc	2770 [kg/m ³]
Negative current collector density	rho_neg_cc	8933 [kg/m ³]
Separator density	rho_sep	1008.98 [kg/m ³]
Positive electrode heat capacity	Cp_pos	300.21 [J/(kg*K)]
Negative electrode heat capacity	Cp_neg	350.4 [J/(kg*K)]
Positive current collector heat capacity	Cp_pos_cc	150 [J/(kg*K)]
Negative current collector heat capacity	Cp_neg_cc	100 [J/(kg*K)]
Separator heat capacity	Cp_sep	200.16 [J/(kg*K)]
Initial temperature	T_init	298.15 [K]
External temperature	T_ext	298.15 [K]

The current consumed by the lithium ion battery during the trip from 124 West Freistadt Road in Thiensville, while the destination is 3200 North Cramer Street in Milwaukee. The current represented for the trip in c-rate is given as below

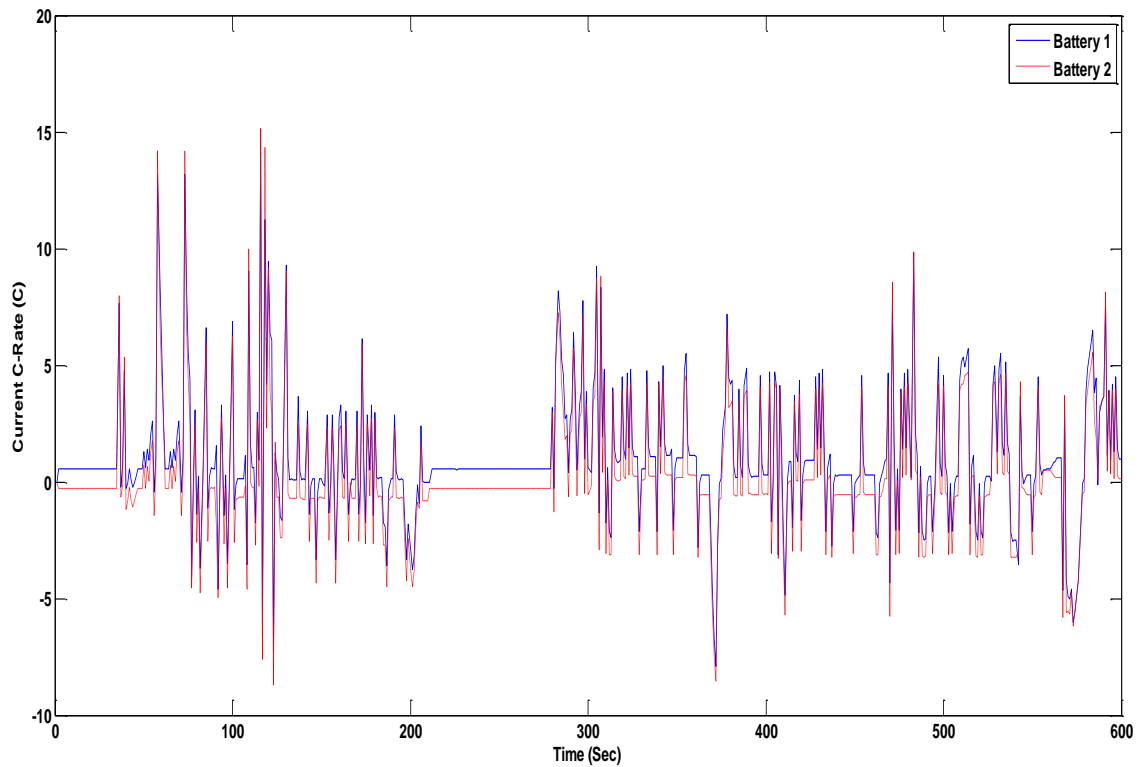


Figure 6.2. C-rate for battery driving cycle

Battery 1 and Battery 2 are simulated with the battery models from Comsol-Multiphysics. We are interested in knowing the exposed temperature in the two batteries. The temperature is a critical factor to be considered in the performance of the lithium ion battery. Battery internal resistance is very sensitive to the instantaneous temperature, as the temperature of the battery rises, the internal resistance also rises.

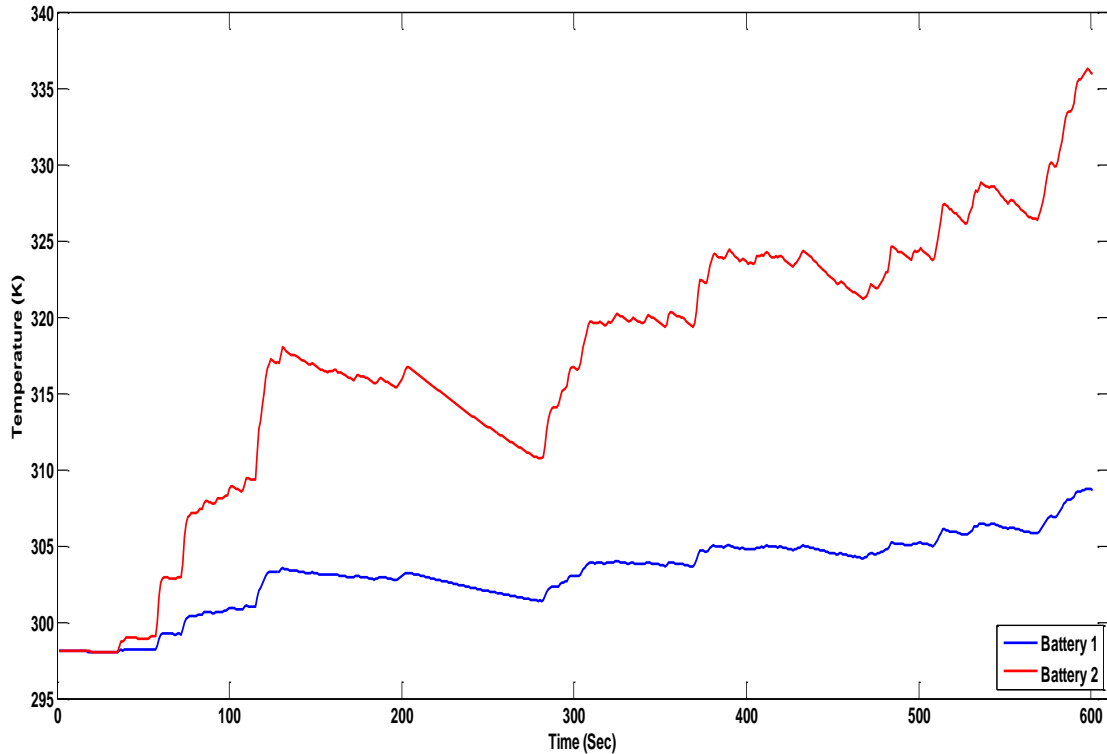


Figure 6.3. Operational temperature of the batteries during the driving cycle

The temperature profiles for Battery 1 and Battery 2 are as given in Figure 6.3. It is evident that battery 2 is exposed to higher temperatures than battery 1. The increased temperature increases the internal resistance of the batteries during the driving cycle which is not accounted for in the circuit based model.

It is impossible to implement physical battery model to estimate the internal resistance or state of charge online for electric vehicle batteries. It is necessary to approximate the internal resistance values based on the temperature the battery is exposed.

Kassem et al represented modeled the effect of temperature on the internal resistance of the batteries with their age and temperature. They conducted a spectroscopic analysis of lithium ion batteries to determine total change in the internal resistance.

Based on their study, we can estimate the internal resistance of the lithium ion battery based on its temperature battery is exposed during the driving trip for battery 1 and battery 2.

This can be done for both batteries battery 1 and battery 2

We use response surface methodology to quantify the internal resistance of battery 1 and battery 2 with the information of the temperature exposure of the lithium ion battery.

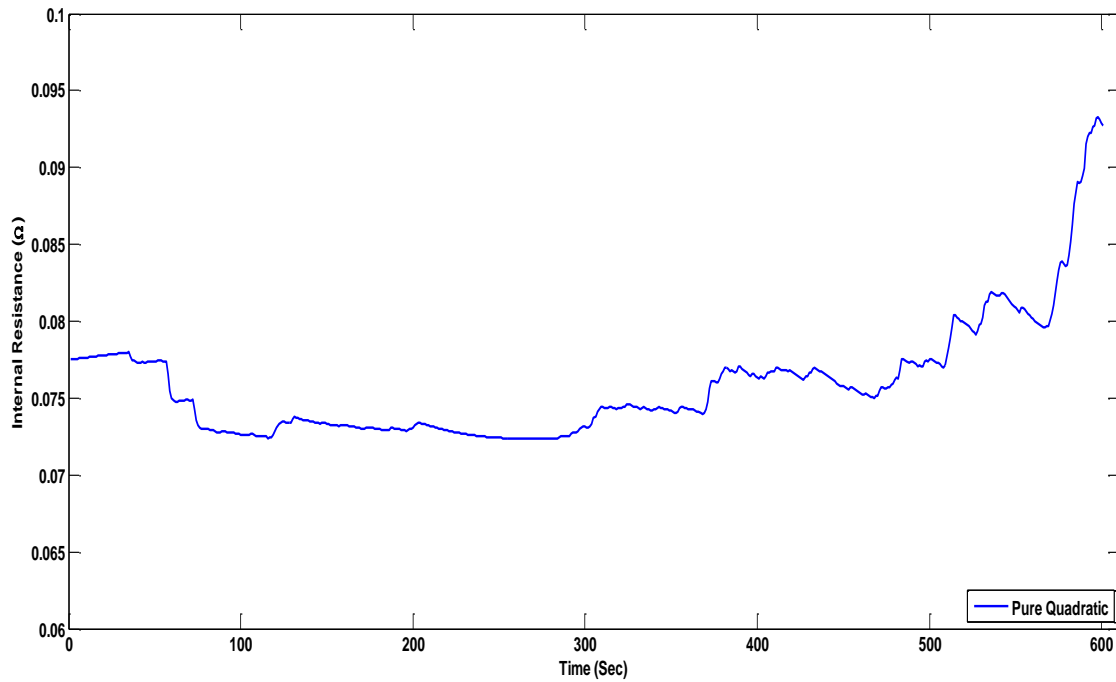


Figure 6.4. Estimated internal resistance for battery 1 from response surface method

It is observed that the estimated internal resistance for battery 2 is close to its initial resistance of 0.075 Ω. There is no significant effect of temperature fluctuations on internal resistance of battery 1.

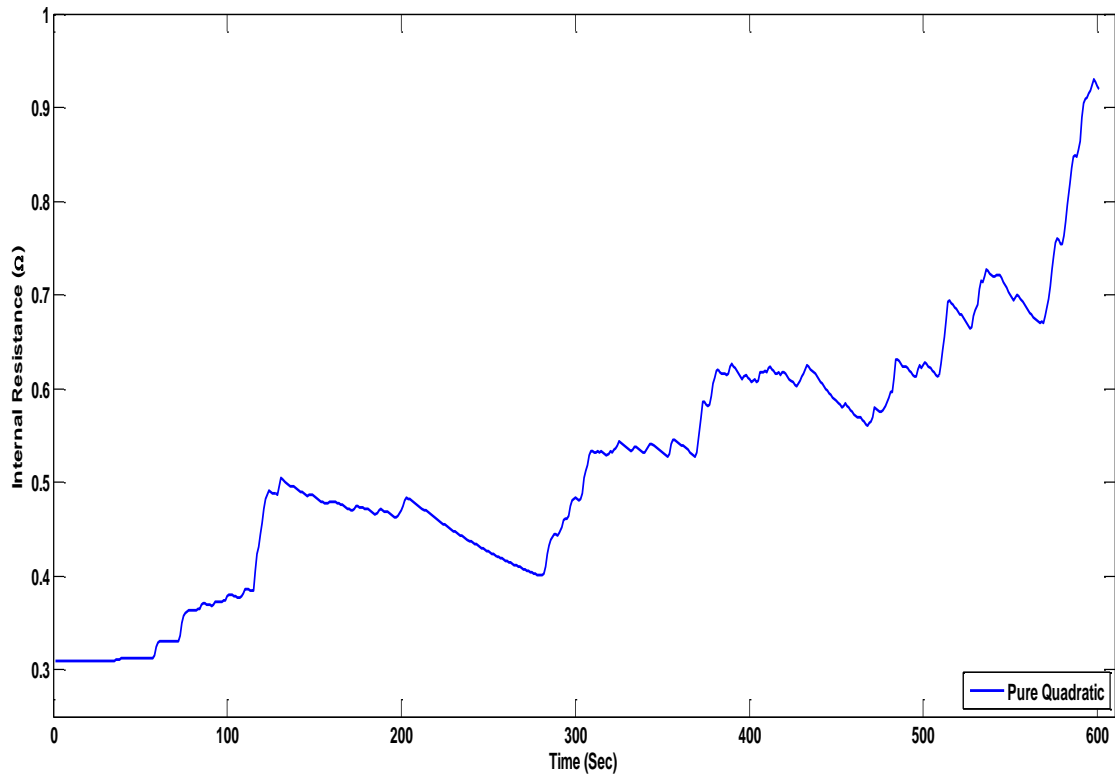


Figure 6.5. Estimated internal resistance for battery 2 from response surface method

It is observed that the estimated internal resistance for battery 2 is significantly influential by its operating temperature. The initial internal resistance of battery 2 is 0.3 Ω. This internal resistance varies from 0.3 Ω to 0.95 Ω during the same driving trip.

Since, the internal resistance of a battery varies with time especially for battery 2. We will simulate the driving trip cycle with the varying internal resistance of batteries as shown in Figure 6.5

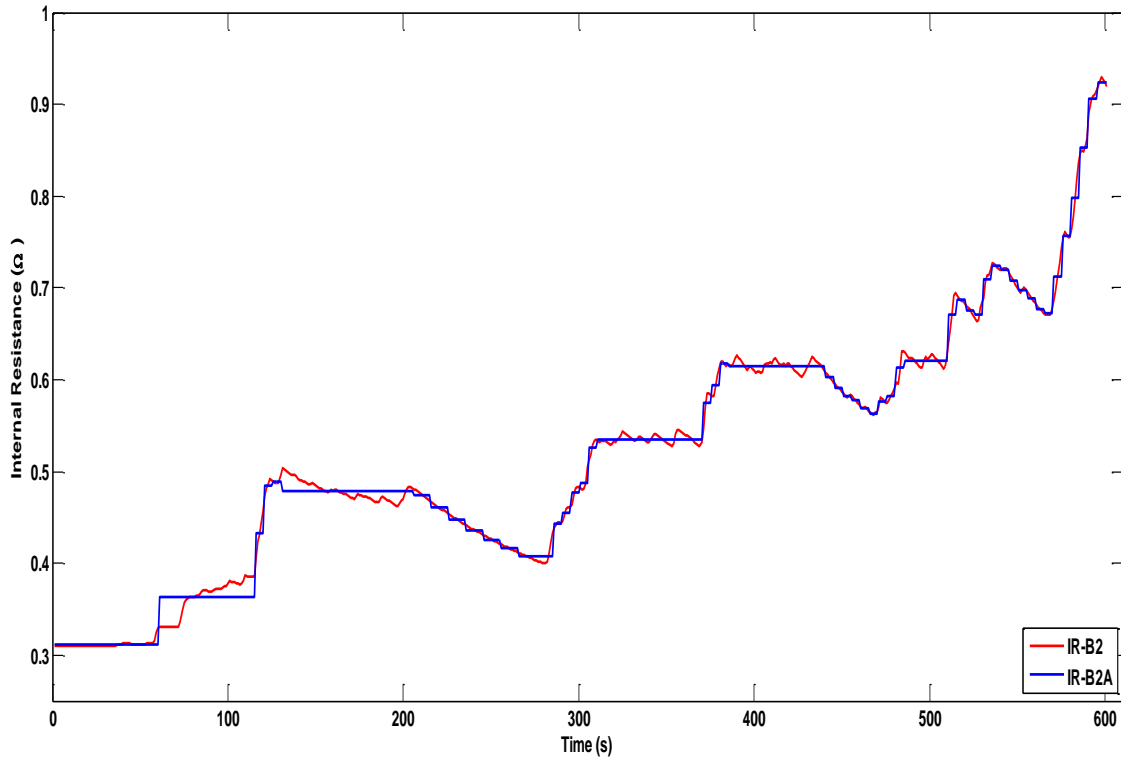


Figure 6.6. Estimated simulated internal resistance for battery 2 vs actual internal resistance applied during the simulation of the trip.

It is practically difficult to simulate with varying resistance. the driving trip for each second, so for simulation convenience the internal resistance values applied in the simulation are represented by IR-B2A as given in Figure 6.6.

The net loss in the energy caused by the rise in the internal resistance can be represented by simulating varying internal resistance valued during the driving trip.

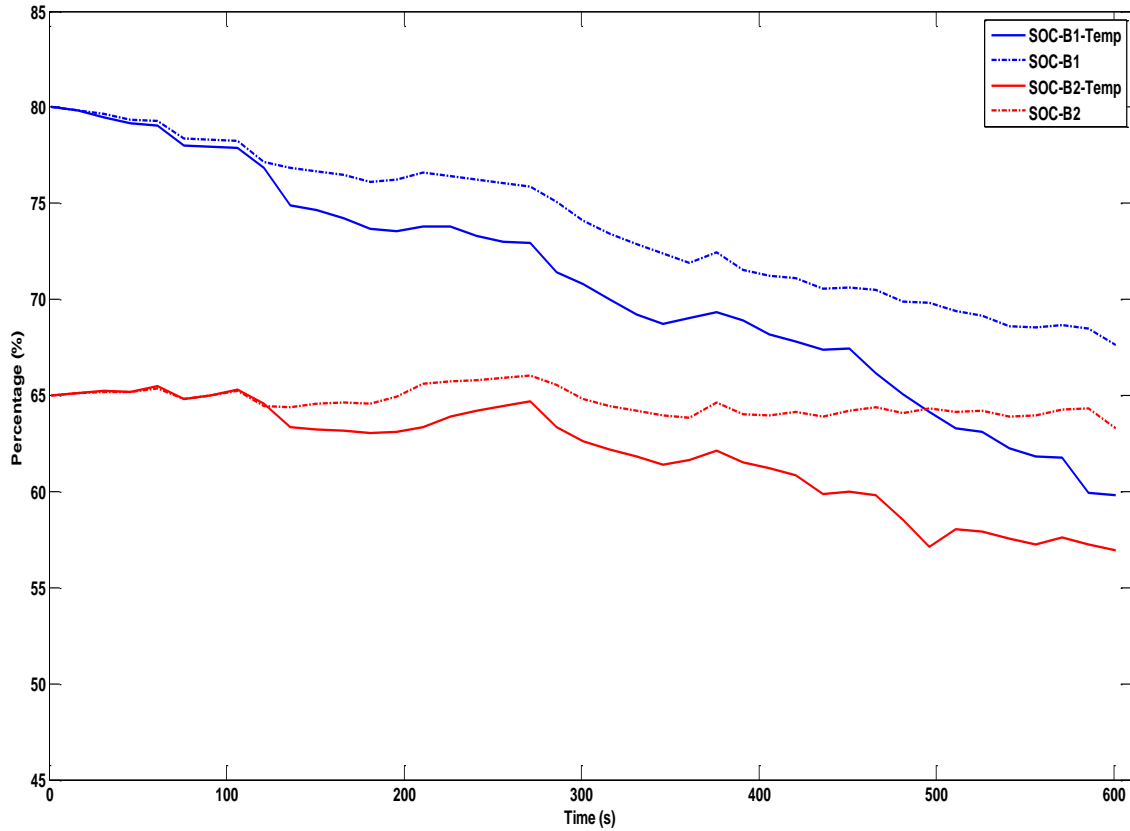


Figure 6.7. Battery SOC with two module equalization with constant internal resistance and varying internal resistance.

We consider the impact of temperature on the performance of lithium ion battery for our driving trip for 600 sec. Ideal lithium ion battery charged to 80% SOC is driven for 600 seconds drops to 76.09% SOC as per Figure 4.5. The SOC for battery with higher internal resistance without the temperature effect, i.e. with constant internal resistance after 600 seconds is 67.63% for battery 1 and 63.31% for battery 2. The average SOC change is 65.47%. The SOC for battery with higher internal resistance with the temperature effect i.e. with variable internal resistance after 600 seconds is 59.82% for battery 1 and 56.92% for battery 2. The average SOC change is 58.37%.

The WOR for battery with constant internal resistance and no temperature effect is 1.79.

The WOR for battery with varying internal resistance based on the operational temperature is 3.61.

Thus, with the knowledge of the exposed temperature and operating conditions we can accurately estimate the battery state of charge. The worthiness of replacement calculation will help us predict the time to change the battery before the battery expires.

6.3 Summary

In this chapter, we emphasized on the fact that battery internal resistance is very sensitive to the change in operational temperature of lithium ion batteries. The internal resistance of the batteries rises with the deviation of the temperature from its normal operational change. We have quantified the internal resistance change during a trip with the Comsol-Multiphysics model. Then we estimated the change in the internal resistance with the Response Surface Methodology (RSM) tool. The response surface modeled RSM accurately estimates the internal resistance within limited tolerances. The proposed methodology will be very effective to estimate the internal resistance during daily driving routes. The internal resistance estimated is used to optimize the daily operation cost and worthiness of replacement of lithium ion battery pack.

7 Summary

The limited availability of conventional energy resources has compelled us to expand the use of non-conventional energy sources for commuting and transportation. Our study was motivated to efficiently utilize and estimate the onboard stored energy in lithium ion battery of the electric vehicle. We also predict the replacement time for the lithium ion battery modules with the knowledge of internal resistance. We have specifically established algorithms which estimate the internal resistance of the lithium ion batteries.

An equalization scheme where energy is transferred from high energy cell to a low energy cell is proposed. The energy loss that takes place in the process of equalization is also quantified. We studied the effect of internal resistance of the battery modules on the performance of the lithium ion batteries. Also, the effect of module to module equalization schemes on lithium ion batteries is also studied. During the process of equalization, energy from higher energy module is transferred to lower energy module. We proved active energy balancing is an effective method of saving the onboard energy. The voltage equalization schemes provides robustness to estimate the state of charge and internal resistance of the lithium ion battery.

As we accurately estimate the internal resistance of the battery modules, we are in a position to qualify the worthiness of battery module replacement. It is proposed here in that battery modules should be replaced instead of the complete battery. The cost of maintaining the battery throughout the life could be reduced as we do not replace the entire battery. We provide a solution to battery maintenance and reduce the cost of battery replacement cost. The battery modules can be replaced in installments over a period of time which helps the user spread out the large cost associated with replacement of entire battery pack.

In chapter 4 it was demonstrated that we can dynamically estimate the internal resistance of the lithium ion modules. This ability provides us with the capability to optimize the performance of the battery during the active driving cycle. Also, in the modern interconnected world, the user has access to the next day predicted energy prices. Based on the internal resistance values, the charging times can be calculated. This helps to minimize the charging time of the electric vehicle. Operational strategies for charging and discharging are prescribed in the research work. In the smart grid system, energy can be transferred from vehicle to the grid. This opportunity is utilized to minimize the trip travel cost by earning some money exchanging energy with the grid. Our optimization algorithm specifies the charging sequencing and energy exchange with the grid which benefits the user. This procedure empowers the user to minimize the battery operational costs.

Battery temperature is a critical parameter to estimate the state of charge and internal resistance of lithium ion batteries. The driving cycle considered in this dissertation is used to obtain the input driving current for the lithium ion battery. The current requirement from the electric motor is used to estimate the state of charge of lithium ion battery. We studied the behavior of internal resistance of lithium ion batteries with changes in the operational temperature of the battery pack. A model of the lithium ion batteries in Comsol-Multiphysics. This model of the lithium ion battery yielded the temperature profile of the battery pack during the driving trip. The temperature profile is then used to estimate the internal resistance of the lithium ion batteries. The internal resistance is related to the operational temperature of the battery. A response surface method is presented to estimate the internal resistance of the lithium ion battery pack. The knowledge of the temperature help us estimate the internal resistance of the batteries. An accurate real-time estimate of

resistance will enhance the predictive capability of the electric vehicle battery. Estimating the internal resistance accurately will enhance the utility of the electric vehicle batteries.

This dissertation has also addressed the patterns and strategies of using lithium ion batteries for electric vehicles. These strategies will help the user to minimize the operating cost of the electric vehicles. The user can reduce the cost of maintenance of the lithium ion batteries by replacing only the underperforming modules without sacrificing the performance of the electric vehicles.

This work has extensive scope in the future as related to diagnostics and prognostics of lithium ion batteries. The digitalization in the automotive sector can help us to monitor the performance of the vehicle throughout its operational period, such that we can accurately estimate the internal resistance and performance of lithium ion batteries. Prognostics of lithium ion batteries is clearly possible based on its internal resistance.

The connected vehicle environment of the next generation of automotive technology will help to share data between vehicles and allow for communication between the vehicles. These electric vehicles utilizing smart technology and wireless charging capabilities can also be used as energy sharing devices.

Future generation smart grids will also include various non-conventional sources of energy that contribute energy to the conventional grid. A Game theory approach can be implemented to optimize the profits for the grid and optimize the cost incurred by the user on end to end operation of various mobile applications.

8 Bibliography

- Energy Information Administration. (2014). (Annual Energy)
- A.S. Masoum, A. S. (2011). Impact of Uncoordinated and Coordinated Charging of Plug-in Electric Vehicles on Substation Transformer in Smart Grid with Charging Stations. *IEEE*, 978-1-4577-0875-6, 807-819.
- A.Y. Saber, G. V. (2012). Resource Scheduling Under Uncertainty in a Smart Grid with Renewables and Plug-in Vehicles. *IEEE Systems Journal*, 6(1), 103-109.
- Akira, Y. (1985). Secondary Battery. *Asahi Kasei*.
- Benedikt Lunz, Z. Y. (2012). Influence of Plug-in Hybrid Electric Vehicle Charging Strategies on Charging and Battery Degradation Costs. *Journal of Power Sources*, 46, 511-519.
- Buller, S, T. M. (2003). Impact Based Simulation Models of Supercapacitors and Lithium-ion Batteries for Power Electronic Applications. *Conf. Rec.*, 3, 15960-16000.
- C. Moo, K. S. (2008). "Parallel Operation of Battery Power Modules. 23(2), 441-452.
- C.R. Gould, C. B. (2009). New Battery Model and State-of-Health Determination Through Subspace Parameter Estimation and State Observer Techniques. *IEEE Transactions on Vehicular Technology*, 58(8), 3905-3913.
- Cassani, P., & Williamson, S. (2010). Design, Testing and Validation of a Simplified Control. *IEEE Transactions on Industrial Electronics*, 57(12), 332-341.
- Chang, L. (1993). Recent Developments of Electric Vehicles and their Propulsion . 8(12).

- Changsun Ahn, C.-T. L. (2011). Optimal decentralized charging control algorithm for electrified vehicles connected to smart grid. *Journal of Power Sources*, 196, 10369-10379.
- Cheng, Y.-S. L.-W. (2005). Intelligent Control Battery Equalization for Series Connected Lithium-Ion Battery Strings. *IEEE Transactions on Industrial Electronics*, Vol, 52(5), 1235-1253.
- Christophe Guille, G. G. (2009). A Conceptual Framework for the Vehicle-to-Grid (V2G) Implementation. *Energy Policy*, 37, 4379-4390.
- Fiji Times Online. (2010, 03 04). Electric car boom.
- G.Gross, C. G. (2009). A Conceptual Framework for the Vehicle-to-Grid. *Energy Policy*, 4379-4390.
- Gold, S. (1997). A P-Spice Macro-Model for Lithium-ion Batteries. *Proc.12 th Annual Battery Conference Applications and Advances*, 215-222.
- Guibin Wang, Z. X. (2013). Traffic-Constrained Multiobjective Planning of Electric-Vehicle Charging Stations. *IEEE Transactions on Power Delivery*, 28(4), 511-519.
- H. Khayyam, H. R. (2012). Intelligent Control of Vehicle to Grid Power. *Journal of Power Sources*, 201, 1-9.
- J. Kiviluoma, P. M. (2011). "Methodology for Modelling Plug-in Electric Vehicles in the Power System and Cost estimates for a System with either Smart or Dumb Electric Vehicles. *Energy*, 36, 1758-1767.
- J. Xu, M. G. (2009). Design and Study of the State of Charge Estimation. *International Conference on Artificial Intelligence and Computational Intelligence*, (pp. 56-61).

- J.G.Lozano, M. M. (2012). Electric Vehicle Battery Charger for Smart Grids. *Electric Power Systems Research*, 90, 18-29.
- Juang, J. (1994). *Applied System Identification*. Prentice Hall.
- K. J. Aström, B. W. (1994). *Adaptive Control* (2nd ed.). Prentice Hall.
- K. Nansai, S. T. (2001). Life-Cycle Analysis of Charging Infrastructure for Electric Vehicles. *Applied Energy*, 70, 251-265.
- K.C.Nyns, E. H. (2010). The Impact of Charging Plug-in Hybrid Electric. *IEEE Transactions on Power Systems*, 25(1), 371-380.
- K.M. Tsang, L. W. (2010). Identification and Modeling of Lithium Ion Battery. 51, 2857-2862.
- Karen L. Butler, M. I. (1999). A Matlab-Based Modeling and Simulation Package for Electric and Hybrid Electric Vehicle Design. *IEEE Transactions On Vehicular Technology*, 48(6), 1778-1793.
- L. Cai, R. W. (2011). Mathematical Modeling of a Lithium ion Battery with Thermal Effects in COMSOL Inc Multiphysics (MP) software. *Journal of Power Sources*, 196, 5985-5989.
- Ljung, L. (1998). *System Identification Theory for the User*. 2 nd ed., Prentice Hall.
- M, C. (2000). New Dynamical Models of Lead-Acid Batteries. *IEEE Transactions on*, 15(4), 1184-1190.
- M. Armstrong, C. M. (2013). Optimal Recharging Strategy for Battery-Switch Stations for Electric Vehicles in France. *Energy Policy*, 60, 569-582.
- M. Dubbarry, N. V. (2009). From Single Model to Battery Pack Simulation. 186, 500-507.

- M. Ecker, J. G. (2012). Development of Lifetime Prediction of Model for Lithium-ion Batteries Based on Extended Accelerated Aging Test Data. *Journal of Power Sources*, 215, 248-257.
- M. Kassem, J. B. (2012, Feb). Calendar aging of a graphite/LiFePO₄ cell. 208, 296-305.
- M. Stadler, C. M. (2012). "Optimal Planning and Operation of Smart Grids with Electric Vehicle Interconnection. *Journal of Energy Engineering*, 138, 95-108.
- M.S, W. (1976). Electrical Energy Storage and Intercalation Chemistry. *Science*, 192(4244), 1126-1127.
- Madeleine Ecker, J. B. (2012). "Development of a Lifetime Prediction Model for. *Journal of*, 215, 248-257.
- Midwest ISO. (n.d.). Retrieved from www.midwestiso.org :
- <https://www.midwestiso.org/Library/MarketReports/Pages/MarketReports.aspx>
- Millner, A. (2010). Modeling Lithium Ion Battery Degradation in Electric Vehicles. *IEEE*, 978, 1121-1132.
- Min Chen, G. R.-M. (2006). Accurate electrical battery model capable of predicting runtime and I-V performance. *IEEE Transactions on Energy Conversion*, 21(2), 504 - 511.
- N. Roterling, M. (2011). Optimal Charge Control of Plug-in Hybrid Electric Vehicles. *IEEE Transactions on Power Systems*, 26(3), 1021-1029.
- Nazri, G. P. (2004). *Lithium batteries: science and* . Springer ISBN 1402076282.
- P. Finn, C. F. (2012). Demand side management of electric car charging: Benefits for consumer and grid. *Energy*, 358-363.

- P.Finn, C. D. (2012). Demand Side Management of Electric Car Charging: Benefits for Consumer and Grid. *Energy*, 42, 358-363.
- Park H.S, K. C. (2009). Design of Charge Equalizer Based on. *IEEE Transactions on Vehicular Technology*, 58(7), 72-79.
- Raviv, T. (2012). The Battery Switching Station Scheduling Problem. *Operations Research*, 40, 546-550.
- S. Bashash, S. M. (2011). Plug-in Hybrid Electric Vehicle Charge Pattern Optimization for Energy Cost and Battery Longevity. *Journal of Power Sources*, 196, 541-549.
- S.C, H. (1993). Simple Spice Models Let You Simulate Common Battery Type. *EDN*, 17-132.
- Salameh Z.M., C. L. (1992). "Mathematical Model for Lead Acid Batteries. *IEEE Transactions on Energy Conversion*, 7(1), 93-98.
- Scott B. Peterson, J. W. (2010). The Economics of using Plug-in Hybrid Electric Vehicle Battery Pack for Grid Storage. *Journal of Power Sources*, 195, 2377-2384.
- V Pop, B. H. (2008). State-of-the-art of battery state-of-charge determination. *Measurement Science and Technology*, 11-45.
- Valvo M. Wicks F.E., R. D. (1996). Development and Application of an Improved equivalent Circuit Model of a Lead Acid Battery. *Proc. Energy Conversion Engineering Conference*, 2, 1159-1163.
- Vasebi A, B. S. (2008). Predicting State of Charge of Lead Acid. *Energy Conversion and Management*, 49, 75-82.
- Weiller, C. (2011). Plug-in Hybrid Electric Vehicle Impacts on Hourly Electricity Demand in the United States. *Energy Policy*, 39, 3766-3778.

- Wencong S, H.-E. W.-Y. (2012). Survey on the Electrification of Transportation in Smart Grid Environment. *IEEE Transactions On Industrial Informatics*, 8(1), 1-10.
- X. Hu, F. S. (2010). Estimation of State of Charge of a Lithium-Ion Battery Pack. *Energies*, 3, 1586-1603.
- X. Wei, B. Z. (2011). Internal Resistance Identification in Vehicle Power Lithium-. *International Conference on Measuring Technology and Mechatronics Automation*, (pp. 221-206).
- Y. Ye, Y. S. (2012). Electro-Thermal Modeling and Experimental Validation for Lithium Ion Battery. *Journal of Power Sources*, 199, 227-238.
- Zhenli Zhang, B. S. (2013). Model-Based Analysis of Cell Balancing of Lithium-ion. *SAE International*, 379-388.

9 Curriculum Vitae

Education

PhD (Mech Engg)	University of Wisconsin at Milwaukee	GPA : 3.73/4.0	Feb '17
MS (Mech Engg)	University of Wisconsin at Milwaukee	GPA : 3.67/4.0	Aug '13
MS (Mech Engg)	San Diego State University	GPA : 3.51/4.0	Aug '09
BS (Mech Engg)	Dr. BAMU University	First Class	Aug '05

Technical Experience

Algorithm Design Engineer **GM Corp** **Jan 2015 - Present**

- Design and develop prognostic and diagnostic algorithms under “Vehicle Health Management” team
- Predict remaining useful life based on physics models and data driven models from machine learning / AI
- Improved the current system of fault detection by designing and developing new algorithms
- Reduce the fault detection time to couple of seconds rather than long hours of trouble shooting
- Collaborate with “Onstar” team to integrate and deploy algorithms for pre-production and production
- Collaborate with service teams to launch the solutions for rigorous testing of the faults

Research/TeachingAssistant **U Wisconsin Milwaukee** **Jan 2010 - Dec 2014**

- Generated 20% savings by strategizing charging and discharging cycles for EV's
- Minimized daily cost of travel for EV users by implementing linear programming and optimization techniques
- Saved cost by ~15% by identifying battery parameters to decide the overhauling time for batteries

- Designed process for MEM's device using local sintering process
- Construction research to study the process capabilities and geometric variations in concrete columns

Publications and Presentations

"Equalization Integrated Online Monitoring of Health Map and Worthiness of Replacement for Battery Pack of Electric Vehicles", Journal of Power Sources Vol. 223 pp. 293-305 2013

"Trip Specific Worthiness of Replacement of Individual Cells for Battery Pack in Electric Vehicles", SAE Technical Paper 2011-01-1361, 2011

"Novel Current Activated Tip based Sintering (CATS) of Advanced Materials", Minerals, Metals and Materials Society/AIME

"Novel Current-Activated Tip-Based Sintering (CATS): Localization of Spark Plasma Sintering", Scripta Materialia, Vol. 60, Issue 9, pp. 745-748, May 2009